MIT/WHOI

Massachusetts Institute of Technology

Woods Hole Oceanographic Institution

Joint Program in Oceanography/ Applied Ocean Science and Engineering

MASTER OF SCIENCE DISSERTATION

Horizontal Linear Array Sensor Localization and Preliminary Coherence Measurements from the 2001 ASIAEX South China Sea Experiment

by

Theodore Herbert Schroeder

September 2002

Horizontal Linear Array Sensor Localization and Preliminary Coherence Measurements from the 2001 ASIAEX South China Sea Experiment

by

Theodore Herbert Schroeder

B.S. Mechanical Engineering, University of Missouri-Rolla, 1989

Submitted in partial fulfillment of the
requirements for the degree of
MASTER OF SCIENCE IN OCEAN ENGINEERING

at the
MASSACHUSETTS INSTITUTE OF TECHNOLOGY
and the
WOODS HOLE OCEANOGRAPHIC INSTITUTION

September 2002

Signature of Author.....
Joint Program in Applied Ocean Science and Engineering
Massachusetts Institute of Technology
and Woods Hole Oceanographic Institution
September 2002

Certified by.....
Dr. James F. Lynch
Senior Scientist, Woods Hole Oceanographic Istitution
Thesis Supervisor

Accepted by.....
Professor Michael Triantafyllou
Chairman, Joint Committee for Applied Ocean Science and Engineering
Massachusetts Institute of Technology/Woods Hole Oceanographic Institution

Horizontal Linear Array Sensor Localization and Preliminary Coherence Measurements from the 2001 ASIAEX South China Sea Experiment

by

Theodore Herbert Schroeder

Submitted to the Massachusetts Institute of Technology/
Woods Hole Oceanographic Institution
Joint Program in Applied Ocean Science and Engineering
On August 9, 2002, in partial fulfillment of the
Requirements for the degree of Masters of Science in
Ocean Engineering

Abstract

This thesis examines data collected in the South China Sea (SCS) component of the 2001 Asian Seas International Acoustic Experiment (ASIAEX), where a fixed Horizontal Linear Array (HLA) was deployed to study transverse array coherence in a coastal environment. Arrays obtain their gain and directivity by coherently adding the energy that impinges on them. Therefore, to maximize the efficiency of an array, the size of the aperture over which the signal remains coherent needs to be determined. Scattering of sound by the ocean environment, especially in coastal areas, reduces the coherence of acoustic signals, and thereby limits the useful aperture of an acoustic array.

During ASIAEX, a horizontal linear array was deployed on the continental shelf of the South China Sea in order to directly measure the acoustic coherence in a coastal environment. 224 Hz and 400 Hz sources were placed on the continental slope to provide an up slope propagation path and a 400 Hz source was placed on the shelf to provide an along shelf propagation path. This thesis analyzes one day of transmissions from these three sources and gives the first look at coherence lengths of the HLA determined by sensor-to-sensor correlations. To achieve this, the thesis analyzes continuous time series data from the Long Base Line (LBL) navigation system and two days of light bulb drops to provide array sensor localization. Accurate sensor positions are needed to determine the correlation versus sensor separation distance and ultimately the array coherence length.

Thesis Supervisor: Dr. James Lynch
Senior Scientist, Woods Hole Oceanographic Institution

Acknowledgements

I thank the Navy for giving me the opportunity and paying the tuition that allowed me to pursue graduate studies at MIT and WHOI. Additionally I thank the Office of Naval Research for providing funding for the ASIAEX experiment through ONR Grant N00014-95-0051 and thereby providing me with some very interesting data to analyze.

I thank my thesis advisor Dr. James Lynch for his guidance, patience and support. He helped make my work exciting and fun. I hope that I will have the opportunity to work with him in the future.

I want to thank my MIT academic advisor Prof. Arthur Baggeroer for his exceptional guidance and support. He was invaluable in helping me navigate my way through the MIT classes.

I thank the fellow ASIAEX contributors, without whom I would not have had the ability to complete this work. I particularly want to thank Arthur Newhall. His computer expertise, willingness to help and patience in teaching were of immeasurable help.

I especially want to thank my wife Shannon and daughter Anna for their love and support, without which I would not have been able to complete such a task.

Contents

List of Tables

List of Figures

1 Background

1.1 Introduction

In the past decade, there has been an increased interest in the performance of sonar arrays in shallow water. This interest has been driven by the U.S. Navy's increase in littoral operations, as well as by increased scientific work conducted in these areas. Sonar arrays are being used in shallow water for everything from tracking ships and marine mammals to making scientific measurements for the determination of ocean dynamics. Because of this, there has been a desire to optimize the performance of sonar arrays.

One of the standard sonar's used is the horizontal array, which is usually towed or bottom deployed. One parameter that limits the resolution and gain of a horizontal sonar array is the transverse coherence length. In general, horizontal arrays can increase their gain and directivity by increasing their length. However, this gain is only achieved when the signal is coherent over the length of the array (the transverse coherence length). The scattering of sound by the ocean environment, especially in coastal areas, reduces the coherence of acoustic signals, and thereby limits the useful aperture of a horizontal acoustic array. In order to maximize the efficiency and resolution of such an array, the size of the aperture over which the signal remains coherent needs to be determined.

1.2 Thesis Objectives

This thesis examines data collected in the South China Sea (SCS) component of the Asian Seas International Acoustic Experiment (ASIAEX), where a fixed Horizontal Linear Array (HLA) was bottom deployed at 125 m depth to study transverse array coherence in a coastal environment. This thesis analyzes one day of signals at frequencies of 224 Hz and 400 Hz. The ASIAEX SCS experiment employed a number of

sources. One of interest was a moored 400 Hz source deployed at approximately the same (125 m) water depth as the HLA, providing an ~20 km along shelf propagation path. Two additional sources, 224 Hz and 400 Hz, were deployed in deeper water (approximately 340 m), providing an ~30 km up slope (or equivalently, cross shelf) propagation path. This thesis takes the first look at the horizontal spatial coherence lengths seen by the ASIAEX HLA, by performing a sensor-to-sensor correlation of the individual signals from these three sources. It also provides some insight into frequency and propagation path effects on coherence. To achieve this, the first part of the thesis analyzes continuous time series data from the Long Base Line (LBL) navigation system and two days of light bulb drops to provide array sensor localization. Accurate sensor positions are needed to determine the correlation versus sensor separation distance and ultimately the array coherence length.

1.3 Spatial Coherence – Some Background

Spatial coherence has been studied for many years in ocean acoustics, but much of the original work was conducted in deep water. Stickler and his colleagues at Bell Telephone Laboratories were some of the first to conduct spatial coherence experiments [1]. In the 1960s, they conducted experiments on the Plantagenet Bank near Bermuda, using 10 ms 400 Hz pulses at ranges of 137-963 km. Analyzing the results from these experiments, Moseley was able to localize a single ray with no surface or bottom interactions that produced $1/e$ correlation lengths of 94-450 λ [2].

Since these first experiments, numerous other experiments have been conducted in many deep ocean basins. The results of these experiments provide accurate measurements and predictions for spatial coherence in these areas. In 1998, Carey looked at many of these deep ocean basin experiments and concluded that for frequencies between 300-400 Hz the measured coherence lengths are of the order 100 λ at ranges of 500 km [3].

Far fewer spatial coherence experiments have been conducted in shallow coastal environments, and the focus has only recently turned to these areas. Additionally,

determining and predicting the spatial coherence lengths in shallow water coastal environments is a more difficult task. The variability of the oceanography and geology in shallow areas greatly complicates the spatial coherence calculations. The main difficulty lies in getting accurate data on the ever changing, range dependent environment. This includes the influence of internal waves, fronts and eddies on the range dependent sound speed profile, along with surface and bottom roughness spectra and bottom geoacoustic profiles. Because of these variables, more experiments that include a wide range of carefully collected oceanographic data are needed to determine the effects of major oceanographic parameters on coherence, in order to thereby achieve better coherence predictions.

To date, only a few experiments have been conducted in shallow water environments with sufficient environmental data. These experiments are summarized in a paper by Carey; Table 1-1 reproduced from that paper summarizes their results [3]. The experiments shown in Table 1-1 indicate that in shallow coastal regions the spatial coherence lengths for frequencies of 135-800 Hz are much shorter than in the deep-water basins, and are on the order of 10-54 λ, with most of the results falling between 18-38 λ. The spatial coherence lengths in the shallow water thus seem to be a factor of 2 to 10 times shorter than in the deep water. This occurs in the shallow water as the acoustic signal experiences more scattering events per unit distance traveled than in deep water. The multiple interactions with the bottom and surface, along with volumetric scatters like internal waves, fronts and eddies cause the signals to scatter and spread far more than in deep water.

1.4 Thesis Outline

Chapter 2 will discuss ASIAEX in more detail and describe the physical environment of the SCS experiment. Chapter 3 provides details about the LBL system and the light bulb drops used for sensor positioning. It also discusses the LBL time series calculations made and the positions of the sensors on 5 and 15 May as obtained by the light bulb drops. Chapter 4 describes the low frequency signals that were analyzed and

correlated for the coherence calculations. The correlation calculations and spatial coherence results are also discussed in Chapter 4. Chapter 5 covers parallel work that has been done by the Naval Research Laboratory, gives conclusions and discusses future work.

Table 1-1: Experiments performed in areas with measured range-dependent sound velocity profiles in sandy-silty areas with known bathymetry. SVP=sound velocity profile; ISV=isovelocity; DR=downward refracting; COV=coefficient of variation in measured results; Exp.=explosive; CW=continuous wave [3].

Reference	4	5	6	7	7	7	7	7
Location	North. Sea	Scotian Shelf	Florida Gulf Coast	West Florida Escarpment	New Jersey Cont. Shelf	Strait of Korea	Strait of Korea	Korean Strait/ Yellow Sea
SVP	ISV	DR	DR	DR	DR	DR	DR	DR
Water Depth	65 m	0.1-1 km	0.1-1 km	200 m	100 m	100 m	100 m	100 m
Bottom	Sand	Sandy-silty-clay	Sandy-silty-clay	Sandy-silty-clay	Sandy-silty-clay	Sandy-silty-clay	Sandy-silty-clay	Sandy-silty-clay
f_1 (Hz)	400	135	173-175	200-400	200-400	354	300	354
f_2 (Hz)	800			400-800	400-600	600	500	604
Range (km)	7.4	100	25	9.3	4-22	7-11	5-45	14-24
$(L_C/\lambda)_1$	18	31	21	30	23	27	29	38
$(L_C/\lambda)_2$	10			32	25	30	31	54
Source	Exp.	CW	CW	Exp.	Exp.	CW	Exp.	CW
Source depth	21 m	18 m	100 m	100 m	52 m	30 m	52 m	33 m
Receiver depth	15 m	750 m	400 m	200 m	100 m	101 m	101 m	94 m
COV	8%	4%	6%	4%	4%	4%	5%	2%-4%

2 ASIAEX

2.1 Background

The Asian Seas International Acoustic Experiment (ASIAEX) was a collaboration between the United States of America, the People's Republic of China, Taiwan (ROC), the Republic of Korea, Japan, Russia and Singapore. The major field experiments of ASIAEX were performed from April to August 2001. These included two major acoustics experiments. The first was a volume interaction experiment conducted in the South China Sea (SCS) during April and May of 2001. The second, a bottom interaction experiment, was conducted in the East China Sea (ECS) in June and July of 2001. These acoustic experiments also included physical oceanography, geology and geophysics components. This thesis will focus on the South China Sea experiment. The three organizations from the USA that contributed to the ASIAEX SCS experiment were the Woods Hole Oceanographic Institution, the Naval Postgraduate School and the Naval Research Laboratory. More detailed information on the 2001 SCS experiment can be found in a Woods Hole Oceanographic Institution technical report [8].

The upper panel of Figure 2-1 shows the location of the SCS experiment, at the edge of the continental shelf east of China and southwest of Taiwan. The lower panel shows the locations of the moored acoustic and oceanographic equipment that was successfully deployed and recovered during the experiment. This panel also shows the overall geometry of the acoustic experiment, in which the horizontal linear array (HLA) and vertical linear array (VLA), deployed in 124.5 meters of water, received acoustic transmissions from two separate source locations. The sources located ~20 km to the east were deployed in ~120 meters of water to provide an along shelf propagation path. The sources located ~30 km to the south were deployed in ~345 m of water to provide an up slope or cross shelf propagation path.

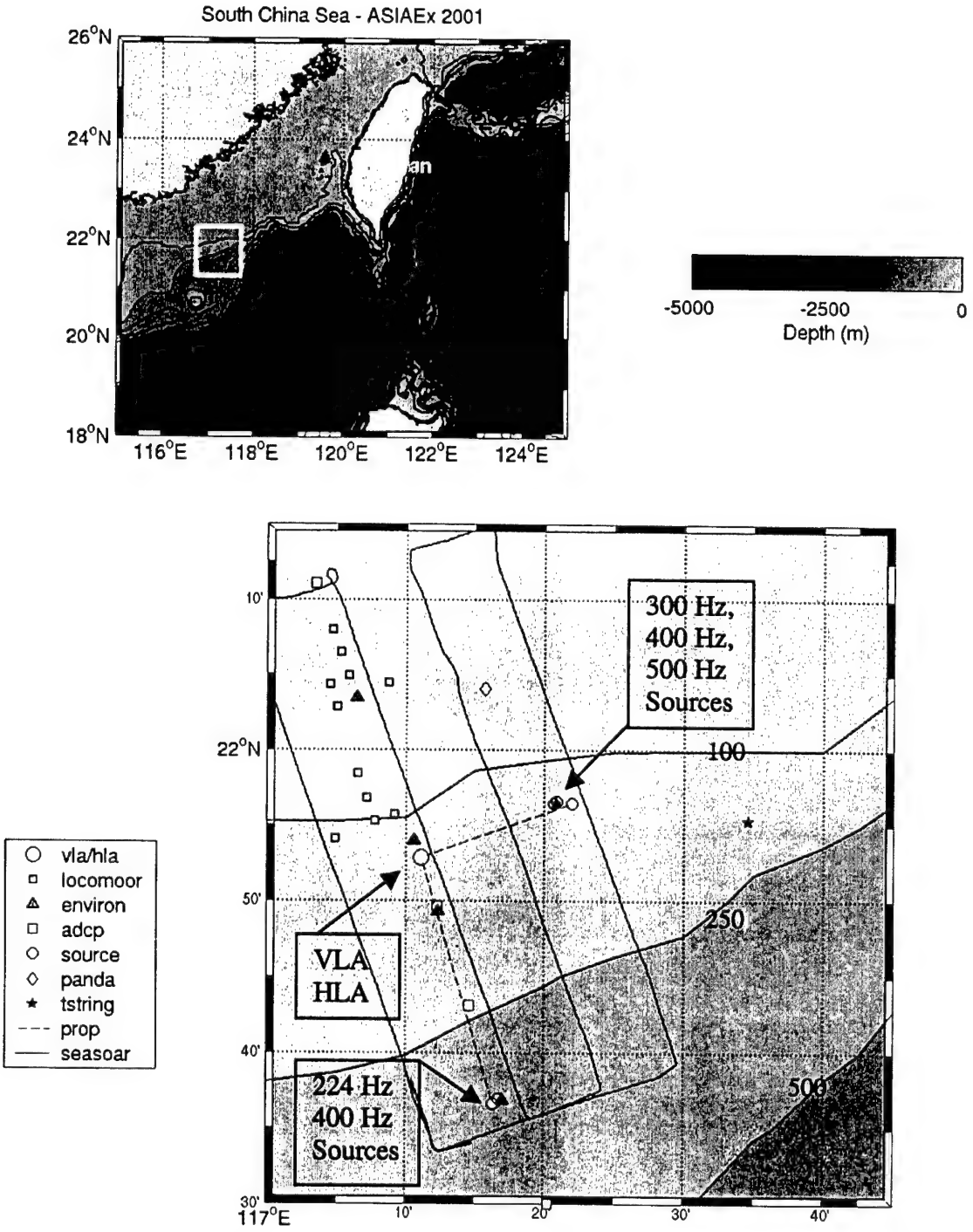

Figure 2-1: ASIAEX South China Sea Experiment. The three sources to the east provided a ~20 km along shelf propagation path and the two sources to the south provided a ~30 km up slope propagation path.

2.2 Goals for ASIAEX SCS Experiment

A major socio-political goal of ASIAEX was to foster collaboration within the scientific community of the Pacific Rim countries by conducting scientific experiments in the area. The main scientific goals of ASIAEX were generally interdependent, but they can be usefully placed into the three broad groups: acoustics, physical oceanography and geology and geophysics.

The data from the experiment can be used to reach a number of acoustic goals. The main goal is to study acoustics in an interesting coastal continental shelf and slope environment that has not previously been extensively studied. Some of the specific areas of acoustic research include measuring horizontal and vertical sonar array coherence (the topic of this thesis); measuring pulse wonder and spread; measuring the frequency dependence of the channel propagation and scattering in the 50-600 Hz band; measuring the ambient noise field; comparison of along shelf and up slope (cross shelf) propagation, and understanding the strong bottom interactions caused by the downward refracting sound velocity profile.

The experiment also concentrated on measuring physical oceanography and geology/geophysics, both to support the acoustics and as studies in their own right. The physical oceanography study can be divided into large scale and fine scale components. For the large-scale study, temperature and salinity profiles were obtained throughout the experimental area, specifically including the acoustic path, to correlate with environmental conditions such as local gyres and currents. For the fine scale study, the generation, propagation and dissipation of internal waves and events of shorter duration were of interest.

The geology and geophysics goals were to study the stratigraphy of the top (approximately) 200 meters of sediment.

2.3 Sensors

Twenty-eight moorings were successfully deployed and recovered during the ASIAEX South China Sea experiment. Additionally, measurements were taken from some of the research vessels such as CTD casts and the towed SeaSoar sled. The data for the geological and geophysics study was collected using high frequency chirp sonar, water gun impulses and core samples. The specific sensors for the acoustic and physical oceanography studies are discussed in the following sections.

2.3.1 Acoustic Equipment

The acoustic equipment deployed was comprised of five moored sources, a towed source, a horizontal linear array (HLA), a vertical linear array (VLA), three high frequency transponders used for the LBL system and light bulbs for HLA sensor location.

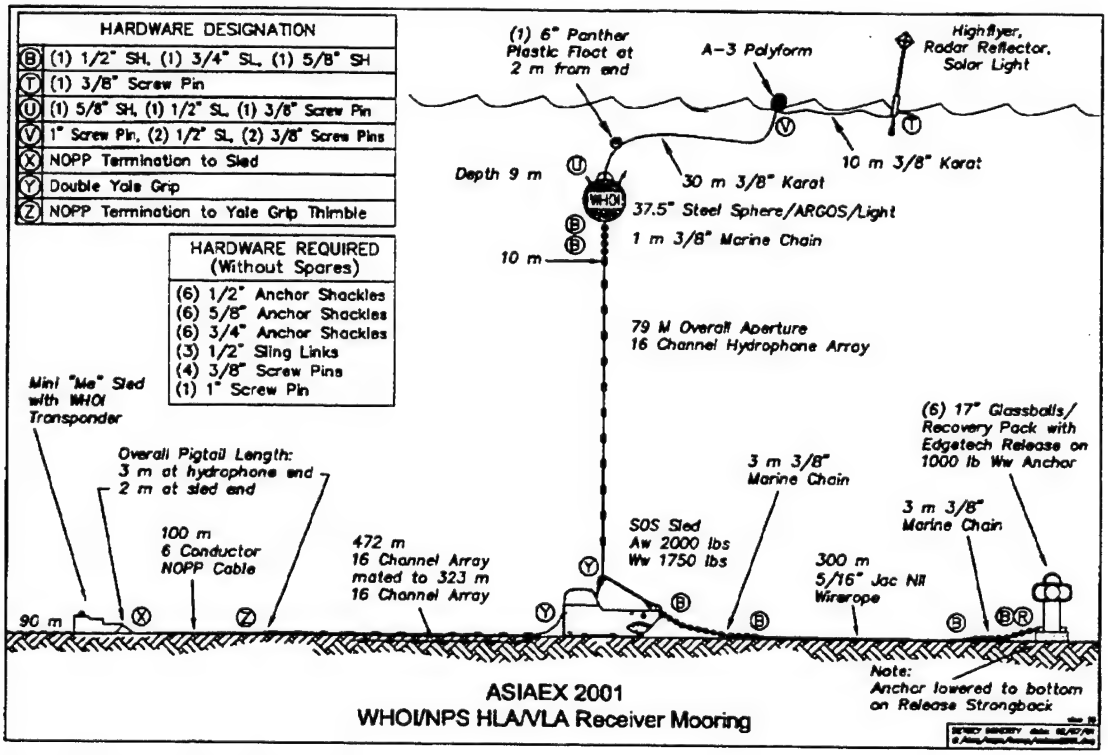

Figure 2-2: Horizontal Linear Array and Vertical Linear Array deployed in 124.5 m of water for the ASIAEX SCS experiment. The HLA consisted of 32 sensors equally spaced at 15 m.

2.3.1.1 HLA and VLA

The horizontal and vertical linear arrays (HLA/VLA) are shown in Figure 2-2. The arrays were designed to be deployed in 90m of water as shown in the figure. However, due to heavy fishing in the area, they were actually deployed at a water depth of 124.5m. The VLA is composed of 16 hydrophones with a spacing of 3.75 m for the top 10 hydrophones and a spacing of 7.5 m for the lower 6 hydrophones. The HLA had 32 elements with a spacing of 15 m giving the HLA a total length of 465 m. The HLA spacing is greater than the optimal sampling spacing of half-wave length (Nyquist sampling) for all but 50 Hz, the lowest frequency used in the experiment. This was done to achieve an array with an adequate length for acoustic coherence studies, i.e., an overall length of greater than 30 times the acoustic wavelength.

2.3.1.2 224 Hz and 400 Hz Sources

The signals analyzed in this thesis are from the 224 Hz and the two 400 Hz sources. The 224 Hz source was a Webb Research Corporation organ pipe tomography source, which transmitted a 224 Hz center frequency, 16 Hz bandwidth phase encoded signal every 5 minutes starting on the hour. It was deployed in deep water to study the up-slope propagation path. Figure 2-3 shows the configuration of the source and Table 2-1 presents specific details about the deployment and transmissions.

The 400 Hz sources were a more modern version of the Webb Research Corporation organ pipe design, featuring 100 Hz of bandwidth. Like the 224 Hz source, these sources transmitted phase encoded signals. Two types of the 400 Hz signals were used in the experiment. For the first part of the experiment, the source transmitted for 449.68 seconds every half hour, to study the temporal decorrelation times of the medium. The transmission schedule changed on 9 May. For the second part of the experiment the sources were transmitting for 117.53 seconds every ten minutes in order to study tidal period (and longer) ocean phenomena. Figure 2-4 shows the configuration for the 400 Hz sources and Tables 2-2, 2-3 and 2-4 present specific information about the deployment and transmission cycles.

The 300 Hz, 500Hz and J-15-3 sources were not analyzed in this thesis, and therefore are not discussed.

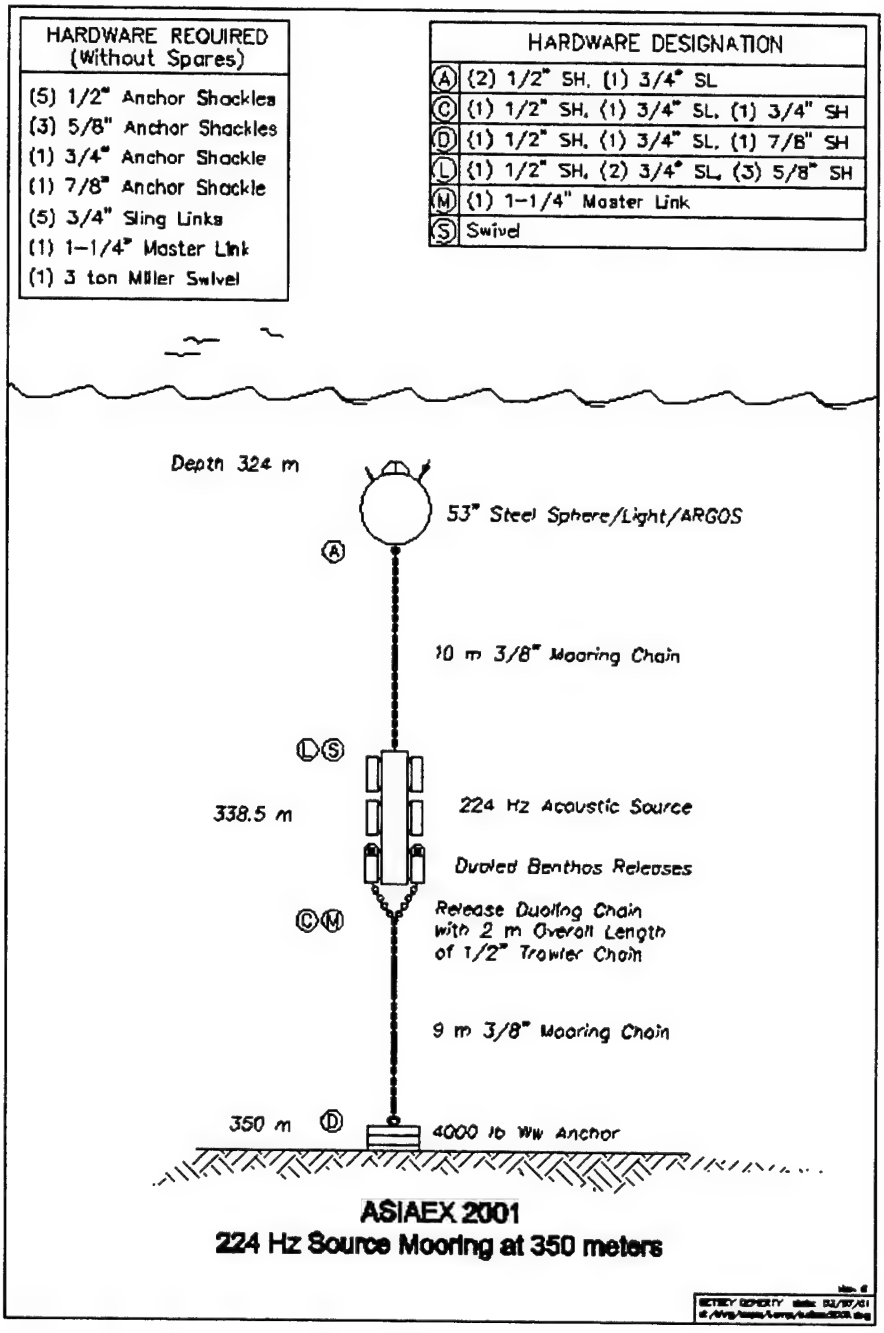

Figure 2-3: Mooring diagram for the 224 Hz source deployed at 345.8 m water depth.

Table 2-1: 224 Hz Source

Water Depth (Log)	345.8 m
Depth, Center of Source	331.3 m
Distance to VLA	31184 m
Transmission Period	Every 5 min
Center Frequency (Hz)	224
Bandwidth (Hz) – Full 3 Db	16
Source Level	183 dB re 1 uPa @ 1m
Cycles Per Digit	14
Digits Per Sequence	63
M-Sequences Per Transmission	30
Sequence Length	3.9375 seconds
Total Transmission Length	118.125 seconds (30*3.9375)

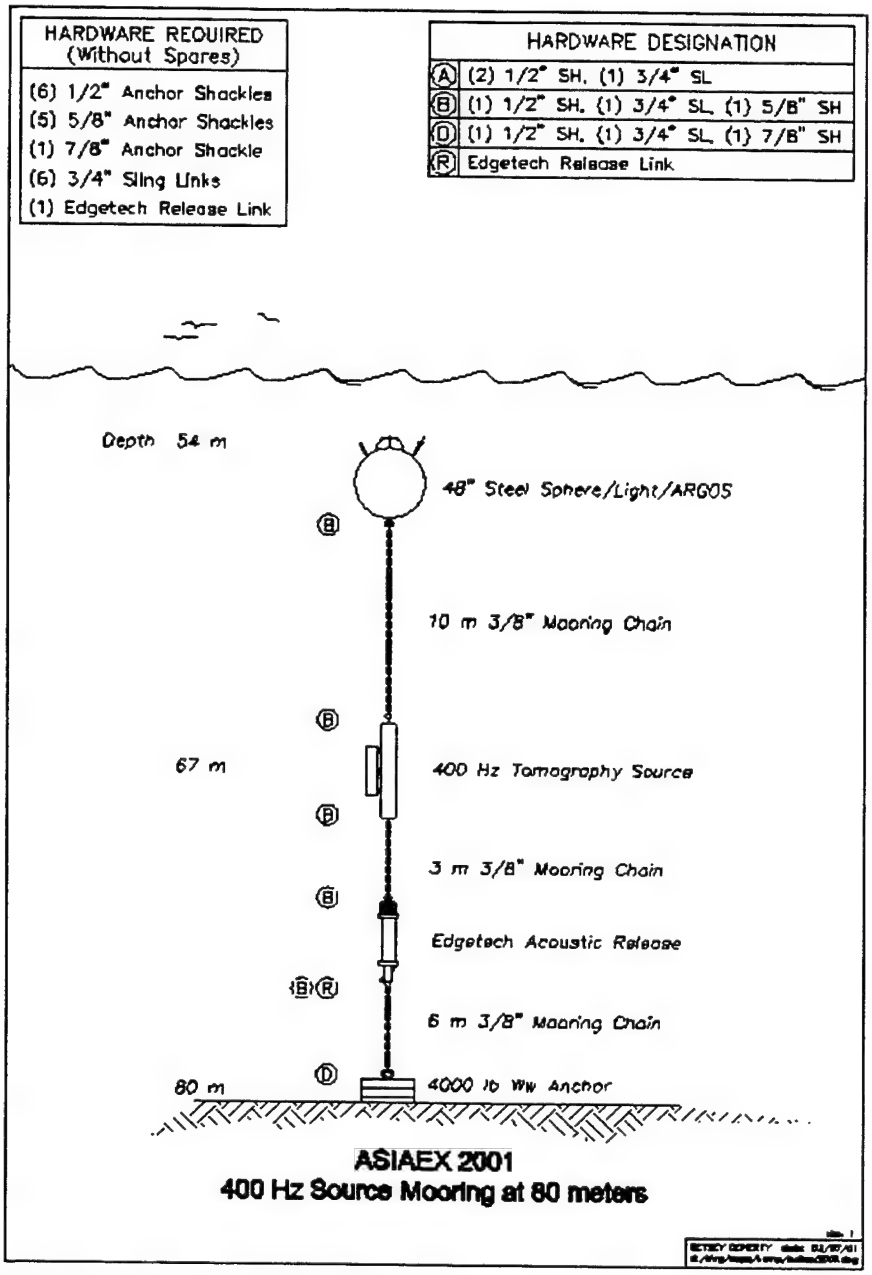

Figure 2-4: Mooring configuration for the 400 Hz sources. Both the deep and shallow sources had the same configuration. The shallow source was actually deployed at 112.7 m depth and the deep source was at 342.5 m water depth.

Table 2-2: 400 Hz Sources

Water Depth (Log)	112.7 m (shallow) 342.5 m (deep)
Depth, Center Of Source	99.7 m (shallow) 329.5 m (deep)
Distance to VLA	19889 m (shallow) 30847 m (deep)
Center Frequency (Hz)	400
Bandwidth (Hz) – Full 3 Db	100
Source Level	183 dB re 1 uPa @ 1m
Cycles Per Digit	4
Digits Per Sequence (Digit length)	511 (10 msec)
M-Sequence Length	5.11 seconds

Table 2-3: 400 Hz Sources, Transmission Schedule 1.

Start time (UTC)	Day 123 (May 3) 12:00:00
Transmission Times (minutes after the hour)	0, 30 (shallow) 15, 45 (deep)
M-Sequences Per Transmission	88
Total Transmission Length	449.68 seconds (~7.5 min)

Table 2-4: 400 Hz Sources Transmission Schedule 2.

Start time (UTC) .	Day 129 (May 9) 00:00:00
Transmission Times (Minutes after the hour)	00, 10, 20, 30, 40, 50 (shallow) 05, 15, 25, 35, 45, 55 (deep)
M-Sequences Per Transmission	23
Total Transmission Length	117.53 seconds (~2 min)

2.3.2 Physical Oceanography

ASAIEX featured the most complete set of physical oceanography data collected for a coherence study to date. Data to study the physical oceanography was collected using numerous environmental moorings (including thermistor strings and different combinations of temperature, pressure, and current meters). Additionally eleven point CTD casts were conducted during the acoustics deployments. These measurements and the picture of the oceanography they provide are discussed in section 2.5. The SeaSoar towed CTD measured the 3-D oceanography throughout the area, and satellite imagery taken during the experiment, gave a 2-D surface picture of both large scale and fine scale oceanography. The sensors used for these measurements are discussed in the following sections.

2.3.2.1 Thermistor Strings

Two thermistor strings (T-strings), each consisting of 11 sensors, were deployed during ASIAEX. One was deployed at the shallow source location and the other was deployed in somewhat deeper water (139 m) on the eastern side of the experimental area. The T-string moorings also had automatic point temperature sensors on the anchor and surface buoy, in an attempt to cover the entire water column. These moorings provide data needed to track the fluctuations in the thermocline due to internal waves and thus to track the propagation of the internal waves themselves. As the temperature is also the dominant determinate of the sound speed, the thermistor data enables the changes in the sound velocity profile to be tracked as well, which is critical to understanding the observed fluctuations in the acoustic field.

2.3.2.2 HLA/VLA Temperature and Pressure Sensors

One Starmon and five Seamon autonomous, point temperature loggers (T-pods), along with four SeaBird Electronics temperature/pressure sensors were attached to the VLA. The data provided by the temperature sensors allows for the tracking of internal

waves. However, since the shallowest temperature sensor was at 39.5 m, it is not always possible to determine the fluctuations of the upper thermocline and thus perfectly create a picture of the SVP at the receiver array. The pressure sensor data enable the tracking of the depth of the VLA as it moved due to currents. The pressure data are also useful for tracking tidal and storm surges, along with indications of increased surface wave activity.

2.3.2.3 Environmental Moorings

A cross shelf line of eight environmental moorings was deployed, spanning water depths of 792m to 71m (Figure 2-1). Four environmental moorings sampled the water column measuring temperature, pressure, salinity and current while the other four solely measured current using Acoustic Doppler Current Profilers (ADCPs). The line of moorings included the up slope propagation path of the 224 Hz and 400 Hz sources. Specifically, three environmental moorings and two ADCP moorings covered the up slope propagation path. The three environmental moorings were placed: at the deep sources, at the HLA/VLA positions, and along the propagation path. The two ADCP moorings were placed between the deep sources and the HLA/VLA, along the propagation path.

2.3.2.4 Low Cost Moorings (Locomoor)

An array of eighteen low cost moorings (dubbed "Locomoors") was deployed on the continental shelf in water depths of 75m to 109m. Eleven of the eighteen were recovered; the others were lost, probably due to fishing operations and failed acoustic releases. The moorings consisted of three sensors attached to a polyester rope and suspended between a 933-pound iron anchor and subsurface float module. The top sensor was a Seabird SBE39 temperature and pressure recorder. Below that were two Star-Oddi Starmon-mini temperature recorders. The sensor depths varied from 50m to 14m. The Locomoors provided an extended array of measurements of the nonlinear internal waves and internal wave packets. These data are used to estimate the wavelength, amplitude, speed and direction of the internal waves.

2.3.2.5 CTD

Eleven CTD (conductivity, temperature and depth) casts were performed during the acoustic array deployment cruise. The three casts of concern for this thesis were taken at the two source locations and the HLA/VLA location. The CTD data provide temperature and salinity profiles from the surface to quite near the bottom.

2.3.2.6 SeaSoar

The SeaSoar sled is essentially a towed CTD with wings that allow the tow-fish to sample the entire water column as it is "flown" between the surface and bottom at speeds of up to 8 knots. During ASIAEX the SeaSoar was towed by the Taiwanese research vessel *OR1*. The track of the SesSoar covers most of the experimental area and can be seen in Figure 2-1. The track crosses the shelf break as the SeaSor samples the environment on the shelf and much of the slope, down to a water depth of approximately 350 m. The SeaSoar was towed in the ASIAEX area from 29 April to 11 May 2001, when the *OR1* had to leave the area because of the passing Typhoon Cimaron.

2.4 Sensor Deployment Timelines

Timelines for the major acoustic support measurements are shown in Figure 2-5. The first timeline shows the deployment of the horizontal and vertical linear receiving arrays. The next five timelines represent the moored acoustic sources. The East 400 Hz source and the 300 Hz and 500 Hz Linear Frequency Modulated sources were deployed on the continental shelf, while the 224 Hz source and South 400 Hz source were deployed on the continental slope in deeper water. The J-15-3 source is a towed source that spans a frequency band of 50-600 Hz. The light bulb drops occurred on 5 and 15 May 2001. Ordinary light bulbs were weighted and dropped to produce a broadband pulse upon implosion, which is then used for HLA sensor location. A thermistor string was deployed next to the shallow sources to give the temperature profiles needed for sound speed calculations. A thermistor string was also deployed on the east side of the area in

"deeper" 139 m of water. The time line for the SeaSoar indicates the days when the system was towed in the experimental area over the tracks shown in Figure 2-1. Additional environmental moorings (the last timeline) were deployed prior to 28, April 2001.

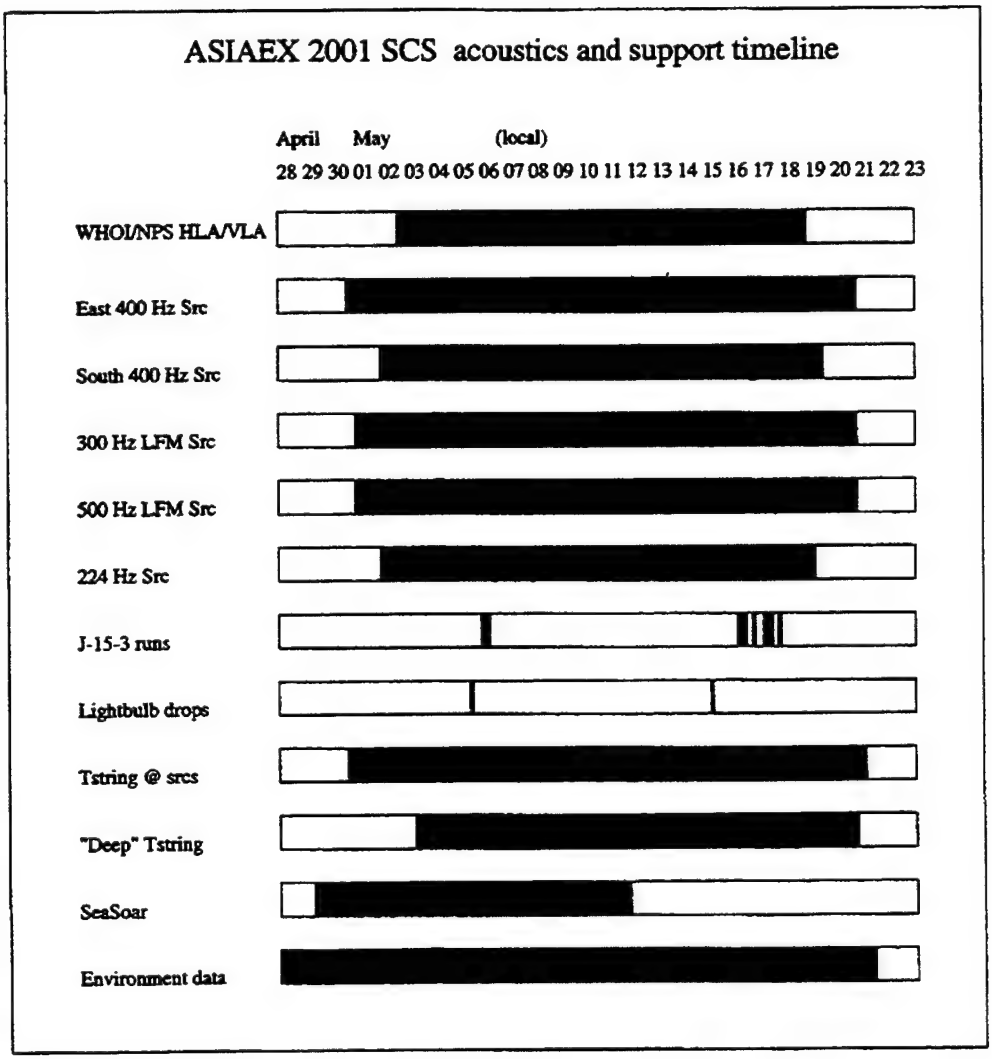

Figure 2-5: Timelines for the ASIAEX 2001 SCS major acoustics and acoustics support equipment deployments.

2.5 Environmental Description

2.5.1 Weather Conditions

During the SCS experiment the weather was generally hot and humid with little wind and no sea swells. The exception to this occurred when increased wind and swells were created by a typhoon that passed to the east of the moorings on 11 May. Because of the refraction of the warm surface layer and the relatively calm seas (especially for 5 May, the day of the coherence calculations), the surface effect is small and will not be discussed further.

2.5.2 Physical Oceanography

Based on prior experience, the physical oceanography of the area was expected to display both large-scale and fine-scale variability. However, the large-scale variability was minimal during the 2001 experiment, as evidenced by the CTD records made during the deployment of the acoustic moorings from the FR-1.

The temperature and salinity profiles are generally constant throughout the experimental area, with the values in shallow water being the same as the top of the deeper water column. Figure 2-6 shows CTD casts 1, 2 and 8 located at the shallow sources, deep sources and HLA/VLA respectively. These temperature plots show a shallow mixed surface layer of a relatively constant temperature, extending to a depth of approximately 25 m. The temperature then uniformly decreases below the surface layer. Figure 2-7 displays the salinity values for the same CTD casts. The plots of salinity show a mixed surface layer with fresher water overlying the deeper water. The salinity becomes constant at depths greater than 50 m.

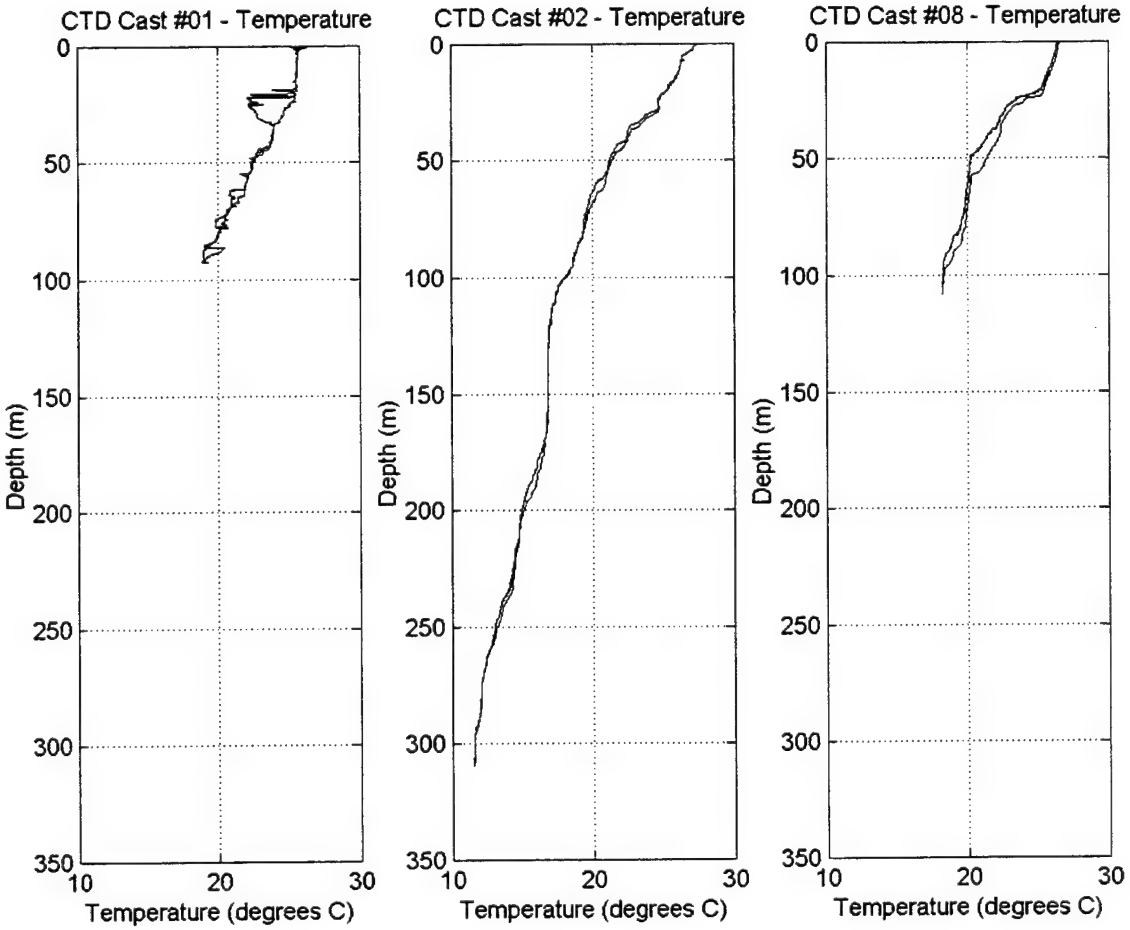

Figure 2-6: CTD temperature from: cast 1 near the shallow sources, cast 2 near the deep sources, and cast 8 near the HLA/VLA.

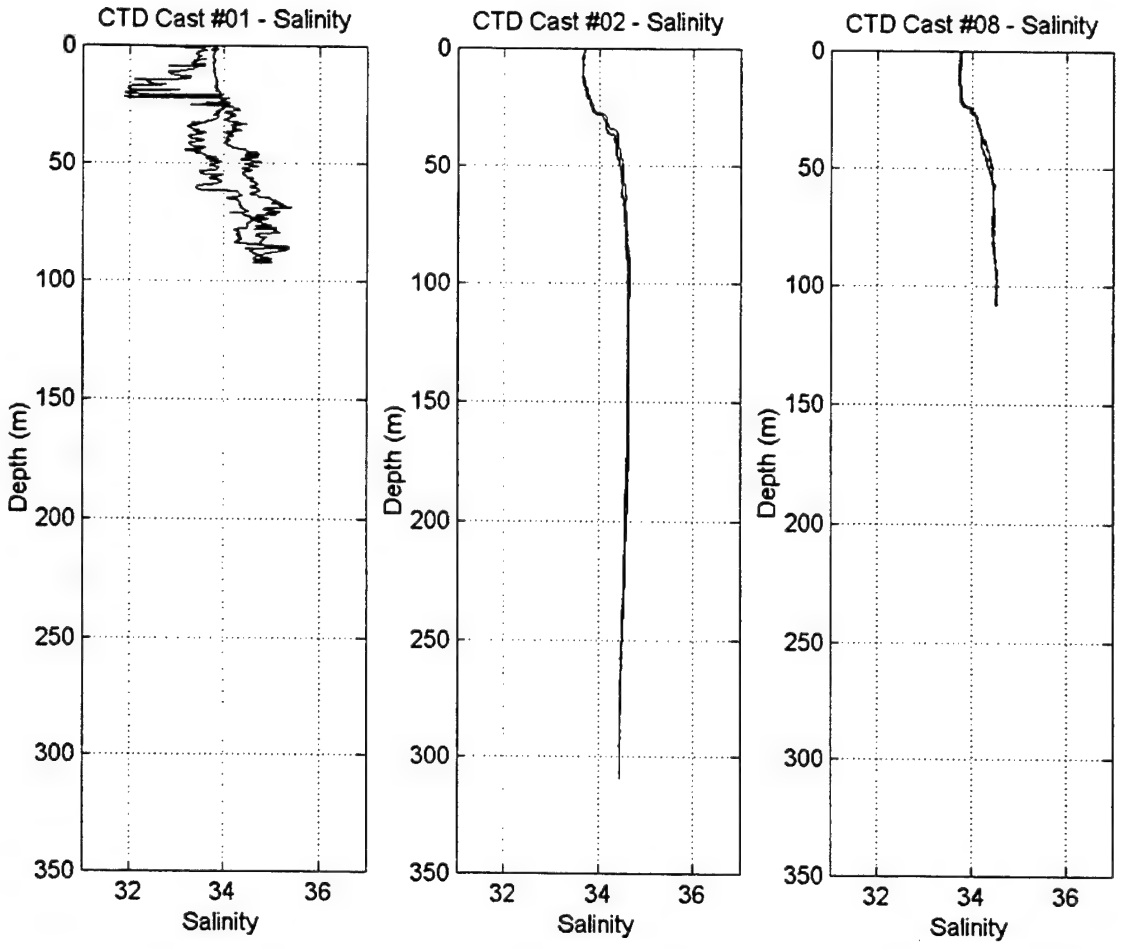

Figure 2-7: CTD salinity from: cast 1 (near the shallow acoustic sources), cast 2 (near the deep acoustic sources) and cast 8 (near the VLA/HLA).

The physical oceanography of the area was dominated by large internal waves. Figures 2-8 and 2-9 are the temperatures recorded by the sensors on the VLA, showing that the internal waves reached depths of over 80 m in the 120 m water depth. These large internal waves are believed to be generated on the Luzon Ridge and then propagate in the general direction of 282 degrees across the basin and onto the continental shelf (Steve Ramp, private communication). There are also some smaller internal waves observed, which are believed to be locally generated.

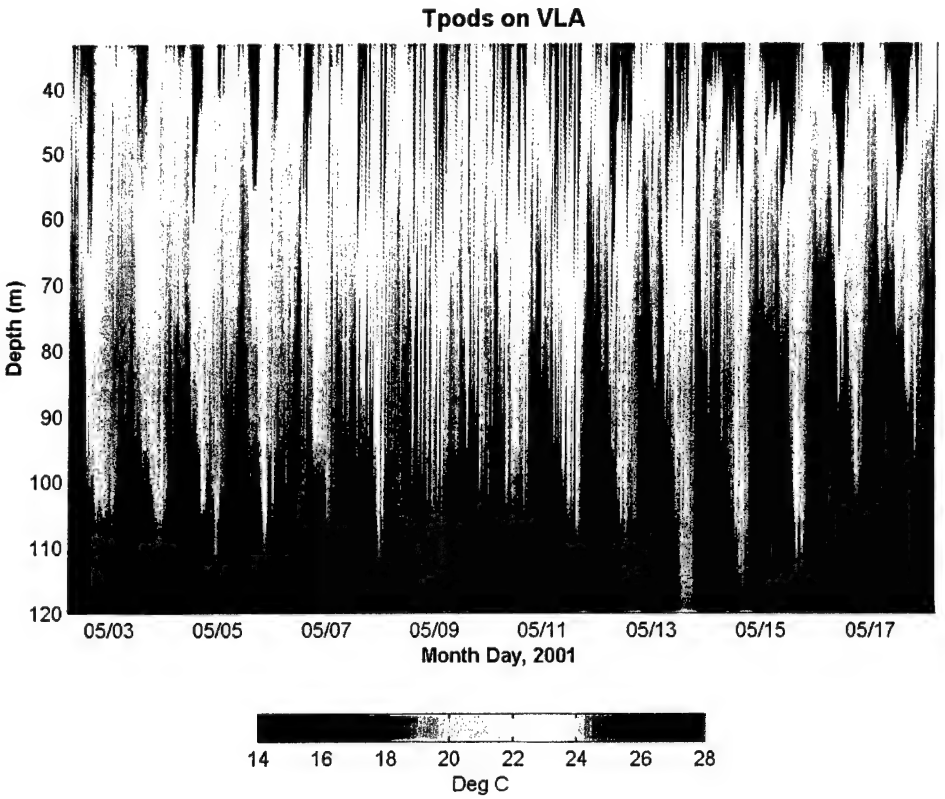

Figure 2-8: Temperature recorded by sensors on the VLA for the entire ASIAEX SCS deployment.

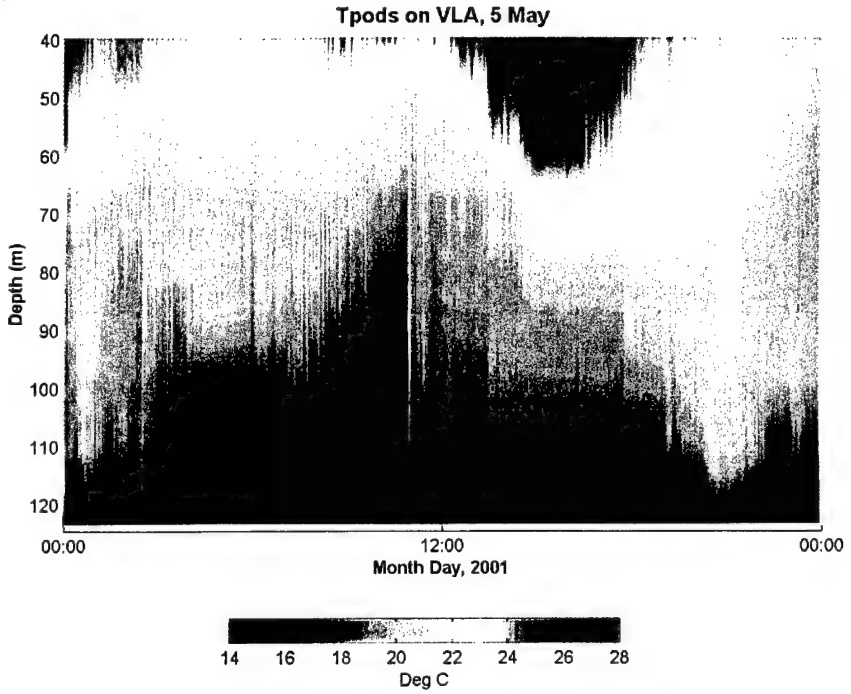

Figure 2-9: Temperatures recorded by sensors on the VLA for 5 May.

2.5.3 Acoustic

During the SCS experiment there was a predominantly downward refracting sound velocity profile (Figure 2-10). The profiles show a nearly constant sound speed shallow surface layer, at depth less than 25 m, followed by a decrease in sound speed with depth. The profiles show little variation throughout the area, i.e., the profiles measured on the shelf in shallow water have the same shape as the top of the deep-water column. The largest variability in the sound speed is caused by internal waves; however, the general shape of the profile remains relatively constant.

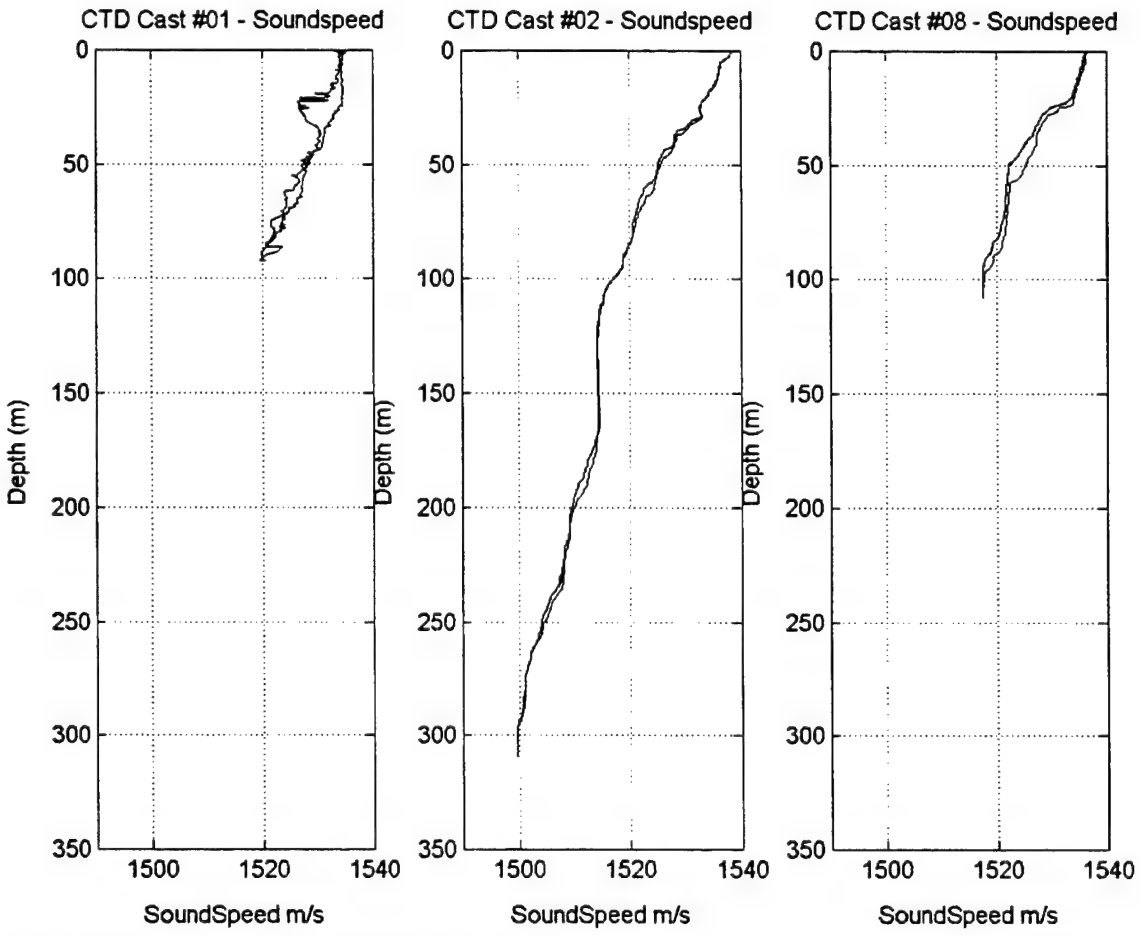

Figure 2-10: Sound velocity calculated from the CTD casts. Cast 1 was near the shallow sources, cast 2 near the deep sources and cast 8 near the VLA/HLA.

2.5.4 Geology and Geophisics

The bathymetry of the ASIAEX SCS experimental area was determined by interpolating data obtained by the three research vessels used in ASIAEX 2001, along with a track completed in September 2000 by the OR3. These tracks are shown by the gray lines in Figure 2-11. The track run by OR3 in September 2000 densely sampled the area along headings of approximately 165 and 345 degrees. The experimental topography consists of a relatively flat shelf to the north, with a steep transition from 140 m to 220 m running through the middle of the area. The transition is more gradual in the center of the region near the shallow sources. There is a steady downward slope between 220 m and 310 m with another short steep transition to approximately 340 m near the deep sources.

A high-resolution chirp sonar system was used to provide detailed stratigraphy and bathymetry information both for the along shelf and cross shelf propagation paths. Figure 2-12 is the raw chirp sonar data for the along shelf propagation path. The HLA/VLA were located on the left side of the figure. Unfortunately, the right side of the figure ends just prior to the location of the 300, 400 and 500 Hz sources. The bottom is mostly flat with a relatively steep, small canyon located next to the sources. Coming out of the canyon to the right the bottom continues to rise to the ~ 113 m water depth where the sources were deployed. Figure 2-13 shows the raw chirp sonar data for the up slope propagation path. The two steep areas, one at the edge of the shelf and the other close to the sources, can be easily seen in the figure.

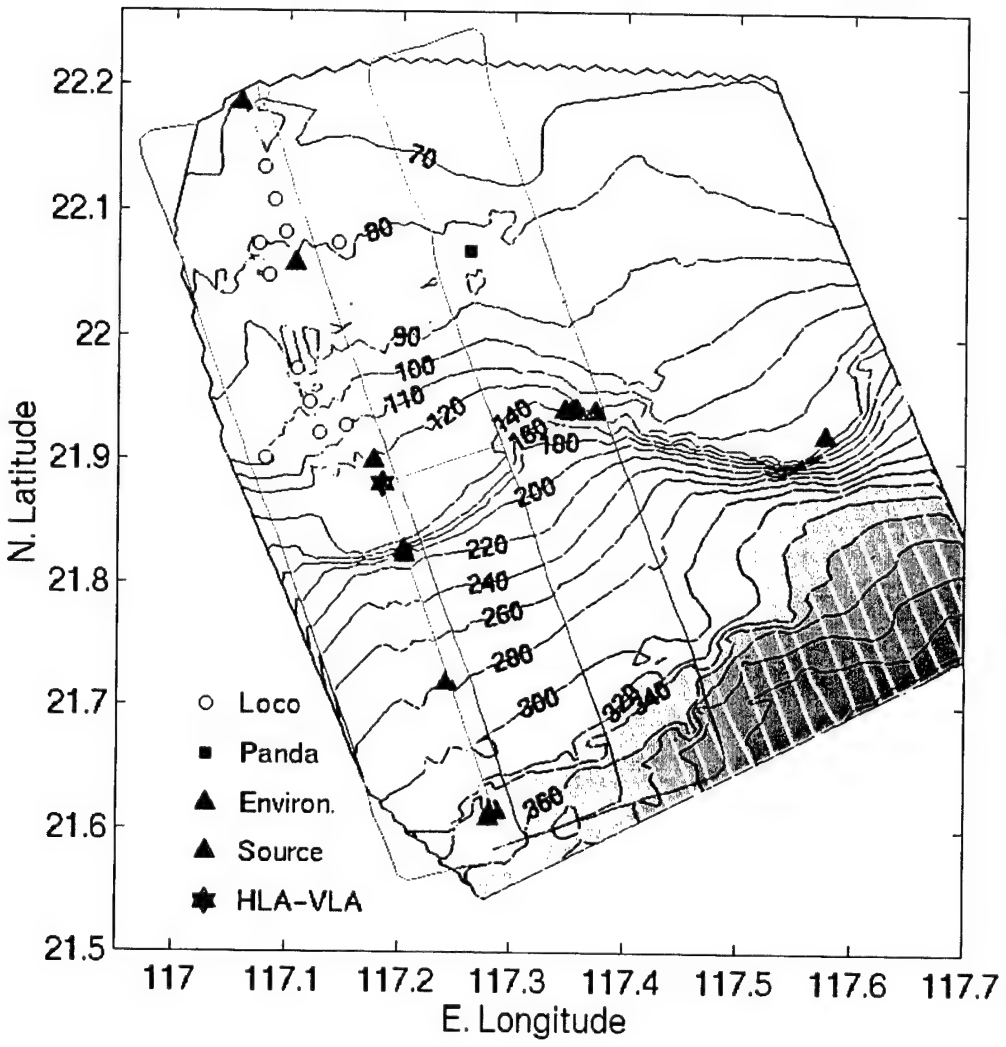

Figure 2-11: Bottom contours for the ASIAEX SCS experiment. The gray lines are the tracks of the research vessels used to interpolate the bottom contours.

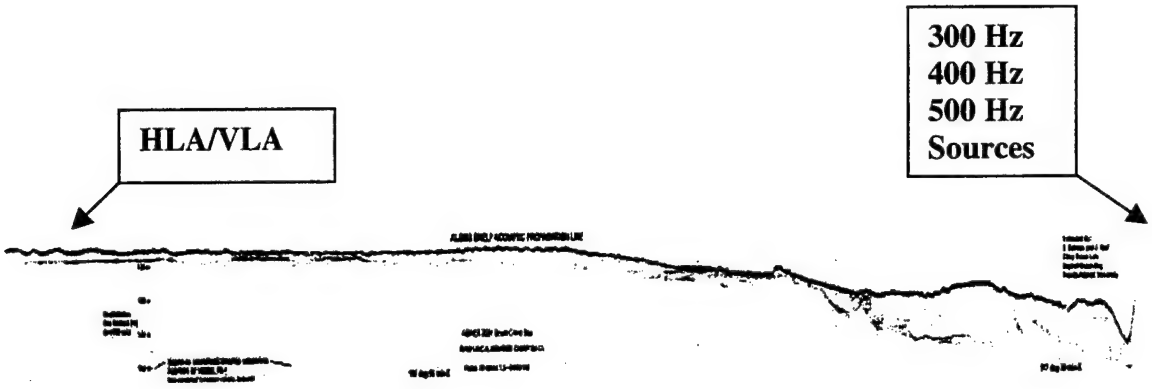

Figure 2-12: Raw chirp sonar data for the along shelf propagation path. The HLA/VLA were located on the left side of the figure and the 300, 400 and 500 Hz sources located just off the figure to the right.

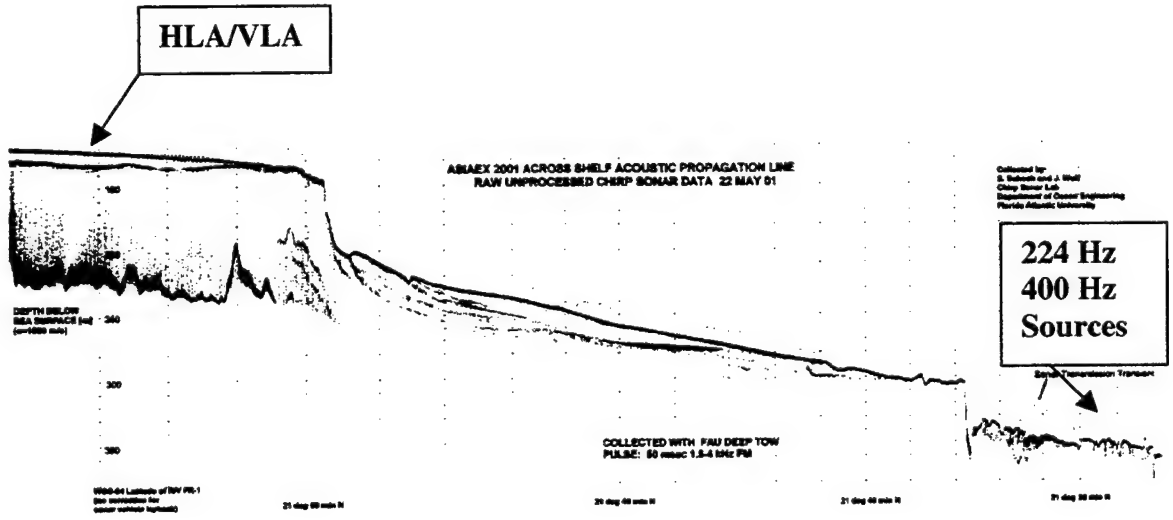

Figure 2-13: Raw chirp sonar data for the up slope propagation path. The HLA/VLA were located on the shelf; the 224 and 400 Hz sources were located in the deeper water on the right side of the figure.

3 HLA Sensor Localization

3.1 Horizontal Linear Array Geometry

To facilitate accurate analysis of the acoustic signals, and in particular to enable the computation of array coherence, the exact geometry of the Horizontal Linear Array (HLA) is necessary. In the ASIAEX SCS experiment, the actual geometry of the HLA was partially unknown, as the array was not fully extended. There was almost 100 m of slack between the sled and the tail anchor. Moreover, the HLA was not heavily weighted, and so the strong bottom current caused the array to move during the experiment. Thus, there is a need to localize the array elements in a time-dependent fashion.

This chapter contains the analysis used to track the movement of the HLA elements and thereby obtain the array geometry as it changed over time. An acoustic long baseline (LBL) array element navigation system was used in hope of being able to track three sensors of the HLA. The LBL system was supplemented by dropping light bulbs from the research ships on 5 and 15 May; this provided low-cost but very effective implosive source signals to assist with location.

The LBL system provided information on the location of three of the HLA sensors for the full duration of the HLA deployment. The daily movement of the HLA and the shifts in the propagation path (multipath "hopping") of the LBL signals made analyzing this data somewhat difficult. However, despite these difficulties, the LBL did provide good information on the general movement of the array, and this chapter will try to quantify the quality of that information.

The broadband impulses produced from the imploding light bulbs dropped on 5 and 15 May provided perhaps the best data for sensor localization. In contrast to the LBL, this method provided a snapshot of the positions for each sensor in the HLA. It

will be seen that there was a good correlation between the positions obtained from the light bulbs and those obtained from the LBL system.

It should also be noted that the broadband low frequency moored sources (224, 300, 400 and 500 Hz) deployed in ASIAEX could also be used as navigation beacons. This chapter will cover the first step of this analysis in section 3.4, where the difference in arrival times at each sensor of the HLA for the deep 400 Hz source transmissions are compared to the time difference calculated using the light bulb determined sensor locations. The actual sensor localization using these low frequency sources is left for future work.

3.2 Acoustic Long Baseline (LBL) Array Element Navigation System

To facilitate the tracking of the HLA and the Vertical Linear Array (VLA) an acoustic long baseline (LBL) array element navigation system was used. Four channels on the VLA and three channels on the HLA were used to record arrival times of signals received from an interrogator OIS transponder, and two Benthos transponder balls. The seven LBL channels used for the measurements correspond to the following array channels:

M0 = CH 0	top of VLA
M1 = CH 6	22.5m from CH 0
M2 = CH 10	42.25m from CH 0
M3 = CH 13	63.75m from CH 0
M4 = CH 16	nominally 467m from sled
M5 = CH 26	nominally 317m from sled
M6 = CH 36	nominally 167m from sled

Figure 3-1 shows the geometry of the LBL system. The interrogator transponder was located on the tail anchor for the HLA, at the end of a 100 m wire rope extension beyond the last channel of the HLA. One Benthos transponder ball was placed to the north of the VLA and the other to the south. The interrogator would then transmit an

11.5 kHz signal every 10 minutes starting on the hour. After receiving the interrogator signal, the north transponder ball replied at 12.0 kHz and the south ball replied at 11.0 kHz. The time between the interrogator's transmission and the detection of the three frequencies by each of the LBL channels was recorded and used to determine the radial distance between the transponders and the LBL channels. The LBL channel positions in x-y coordinates were determined by using these distances in a standard least squares calculation.

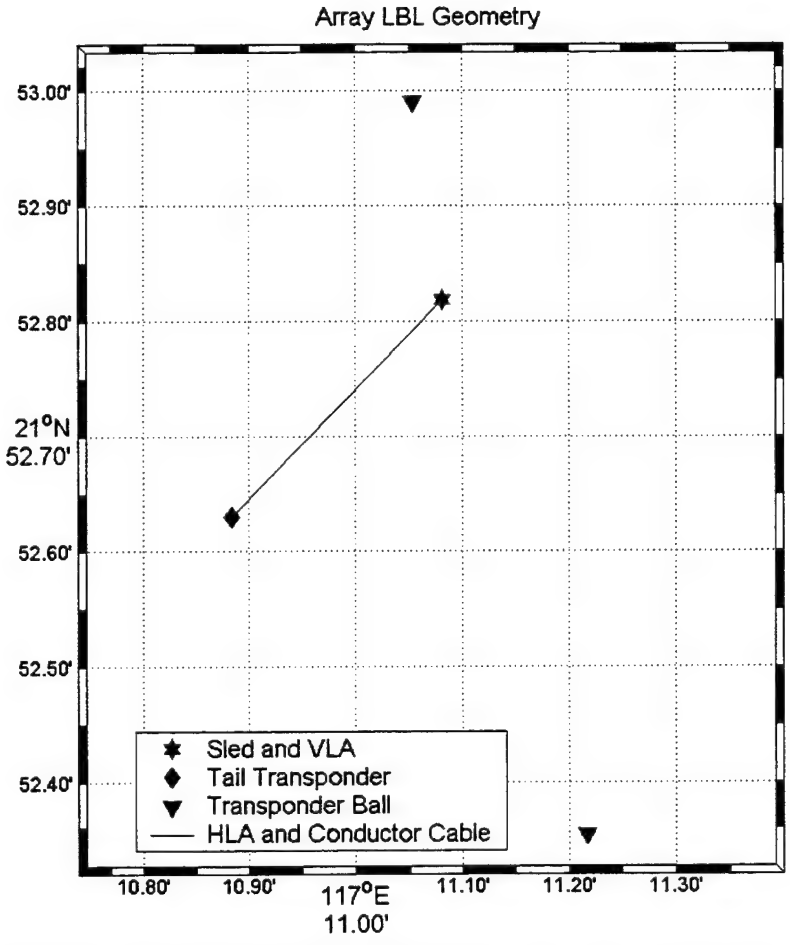

Figure 3-1: Location of the LBL system components. The tail transponder transmitted an 11.5 kHz interrogation signal. After the transponder balls received the interrogation, the north ball replied at 12.0 kHz and the south ball replied at 11.0 kHz. The time difference between the interrogation transmission and the reception of the three frequencies by the four LBL channels on the VLA and three LBL channels on the HLA was recorded to obtain positions.

3.2.1 Ranges from Transponders to LBL Channels

This section will discuss the determination of sound speeds and propagation paths used to calculate the ranges between the transponders and the LBL channels. In order to convert time differences recorded by the LBL system into accurate distances, a good estimate of the sound speed field is needed. Just as important is an accurate determination of whether the propagation is a direct path or a surface bounce path.

3.2.1.1 Sound Speed

The general shape of the sound velocity profile (SVP) near the VLA/HLA can be seen in Figure 3-2, which is a plot of the sound speed calculated from the CTD cast taken near the receiving arrays. The sound velocity profiles for the ASIAEX SCS experimental

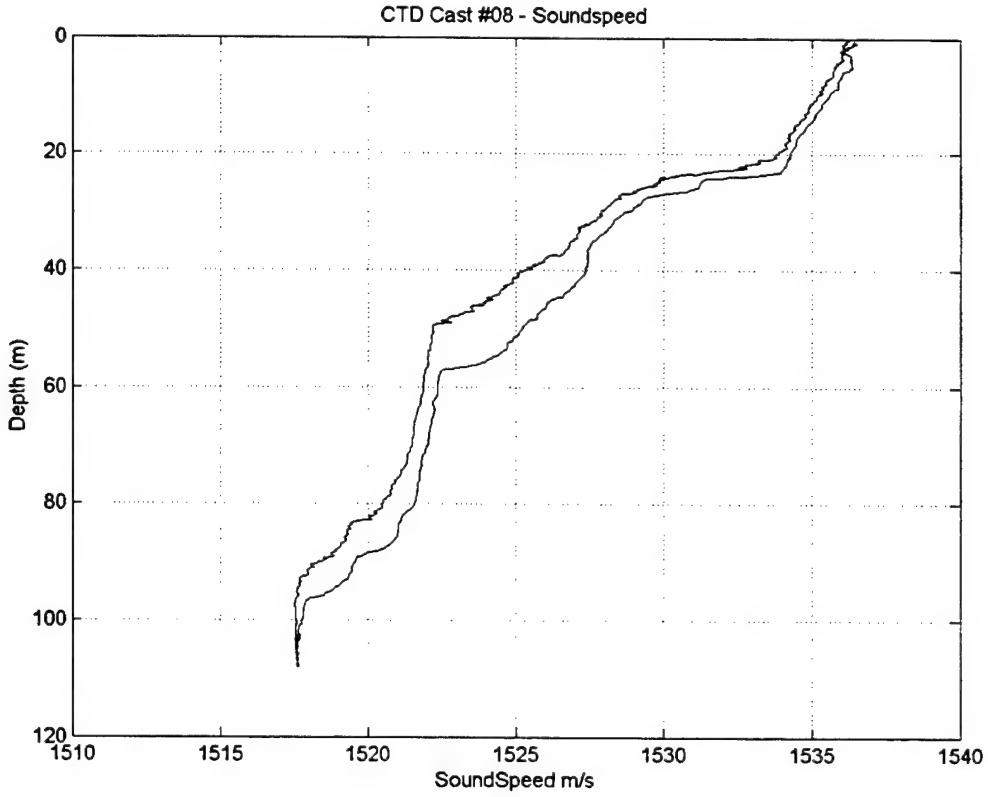

Figure 3-2: Sound velocity profile calculated from CTD Cast #08 taken near the VLA/HLA.

area are discussed in more detail in section 2.5.3. The profiles are downward refracting with little spatial variability. The largest disturbance to the basic SVP is the internal waves that cross the area.

The change in sound speed caused by the internal waves was accounted for by using the temperature and pressure recorded every two minutes by the four SBE T/P probes located on the VLA (the probes were located at 78 m, 57.3 m, 37.1 m, and 16.9 m above the bottom). This data was used to calculate a depth averaged sound speed. For M0 at 82 m above the bottom the sound speed calculated from all four SBE probes was averaged. For M1 at 59.5m above the bottom the lower three probes were used, for M2 at 40.5 m above the bottom the lower two were used and for M3, the HLA channels and the interrogator to transponder propagation times, the deepest probe was used.

These depth averaged sound speeds proved to be adequate for the short ranges and the downward refracting environment. With a maximum sound speed difference of 20 m/sec and travel times between 0.3 and 1.1 seconds, the error in range for direct path propagation should be less than 5 m and for surface bounce the range errors should be less than 10 m. These small possible errors in ranges from the three transponders would cause a negligible effect in the accuracy of the determination of the sensor positions.

3.2.1.2 Initial Slant Ranges

Using the corrected sound speeds and the time differences between transmission and reception, the propagation lengths (or "slant ranges") were calculated from each of the LBL transponders to each of the LBL channels. The original data showed much spiky noise, so the curves were cleaned by replacing any spikes greater than 3 standard deviations away from a running mean with that mean. Figure 3-3 is a representative example of the ranges seen from the transponders to the HLA. The ranges have large jumps resulting from array movement and shifts between direct and surface bounce propagation paths. Since the HLA was free to move between the anchored ends, it was hard to determine what might be movement and what was a shift in the signal

propagation path. Therefore, the data for the VLA channels with a known position were analyzed first, hoping this would aid understanding and thus reduce ambiguity.

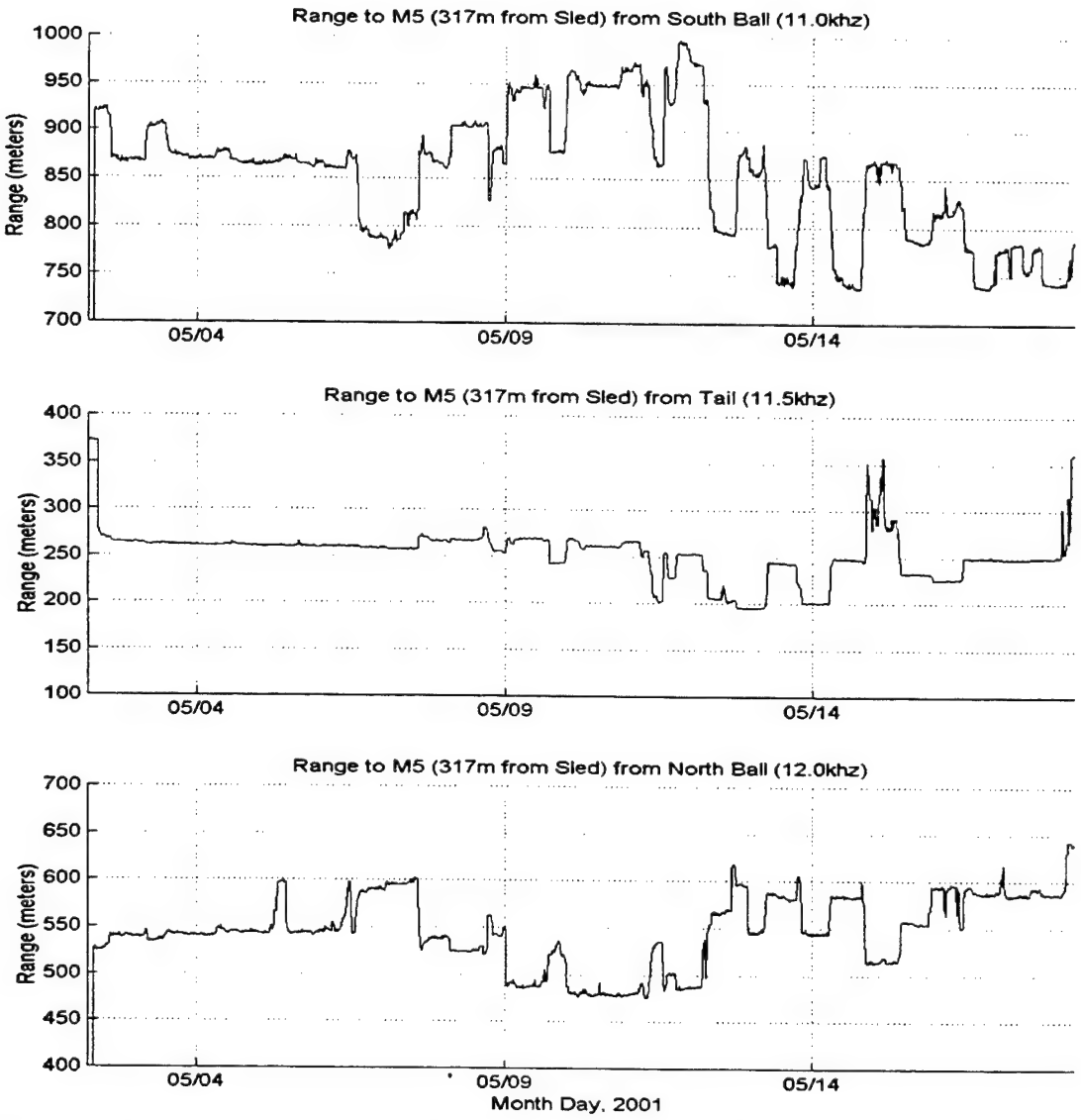

Figure 3-3: Initial calculated ranges between the transponders and LBL channel M5 (CH26 on the HLA). The calculation used a depth averaged sound speed and the recorded time difference between the interrogation transmission and the reception of each of the three frequencies. This figure is representative of the results seen at each of the three HLA LBL channels. The jumps in range are due to array movement as well as propagation shifts between direct path and surface bounce.

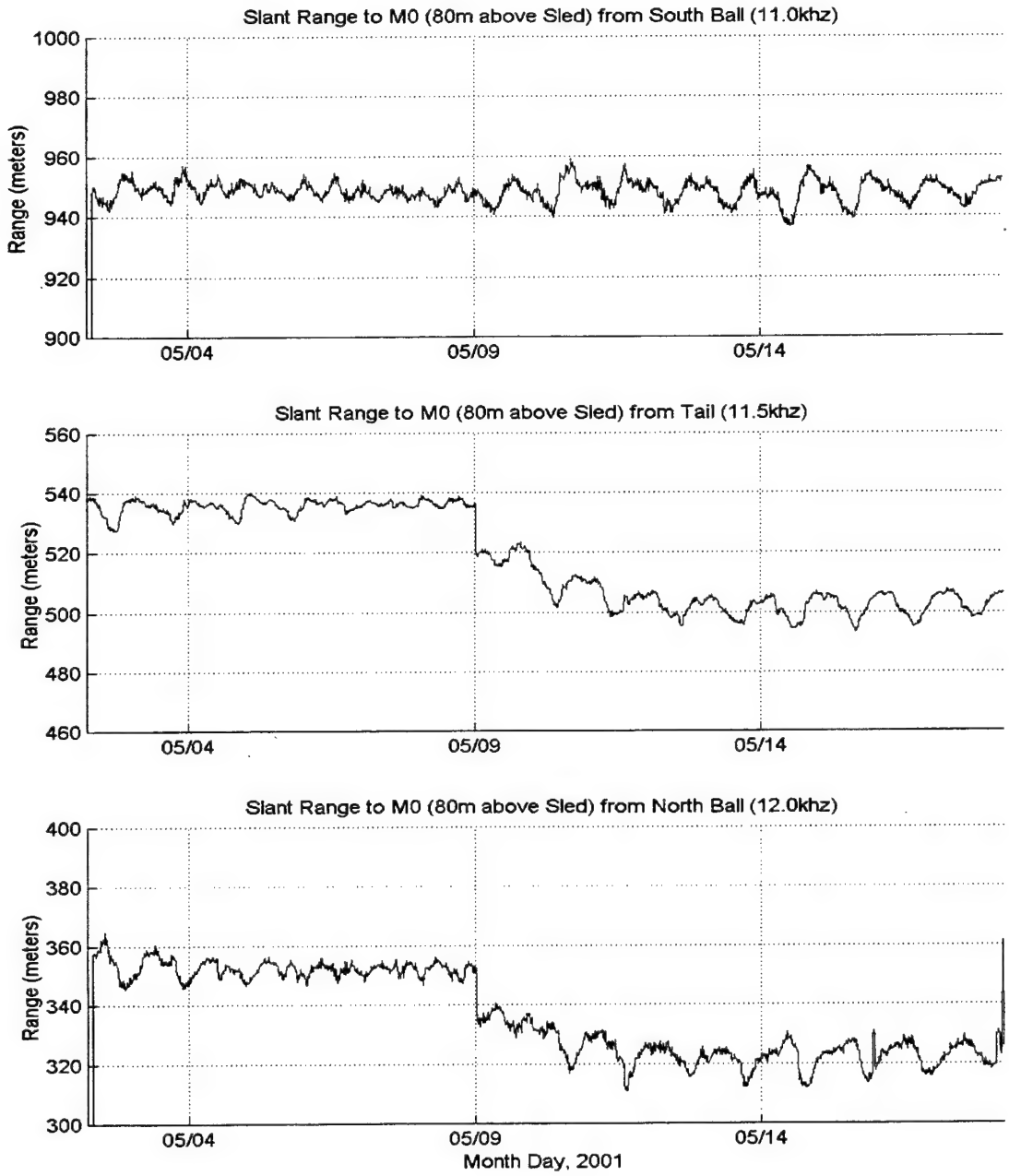

Figure 3-4: Slant Ranges from the transponders to LBL channel M0 located at the top of the VLA. These data are representative for all four VLA LBL channels. The oscillations are produced by the tidal cycle. The estimates of the ranges from the south ball to the VLA LBL channels were determined to be too long due to a surface bounce propagation path. Also a jump can be seen in the ranges at 0030 on 9 May for the tail and north ball to the VLA. This jump was caused by a change from a surface bounce propagation path (between the tail and the VLA and the tail and the north ball) to direct path propagation.

Figure 3-4 shows the slant ranges to LBL channel M0 at the top of the VLA and is representative of the other channels on the VLA. The general oscillations in the curves are expected as the VLA moves in a watch circle with the tidal currents (M0, being at the top of the array, will have the most movement due to tidal currents and therefore the largest cyclical changes in range). There are, however, some irregularities. First, on 9 May between 0020 and 0030, there is a sudden drop in the range from the tail and the north ball to all four VLA LBL channels. This drop is also seen in the data for the north ball to the HLA LBL channels. Using simple geometry, it was determined that prior to 9 May the ranges from the north ball and tail to the VLA were in fact too long, and they appear more accurate after the jump. Second, while there are no sudden changes in the ranges from the south ball to the VLA, those ranges are also too long. These over-estimates in range were too large to be accounted for by an error in the sound velocity profile, which implied that either the LBL elements moved or there was a change in the propagation path. These possibilities were then investigated.

3.2.1.3 Movement of LBL System Components

Analyses of the slant ranges for the LBL system were first calculated using the positions obtained by the deployment survey. Since it is not unusual for fishing nets to snag oceanographic equipment, especially in this area, the possibility of the before-mentioned range discrepancies being caused by a movement of LBL system components after the deployment survey was investigated.

The surveys are accomplished by taking the time difference between the transmission of an interrogator pulse from the research vessel and the reception of the answer pulse sent by the desired component. This is done at different positions around the component and the travel times are used to calculate range arcs from the ship to the component. These range arcs are used in a least squares fit to give the position. The accuracy of the survey is dependent on the accuracy of the time measurement and can be estimated by how well the range arcs cross at a specific point.

A recovery survey had also been conducted, so a comparison of the before-and-after positions from the two surveys was performed. The distances between the LBL system positions determined by the two surveys were 9.85 m for the sled, 5.95 m for the tail interrogator, 9.76 m for the south ball and 19.41 m for the north ball. While the change of 19.41 m for the north ball seems large enough to be significant, the recovery survey data did not provide as reliable an accuracy, certainly not as useful as the deployment survey. This was indicated by the fact that the range arcs for the recovery survey did not provide as effective a fit. All differences were then determined to be within the accuracy of the surveys.

Additionally, for a jump in the ranges calculated from the tail to the VLA to be caused by movement, either the tail or the sled/VLA would have to move. Since the interrogator is located on the tail, a movement in either the tail or the sled would have been seen in the ranges for all three transponders. Since the jump was only seen in the data from the tail and the north ball, it is unlikely that movement of the LBL system components caused the discrepancies in range.

3.2.1.4 Propagation Paths

Since the LBL system uses high frequency transmissions at short ranges, it is appropriate to use a ray code to model the propagation. For an accurate ray path calculation, a sound velocity profile (SVP) is needed. Minimum and Maximum sound velocity profile were used. The maximum SVP was determined by using the temperature data recorded by the T-pods on the VLA to find times at which high temperature dominated the water column. The SVP was calculated for these times and the one with the highest sound speeds was chosen. The minimum SVP was determined in the same way; however, it was found during the times that colder water dominated the water column. With these profiles, the ray code determined the ray lengths and propagation times of the different paths to each of the VLA LBL channels. Using this information, it was concluded that the path from the tail to the south ball was surface bounce the entire time, whereas the path from the tail to the north ball and the tail to the VLA channels

shifted from surface bounce to direct path on 9 May. The propagation shift accounts well for the sudden change in range that is seen on 9 May.

Next, the geometric surface bounce corrections for the tail to the transponder balls was applied to the HLA ranges, and positions of the LBL channels were calculated using a least squares fit. Some of the position estimates exceeded the maximum possible ranges to the sled or the tail, indicating there were additional propagation shifts between the transponders and the HLA channels. Returning to the ray code, the ray lengths and propagation times for the signals traveling from the transponders to the HLA LBL channels were determined. Using distances between the HLA LBL channels, distances between the LBL channels and the sled and tail, and examining the three "slant" range curves for corresponding movement, many of the propagation shifts were able to be determined.

3.2.2 HLA LBL Channel Positions

The differences in ray lengths due to the shift in propagation between direct and surface bounce paths was then applied to the code, which calculated the ranges from transponder to LBL channel. The correction values are shown in Table 3-1. The corrected ranges from transponders to M5 are shown in Figure 3-5.

3.2.3 Summary Array Motion and LBL Error Estimates

Comparing Figure 3-5 and Figure 3-3,after compensating for surface bounce propagation paths, it is evident that the overall shape of the curve does not change. However, the size of some of the peaks have been reduced. While this process is not infallible, it certainly does provide more accurate data to be used in the least squares calculation.

Figure 3-6 shows a plot of the positions of the LBL channels using these corrected ranges. While there likely are still uncorrected propagation shifts, this method does give a good indication of the general array position and geometry. As is seen in the figure, almost all of the

positions fall within the maximum range arcs to the sled and tail anchors. The lengths between the LBL channels also checked satisfactorily.

Table 3-1: Corrections applied to ranges between transponders and LBL channels to compensate for changes between direct and surface bounce propagation paths.

Surface Bounce Propagation Path	Correction	Date and Time
Tail to north ball	-38m	Start to 9 May 0025
Tail to south ball	-36m	Entire Time
M4		
North ball to M4	-44m	10 May 2100-10 May 2320
North ball to M4	-44m	12 May 1800-12 May 2340
North ball to M4	-44m	13 May 0330-13 May 0540
Tail to M4 correction	-13m	Entire Time
South ball to M4	-37m	10 May 0000–12 May 0750
South ball to M4	-37m	12 May 1650-13 May 0540
M5		
North ball to M5	-54m	05 May 0650-05 May 1045
North ball to M5	-54m	06 May 0930-06 May 1200
North ball to M5	-54m	12 May 1600-12 May 2300
North ball to M5	-54m	13 May 1830-13 May 1930
North ball to M5	-54m	15 May 2030-16 May 0900
Tail to M5 correction	-10m	Entire Time
Tail to M5 correction	Set range to 255m	14 May 2000-15 May 0900
South ball to M5 correction	-4m	Entire Time
South ball to M5	-35m	11 May 1350-12 May 0700
South ball to M5	-35m	16 May 2100-17 May 1600
M6		
North ball to M6	-70m	12 May 1840-12 May 2315
North ball to M6	-70m	13 May 1700-13 May 2200
North ball to M6	-70m	14 May 1900-15 May 0845
North ball to M6	-70m	15 May 2100-16 May 0945
North ball to M6	-70m	17 May 0540-17 May 0755
Tail to M6 correction	-15m	Entire Time
Tail to M6 correction	Set range to 350m	12 May 1300-12 May 1840
Tail to M6 correction	Set range to 380m	13 May 1500-13 May 1930
Tail to M6 correction	Set range to 360m	14 May 2100-15 May 0415
South ball to M6	-69m	09 May 0025-12 May 0600

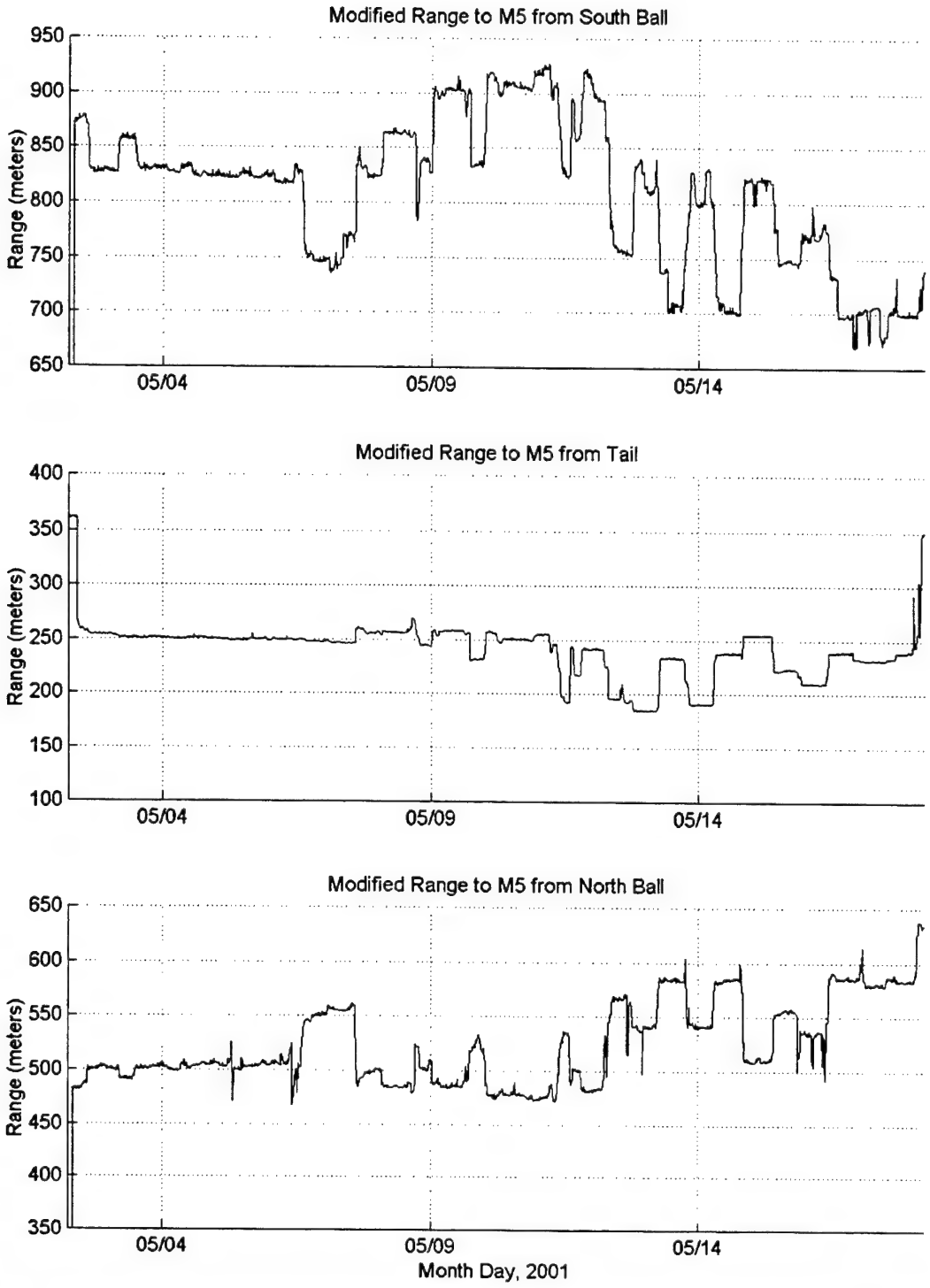

Figure 3-5: Ranges from transponders to LBL channel M5 using the correction in Table 3-1 to correct for changes between direct and surface bounce propagation.

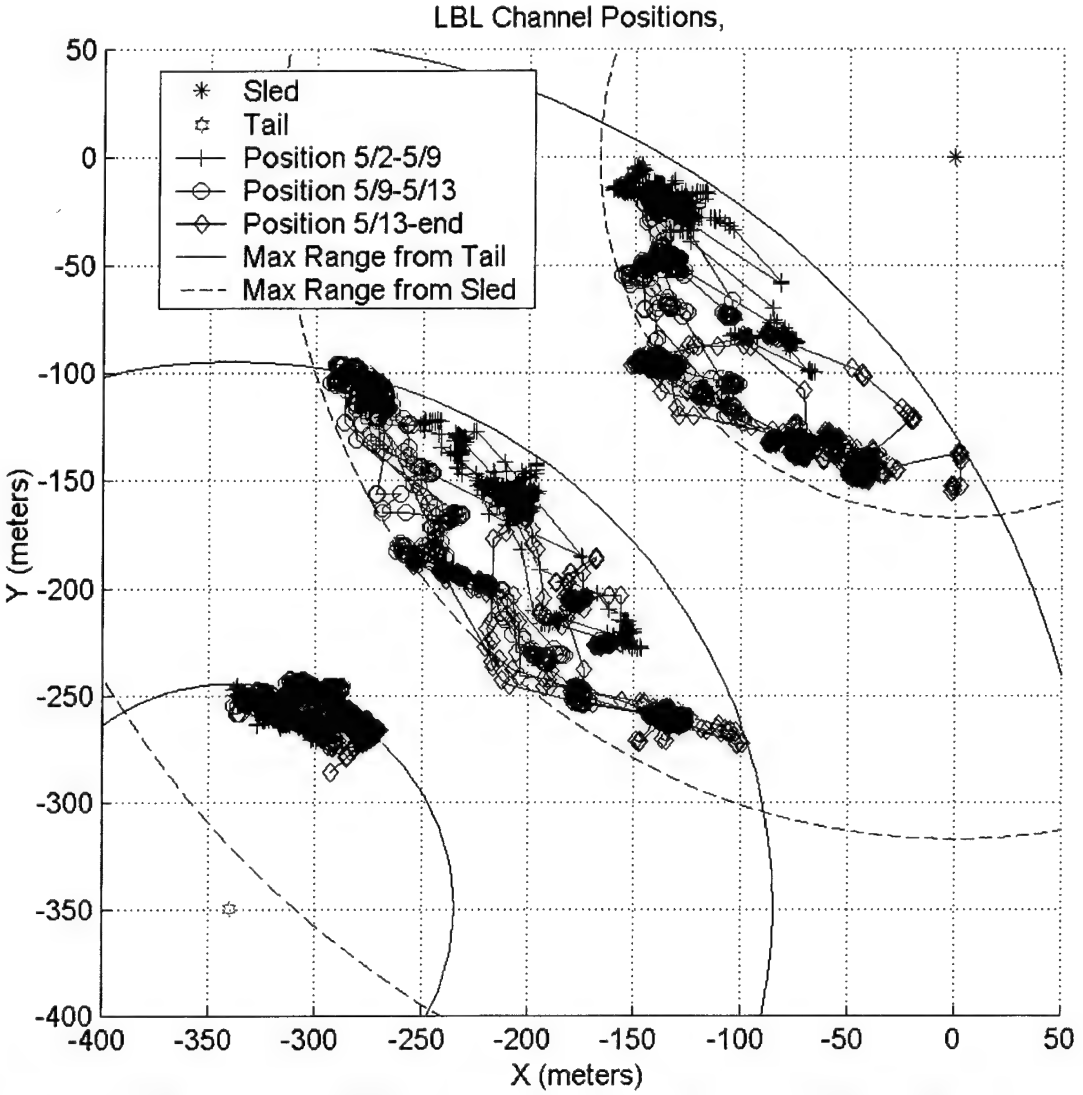

Figure 3-6: Positions of the LBL HLA channels using ranges corrected for surface bounce propagation paths listed in Table 2-1. The positions provide the general movement of the array throughout the experiment.

While the absolute position error may be rather large, this system does give good general array geometry. When there are possible uncorrelated propagation path shifts, the absolute accuracy of this data alone for exact LBL sensor location is probably no better than plus or minus 100 m. However, when a position is confirmed by other sources, verifying the correct propagation path, the absolute accuracy will be on the order of 30 m or better. Additionally, since the distance between the LBL channels has been

checked, the error for the relative distance between them should be on the order of 20 m or less (again, if the proper propagation path is confirmed). For the frequencies used in ASIAEX this gives possible absolute position errors of 30 times the wavelength to less than a wavelength, depending on the correct determination of the propagation path. These absolute position errors should be maximum errors and, due to the physical constraints in the HLA, the relative distance between each sensor should see smaller errors. In fact, the relative errors may be small enough to attempt beam forming the array, but that is left for future work.

Perhaps the most valuable information gained from the LBL system is the general motion of the array and a confirmation that the array was moving throughout the experiment. Since the wire cable connecting the end of the HLA with the tail sled weighed more than the HLA, and ch16 was closer to an anchor (tail anchor) than the other LBL channels, it moved the least. As expected, the middle of the array showed the largest movement.

Better accuracy could be obtained by further analysis of the data. However, this is left for future work. Nevertheless, these results will be compared to other methods in the thesis, to further demonstrate the accuracy of the results obtained by the LBL data.

3.3 Light Bulb Localization

On two days, May 5 and 15, 2001, light bulbs were dropped from the research vessel OR3 at selected locations around the HLA. The arrival time of the broadband pulses produced by the implosion of these light bulbs was used to calculate the position of each sensor on the HLA. A range was calculated from the implosion point to each of the sensors and used in a least squares fit. The following sections discuss this localization scheme and its results.

3.3.1 Light Bulb Drop Positions

Three of the light bulbs dropped on 5 May and five light bulbs dropped on 15 May provided strong enough signals to be used. Figure 3-7 shows the relative positions in meters of the logged locations of the light bulb drops along with the LBL system provided as a reference.

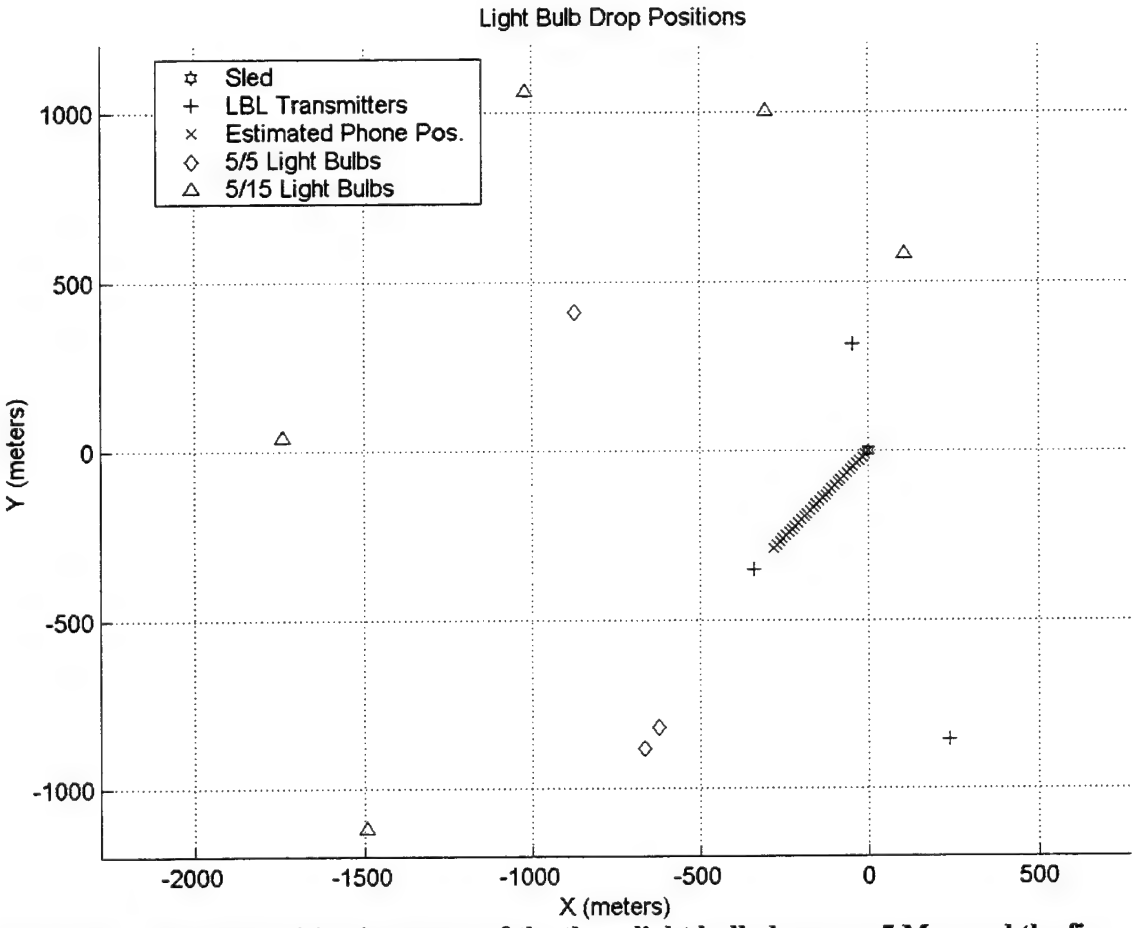

Figure 3-7: Relative position in meters of the three light bulb drops on 5 May and the five light bulb drops on 15 May that provided strong enough signals to be used in the least squares calculation. The LBL system components are provided for reference.

3.3.2 Light Bulb Pulse Arrival Times

The signal received at each of the HLA sensors was examined to determine the arrival time of the light bulb pulse. A representative pulse created by the implosion of a

light bulb, as recorded by hydrophone 47, is shown in Figure 3-8. The direct path and at least two reflected multipath arrivals are seen in the figure. Since the light bulbs provided such a strong signal above the background noise, a simple code was used to record the time at which the signal exceeded a set SNR threshold for each hydrophone.

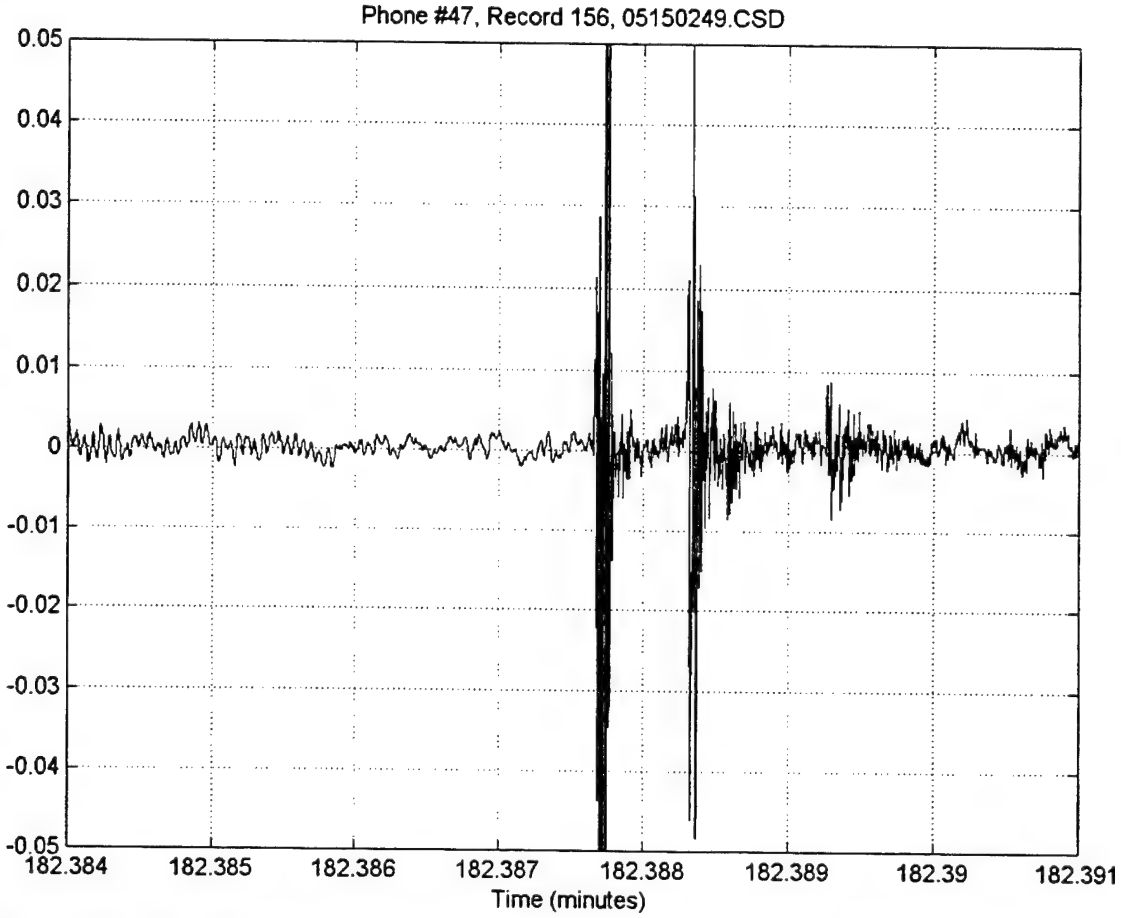

Figure 3-8: Light bulb pulse recorded by hydrophone 47 on 15 May. This signal is representative of all the pulses used in the localization. The time of arrival was determined by recording the time at which the signal exceeded a set threshold. Direct and surface reflected multipaths are clearly seen.

To determine the best threshold, the difference in arrival time between successive hydrophones was compared. The threshold that provided the smoothest curve and did not have any time differences greater than .01 seconds, the maximum possible difference given the 15 m maximum spacing of the sensors, was chosen. Figure 3-9 shows the time differences for each of the five different light bulb drops used in the analysis for 15 May.

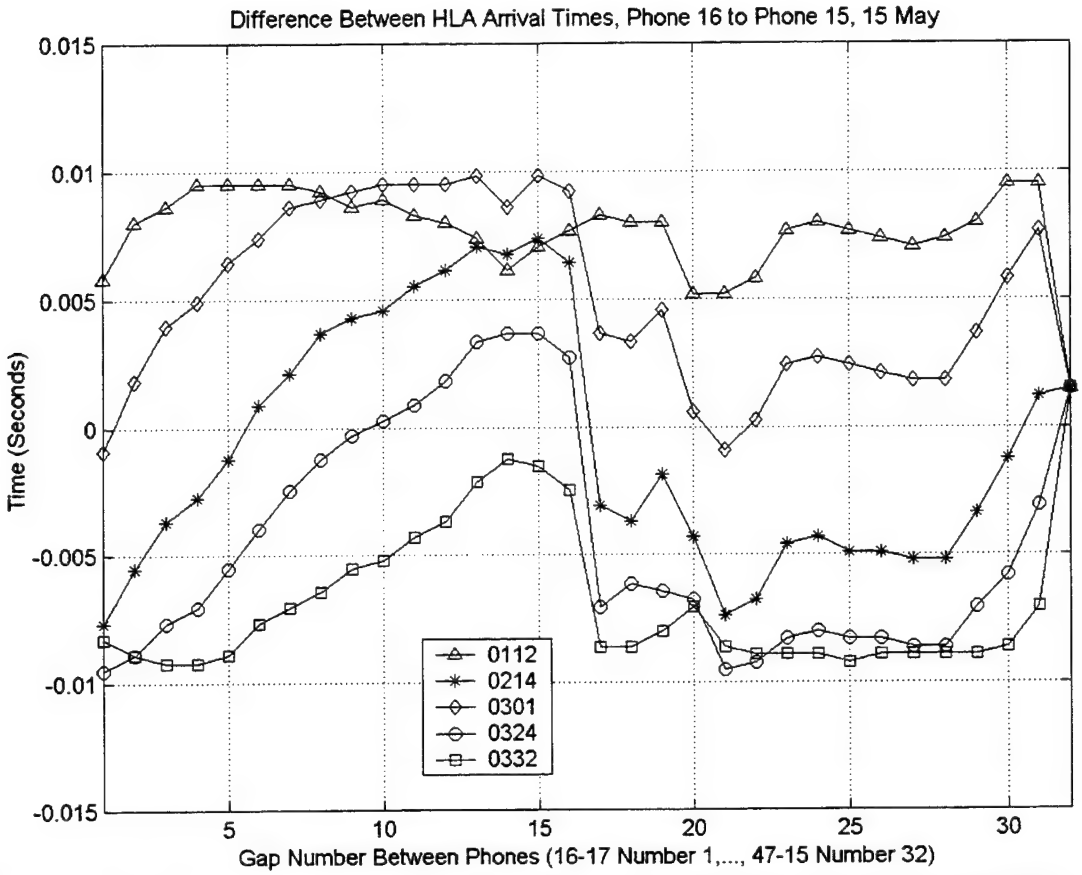

Figure 3-9: Difference between arrival times for successive hydrophones along the HLA, including the time difference between CH47, closest to the sled, and CH15, lowest on the VLA. The x-axis is the number index of the gap between the hydrophones starting with CH16 and CH17, the farthest from the sled. Each of the five drops of 15 May is plotted. The graph verifies good thresholds were used for each drop, as the curves are relatively smooth and none of the time differences exceed .01 seconds, the maximum allowable for the 15 m "fully stretched" sensor spacing.

3.3.3 Sensor Localization from Light Bulb Drops

For the least squares calculation, range arcs are needed from the light bulb implosion points. A practical problem was encountered since the exact time and location of the light bulb implosion was not recorded. The only information recorded in the science log was the time the light bulb was dropped in the water. The locations of the drops were then obtained from the GPS position logs; however, the time between the drop and the implosion, and any change in position that occurred during the light bulb's

descent still needed to be accounted for. An iterative method was thus used to determine the best implosion location and propagation distance.

To determine the best estimate of the implosion location, an error circle was set around the drop positions and four possible implosion positions were picked on the error circle, two perpendicular to and two along the axis of the HLA. Figure 3-10 shows an example with a 100 m-error circle for the light bulb drops on 15 May.

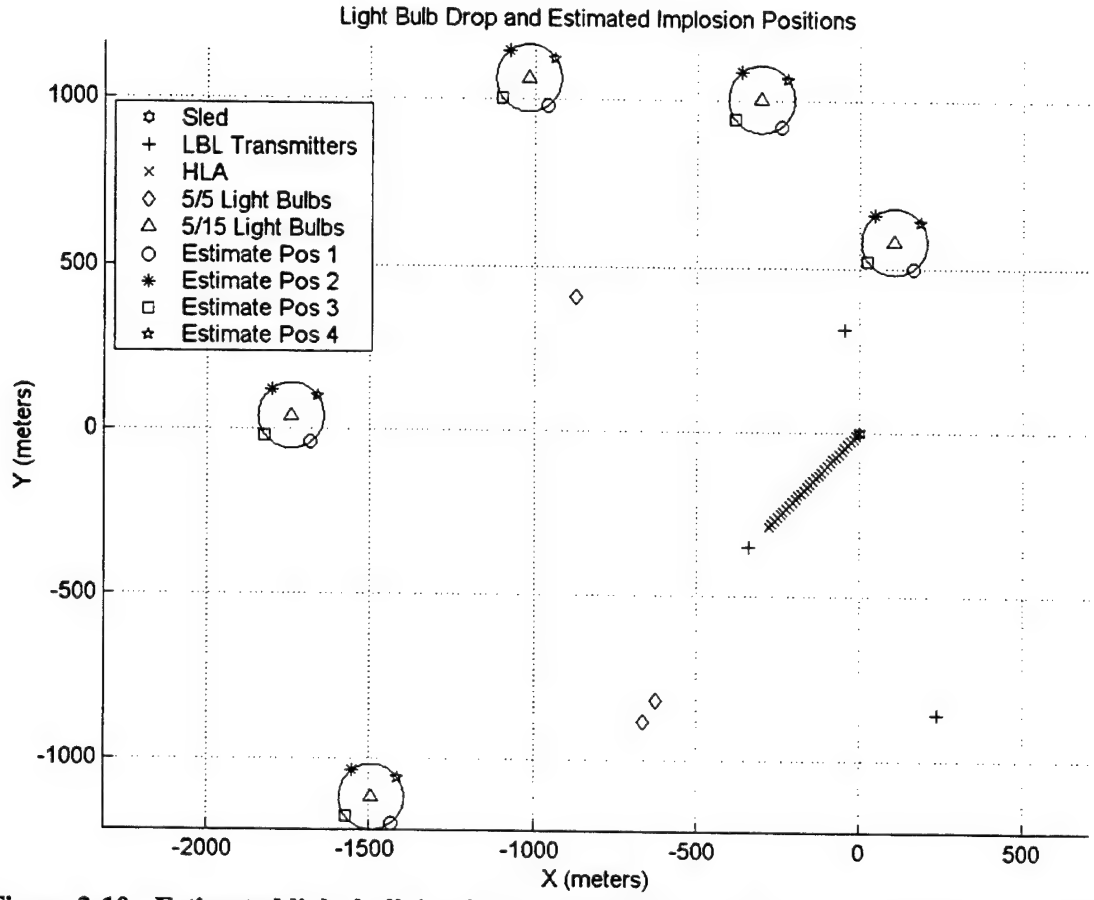

Figure 3-10: Estimated light bulb implosion positions for 15 May 2001 using 100 m-error circle. The estimated positions are chosen perpendicular to and along the HLA axis.

To determine a maximum radius for the error circle the pulse arrival times were compared to the drop times and it was found that it took between 80 and 120 seconds for the light bulbs to break. This corresponds well to a weighted light bulb sinking at 1 m/sec and imploding at a depth of approximately 100 m. The maximum possible

position error was established at 120 m, which corresponded to a maximum current of 1 m/sec or ~2 kts (a good estimate for the maximum current in the experiment area). The assumption that the current would be traveling in the same direction for all drops was also made. This reduced the number of required calculations to five, with four different error positions (grouping the positions on the same side of the error circle) and the drop position.

To determine the propagation distance, the arrival time at VLA CH15 was used. Since VLA CH15 was less than 2 m above the sled, the known position of the sled was used for the position of CH15. The distance between the estimated implosion positions and the sled was then used to calculate the required transit time to CH15. Subtracting that time from the arrival time at CH15 gives the time of implosion. Subtracting the implosion time from the arrival time at each of the HLA hydrophones gives the respective transit time. Each of those times is then converted into ranges for the least squares localization of the hydrophones.

Different sized error circles were tried to determine the best sensor location. Figure 3-11 shows the sensor locations calculated using the five drop positions and their corresponding 100 m estimated error implosion positions shown in Figure 3-10. The LBL positions for the entire day of 15 May are shown together with the light bulb positions in Figure 3-11 for cross-comparison. The small group of obviously erroneous LBL positions for CH26 and CH36, located farther away from the positions from the light bulbs, occur at different times of the day than the light bulb drops. They are likely uncorrected propagation path shifts in the LBL system transmissions.

For these five different drops on 15 May, there is little change in the HLA sensor locations for each of the different postulated implosion positions, with the biggest effect coming from postulated error positions 3 and 4. These are the postulated error positions that correspond to movement of the light bulb along the axis of the array. As these positions are moved the 200 m from position 3 to 4 the curvature of the range arcs cause the sensor position to move perpendicular to the array axis. In comparison, moving

between error positions 1 and 2 (in the direction perpendicular to the array) provides only a small amount of movement in the sensor locations.

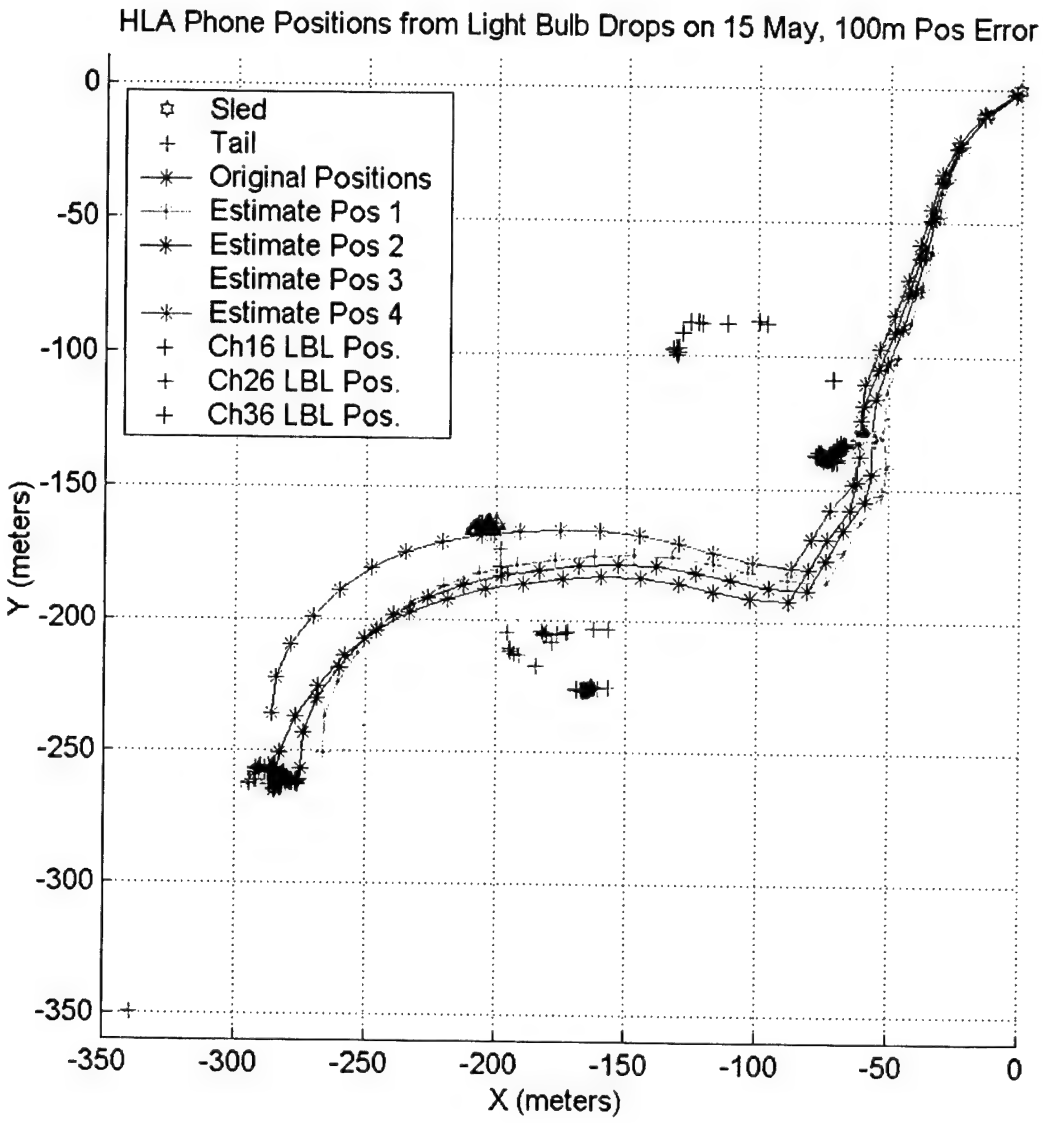

Figure 3-11: Possible HLA hydrophone positions on 15 May using initial drop position and the four estimated implosion positions using a 100m error as shown in Figure 2-9. Changing the estimated position in the direction of the HLA axis (estimated positions 3 and 4) gives a larger variation in the hydrophone positions. The LBL data is provided for reference and correlates well. The spurious LBL positions are most likely due to uncorrected propagation path shifts for the LBL transmissions.

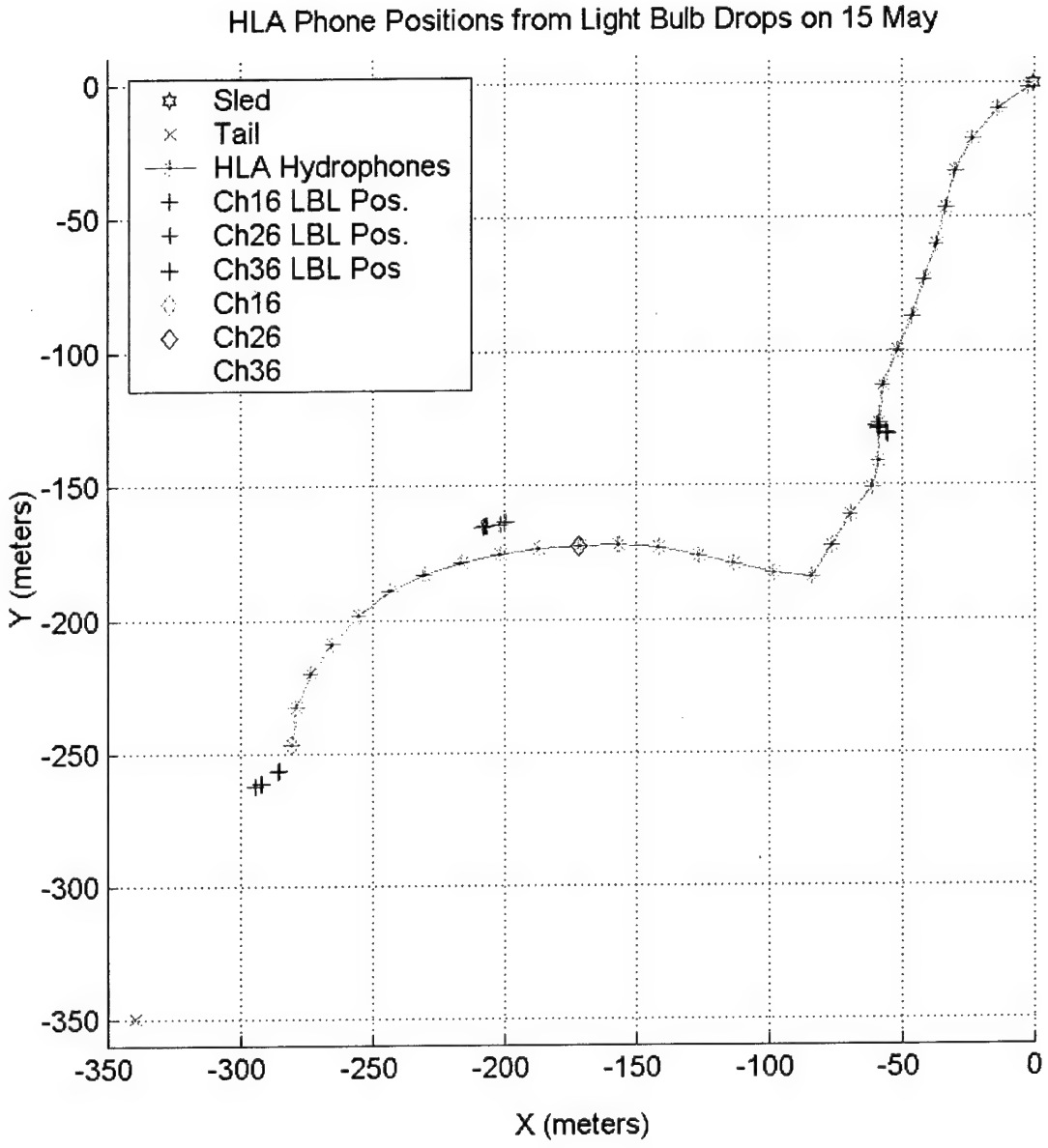

Figure 3-12: Final hydrophone positions determined from the light bulb drops on 15 May. They are plotted with the LBL positions for the same time. There is good correlation between the light bulb and LBL positions.

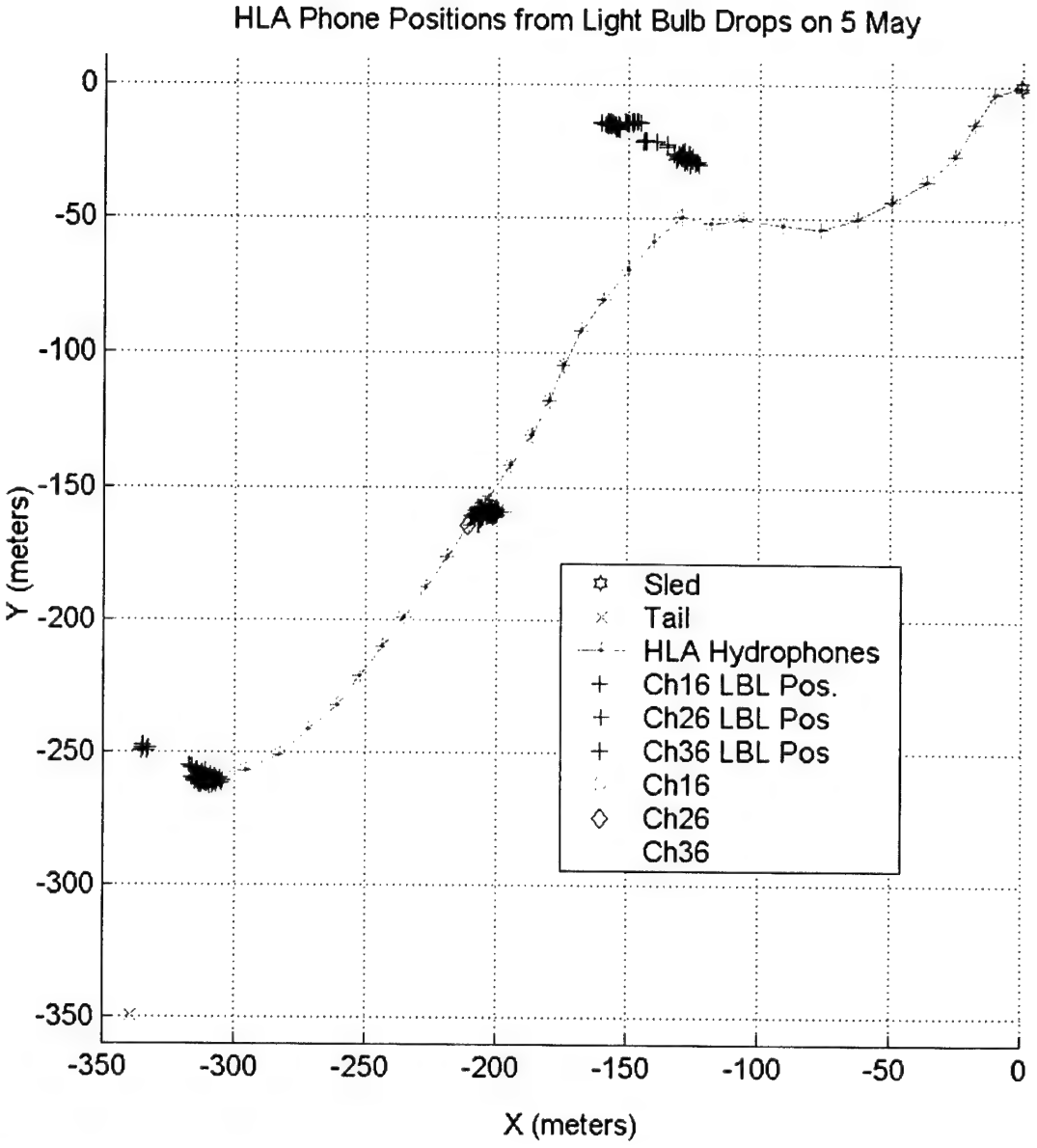

Figure 3-13: Final hydrophone positions determined from the light bulb drops on 5 May. LBL positions are also plotted for the same period. Once again, there is good correlation between the light bulb and LBL positions.

Table 3-2: HLA hydrophone positions from light bulb sources for May 5th.

Hydrophone	Latitude N	Longitude E
16	21 52.67921	117 10.90144
17	21 52.67968	117 10.90879
18	21 52.68302	117 10.91657
19	21 52.68815	117 10.92263
20	21 52.69305	117 10.92906
21	21 52.69902	117 10.93412
22	21 52.70505	117 10.93906
23	21 52.71128	117 10.94366
24	21 52.71746	117 10.94884
25	21 52.72368	117 10.95346
26	21 52.73013	117 10.95818
27	21 52.73633	117 10.96281
28	21 52.74246	117 10.96758
29	21 52.74865	117 10.97224
30	21 52.75532	117 10.97608
31	21 52.76231	117 10.97936
32	21 52.76929	117 10.98318
33	21 52.77552	117 10.98828
34	21 52.78155	117 10.99372
35	21 52.78718	117 10.99934
36	21 52.79214	117 11.00558
37	21 52.79073	117 11.01192
38	21 52.79170	117 11.01917
39	21 52.79057	117 11.02770
40	21 52.78972	117 11.03608
41	21 52.79190	117 11.04441
42	21 52.79546	117 11.05201
43	21 52.79963	117 11.05960
44	21 52.80476	117 11.06578
45	21 52.81116	117 11.07013
46	21 52.81726	117 11.07445
47	21 52.81852	117 11.08031

Table 3-3: HLA hydrophone positions from light bulb sources for May 15th.

Hydrophone	Latitude N	Longitude E
16	21 52.68557	117 10.91766
17	21 52.69306	117 10.91841
18	21 52.70000	117 10.92168
19	21 52.70603	117 10.92654
20	21 52.71177	117 10.93231
21	21 52.71649	117 10.93905
22	21 52.71992	117 10.94659
23	21 52.72244	117 10.95490
24	21 52.72403	117 10.96352
25	21 52.72495	117 10.97211
26	21 52.72570	117 10.98099
27	21 52.72577	117 10.98977
28	21 52.72531	117 10.99852
29	21 52.72382	117 11.00731
30	21 52.72201	117 11.01496
31	21 52.72028	117 11.02362
32	21 52.71947	117 11.03206
33	21 52.72566	117 11.03643
34	21 52.73178	117 11.04041
35	21 52.73726	117 11.04522
36	21 52.74288	117 11.04666
37	21 52.75051	117 11.04673
38	21 52.75802	117 11.04766
39	21 52.76508	117 11.05064
40	21 52.77208	117 11.05389
41	21 52.77933	117 11.05670
42	21 52.78649	117 11.05919
43	21 52.79374	117 11.06131
44	21 52.80113	117 11.06349
45	21 52.80767	117 11.06710
46	21 52.81366	117 11.07269
47	21 52.81798	117 11.07967

3.3.4 Results of Light Bulb Sensor Localization

Comparing the results of different light bulb drop error magnitudes and directions to the LBL data, combined with comparing the distances between each hydrophone and distances to the sled and tail, the best positions for the implosions and therefore the best estimates of the hydrophone locations were determined. The radius of the error circle that produced the best results was 90 m for 5 May and 50 m for 15 May. The positions of each hydrophone are recorded in Table 3-2 for 5 May and in Table 3-3 for 15 May. The hydrophone positions are also plotted in Figures 3-12 and 3-13 with the LBL positions for the same period. The data show that there is good correlation between the LBL and light bulb calculated positions. For 5 May there is less than a 5 m error between the light bulb and LBL positions for CH16 and CH26 and less than 25 m for CH36. On 15 May there is less than a 10 m difference for CH16 and CH36 and about a 30 m difference for CH26.

3.4 Comparison of Sensor Locations to Low Frequency Transmission Arrival Times

Another method to localize the sensor positions that should be pursued is the use of the distant moored low-frequency sources. Though the use of this data for sensor location negates using it simultaneously for other purposes, there is enough data that using a little poses no real problem. This thesis will only look at the beginning of such an analysis.

The first step is determining the arrival times at each sensor for the transmissions from each distant source. The arrival times for many of the East 400 Hz, South 400 Hz and 224 Hz source transmissions on 5 May have been determined. They will be used for the correlation study in Chapter 4. To give an indication of the sensor location accuracy, the time difference between the arrival time of the transmission at phone 16 and the arrival times at the other hydrophones was determined. Additionally, the time differences between the arrival times at each subsequent hydrophone were determined. These time differences were compared to the time difference calculated from the distance between

the sensor locations in the direction of the transmission, using the positions derived from the light bulb drops.

The south 400 Hz source gave the best information, because it was the higher frequency of the two sources located the closest to the broadside aspect of the HLA. Figure 3-14 shows the time differences between the arrival time at CH16 and the arrival times at the other hydrophones for 21 transmissions of the south 400 Hz source on 5 May. The thick black line on the plot was determined by taking the distance between the location of CH16 and the location of the other sensors in the direction of the South 400 Hz signal propagation. That distance was then converted to time using 1500 m/sec for the sound speed. The plot shows that the light bulb drop generated sensor location times correlate well with the 400 Hz pulse arrival times. There is a maximum difference after hydrophone 36 of 0.01 sec, or equivalently a possible error of 15 m.

Figure 3-15 is similar to the previous plot, but looks at the time difference between subsequent hydrophones. The x-axis is the numbered space between the hydrophones starting at 1 with CH16 and CH17 (closest to the tail) and ending with gap 31 between CH46 and CH47 (closest to the sled). Again, there is a good correlation between the 400 Hz arrival time calculation and the values using the sensor locations from the light bulb drops. This shows that the sensor locations (distances between each hydrophone) are relatively well estimated. The maximum errors seem to occur in gaps 4, 6, 15, 16, 24, and 25 with the sensor location tending to be about 0.004 seconds shorter, or about a 6 m difference. These shorter gaps are probably part of the possible loss in overall length seen in Figure 3-14.

The differences between the actual 400 Hz arrival times and those calculated from the light bulb drop sensor locations could be caused by a number of effects. First, the South 400 Hz source is located just inside the near field for the HLA. Thus, there will be some wave front curvature at the array, which was not accounted for. Second, as the wave propagates from the South 400 Hz source, there will be some phase front variability due to scattering, causing the wave front to be non-uniform. Third, the array could have moved in the time between some of the transmissions and the light bulb drops. Fourth,

since there were only three light bulbs (one at broadside and two at endfire) usable on 5 May, and the actual light bulb implosion points were unknown, there could be some error in the location data. Since there are five light bulbs used on 15 May, there would be a smaller error on that day.

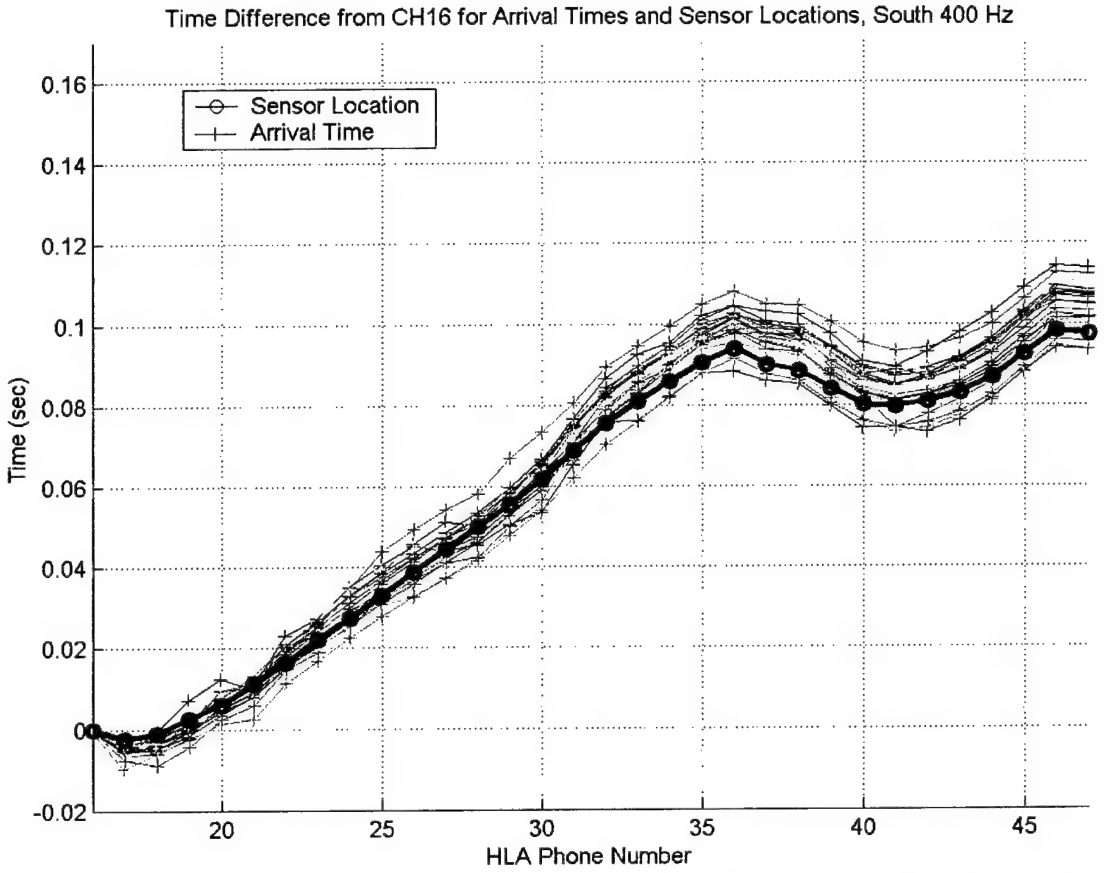

Figure 3-14: Time difference between the arrival time at CH16 to the arrival time at the other sensors. These times were found by taking the difference in the arrival times of the 400 Hz source on 5 May and by using the acoustic sound speed and the distance between sensor locations (derived from the light bulb drops) in the direction of propagation.

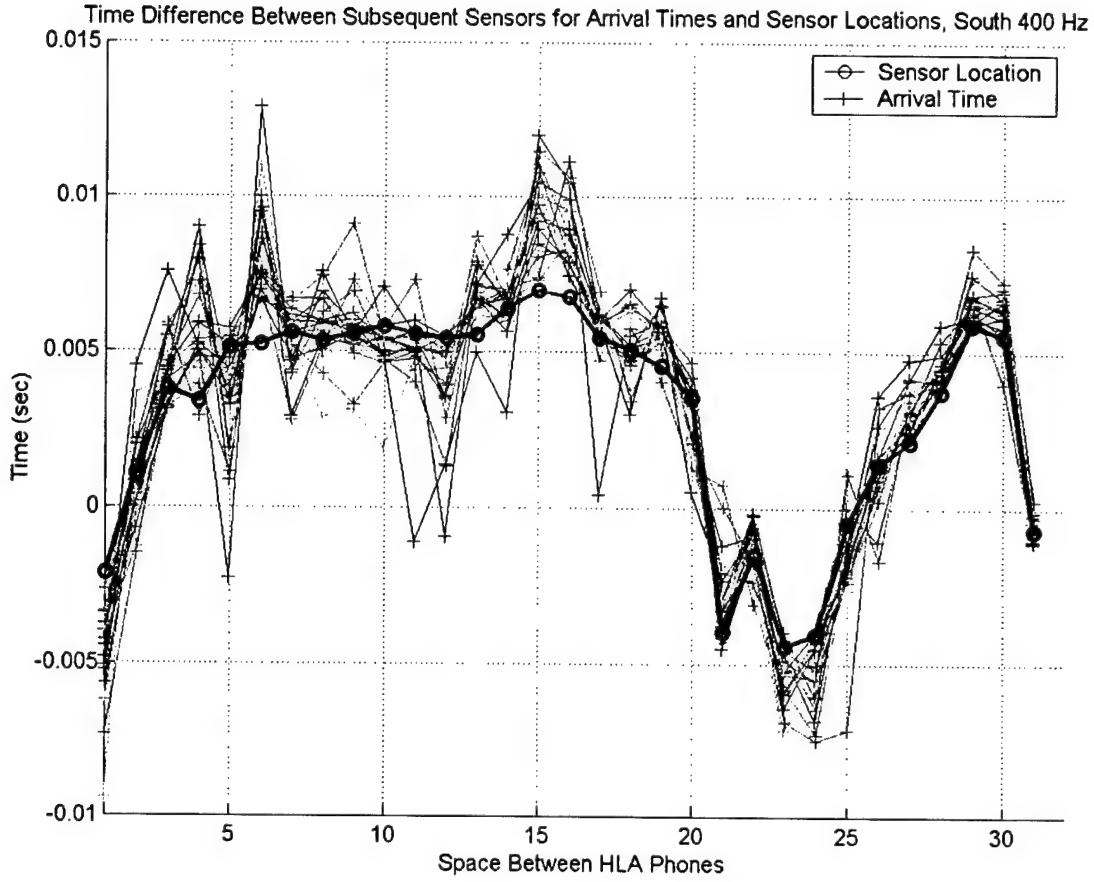

Figure 3-15: Time difference between the arrival times of subsequent hydrophones (space 1 is between Ch16 and Ch17) calculated by taking the difference between the arrival times found from the 400 Hz source transmissions on 5 May. This is compared to the time difference calculated from the sensor locations determined from the light bulb drops on 5 May.

3.5 Conclusions on HLA Element Localization

The LBL data provides a good way to track the general movement of the HLA. The positions of the three tracked hydrophones also give some indication of the general geometry of the array. Using the actual physical constraints of the hydrophone spacing and a spline fit between the LBL hydrophones could give useful relative positions of the HLA sensors, with maximum relative errors on the order of 10m. This accuracy however still needs to be confirmed by other methods, such as beam forming the array. The

accuracy of the absolute position of three LBL hydrophones with the current analysis is on the order of 100 m unless the propagation path has been verified, in which case it should be better than 30 m.

The sensor localization obtained from the light bulb drops, and verified using the LBL data and arrival times of three of the low frequency sources on 5 May, seems to be accurate to within a 15 m maximum absolute error. The relative sensor location is even better, with an accuracy within 6 m. The accuracy of the light bulb drop based locations on 15 May are at least as good as the locations on 5 May, and should be even better because they were localized using 5 light bulb drops. However, their accuracy still needs to be confirmed.

4 Sensor-to-Sensor Correlations and Coherence Length.

4.1 Introduction

This chapter discusses the results of a first look at horizontal coherence length calculations for the HLA in the ASIAEX SCS experiment. In particular, the transmissions on 5 May from the 224 Hz source, along with the deep and shallow 400 Hz sources, have been analyzed. This analysis included pre-processing the signals and then completing the sensor-to-sensor cross-correlation of the signals on the hydrophones of the HLA. The correlation values between each hydrophone were then interpolated to give the correlation function versus hydrophone separation. The distance to the correlation value of 0.5 was then used as the determining factor for coherence length.

Section 2 of this chapter will discuss the 224 Hz and 400 Hz signals used for the coherence analysis, with emphasis on the signal processing and the resulting signals. Section 3 looks at the coherence and correlation theory and calculations. Section 4 presents a discussion of the results and the conclusions.

4.2 224 Hz and 400 Hz M-Sequence Signals

4.2.1 Signal Transmissions

The signals considered in this thesis were produced by the 224 Hz and 400 Hz Webb Research Corporation organ pipe tomography sources. The signals were standard tomographic m-sequences. The m-sequence signal was chosen because it allows for low energy sources with a specified bandwidth to provide improved time resolution [9]. This is beneficial for oceanographic studies as it reduces battery requirements and minimizes the amount of sound energy needed to achieve the desired SNR at the receiver. The specifics for the m-sequence signals are shown in Table 4-1.

Table 4-1: Parameters of the source signals used for the analysis in this thesis (transmissions occurred on 5 May). Both the deep and shallow 400 Hz sources had the same signal characteristics.

Carrier Frequency (Hz), f	224	400
Cycles per digit, c	14	4
Digits per sequence, N	63	511
Number of sequences transmitted, R	30	88
Digit duration (sec), d=c/f	.0625	.01
Bandwidth (Hz), f/c	16	100
Sequence duration (sec), Nd	3.9375	5.11
Total transmission time (sec), RNd	118.125	449.68
M-sequence law (octal)	0103	1533
Modulation angle (deg), $\tan^{-1}\left(\sqrt{N}\right)$	82.8192	87.467
Transmission times	Every 5 min Starting at time 00	15,45 (deep) 00,30 (shallow)

4.2.2 HLA/VLA Data Acquisition

The following section was taken from the Woods Hole Oceanographic Institution technical report on the ASIAEX South China Sea experiment [8] to provide information on the acoustical data acquisition by the HLA and VLA.

Sixteen days of continuously sampled acoustic data was stored on hard drives located in the anchor sled of the HLA/VLA. Nine 75 GB disks were employed to store the 650 MB of acoustic data. The system recorded forty-eight channels at 3255.208 Hz. The exact sampling rate for the 5-megahertz sampling clock was 5E6/(6*256). The channel assignments put the VLA channels in positions 0-15 and the HLA channels in positions 16-47 (with channel 47 being the closest to the sled) [8].

The hydrophone preamps are current mode and each derives power and transmits signals over a separate pair of twisted conductors. All hydrophones have a sensitivity of –170 dB, linearly handling signals up to an acoustic receive level of 160 dB corresponding to a maximum amplitude at the differential receiver of about 1 Vpp (-10dB V rms). The receiver applies a fixed gain of 20 dB to each channel. The amplitude match between channels is approximately +/- 1 dB. All channels are sampled on a

common time base, simultaneously, with a constant group delay of 28 samples. The amplitude response is flat to 0.375*sample rate (1221 Hz) and the –3dB point is 0.41*sample rate (1335 Hz). The sampling elements are sigma-delta converters of 24-bit resolution with about 21 bits of dynamic range. The 24-bit sample values are converted on the fly to 16-bit values comprised of a 13-bit mantissa, sign bit and 2 bit gain word. The gain bits represent the position in the raw 24-bit word of the most significant 13 bits used as the mantissa [8].

4.2.3 Signal Processing

The signal processing of the data required the following steps: (1) generate a replica of the transmitted m-sequence signal, (2) extract desired transmission from the data file, (3) bandpass filter, (4) beat the signal to baseband and quadrature demodulate to get the complex envelope, (5) pulse compress the signal to remove the m-sequence coding, and (6) downsample the result to reduce storage requirements. Additionally, on the time scales used in this processing, mooring motion could be neglected, so no correction for motion-induced Doppler shifting was required.

Creating the replica m-sequence is accomplished by using equation (4.1):

$$w = \sin(2\pi f_c t + \theta A) \tag{4.1}$$

where f_c is the carrier frequency, t is the sampled time vector, θ is the modulation angle, and A is the scaled m-sequence. For example, the m-sequence for 224 Hz source using octal code 0103 is:

0 0 0 0 0 1 0 0 0 0 1 1 0 0 0 1 0 1 0 0 1 1 1 1 0 1 0 0 0 1 1

1 0 0 1 0 0 1 0 1 1 0 1 1 1 0 1 1 0 0 1 1 0 1 0 1 0 1 1 1 1 1 1

After generating the replica code, it is used in the pulse compression.

The pulse-compressed signal of the j^{th} hydrophone may be expressed in the form of a discrete Fourier transform (equation 4.2):

$$s_j(n) = \frac{1}{N}\sum_{k=1}^{N}\left(P_j(k)W^*(k)e^{-i2\pi k(f_c/f_s)\theta_t}\right)e^{i2\pi kn/N} \tag{4.2}$$

where P_j is the demodulated Fourier transform of raw digitized signal at hydrophone j, W^* is the conjugate Fourier transform of the replica pseudo-random signal transmitted, f_c is the m-sequence carrier frequency (224 Hz or 400 Hz), f_s is the sampling rate, and θ_l is the phase correction for timing errors (such as clock drift, delays of writing data to disk, etc.). This pulse compression removes the m-sequence and gives a signal of much shorter duration than the original sequence length – in particular, it gives a pulse of length 1/(digit bandwidth).

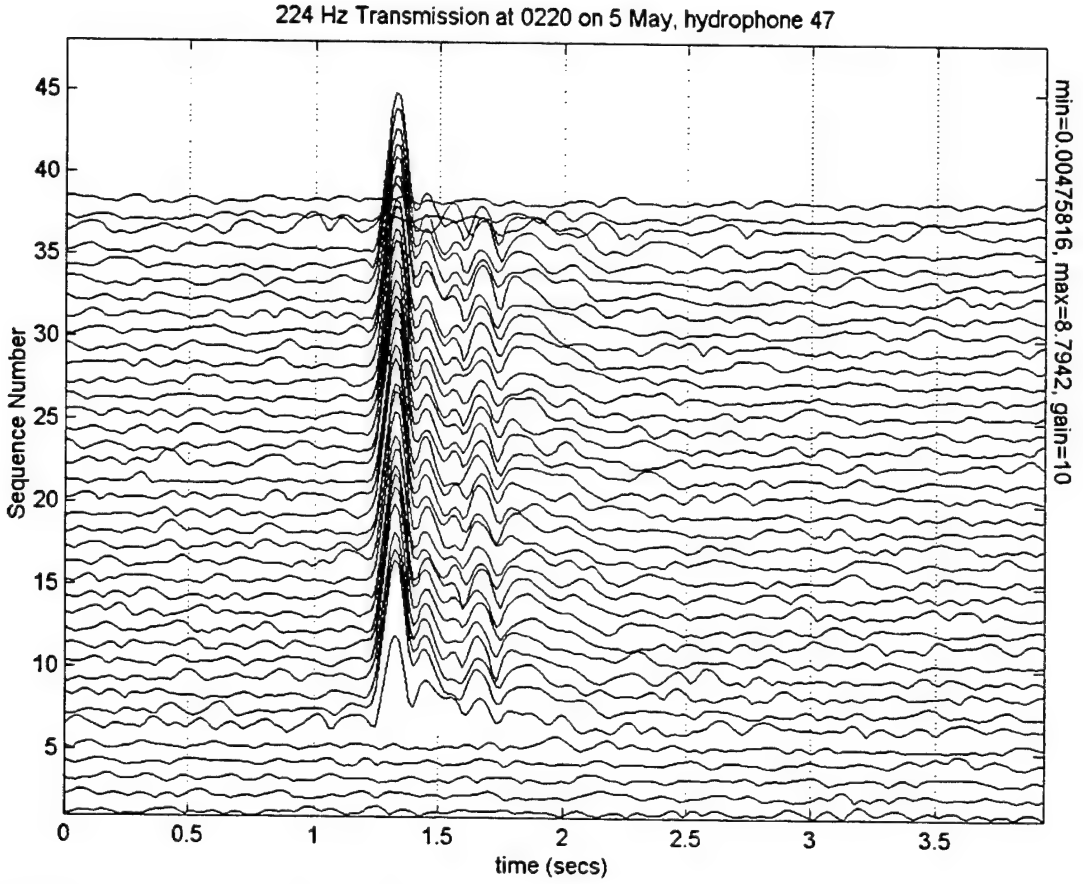

Figure 4-1: The absolute value of the signal processed 224 Hz transmission (at 0220 on 5 May) as it was received on hydrophone 47. The sequences are stacked vertically along the y-axis enabling the comparison of each sequence. Sequences 1 to 5 are processed noise, 6 to 35 are the actual signal and 36-38 are again processed noise (giving 30 signal and 8 noise sequences).

4.2.4 Signal receptions

An example of a processed 224 Hz signal can be seen in Figure 4-1. This transmission was received on hydrophone 47 at 0220 on 5 May, and the plot shows the absolute value of the complex signal. The signal consists of 30 consecutive 3.9375 sec sequences, making the total transmission 118.125 sec long. Each sequence is stacked vertically to allow for comparison. The processing of the signal started at the time of the transmission and ended after the completion of the reception. This results in the first 5 sequences and the last 3 sequences being processed noise, giving a total signal processed file of 38 sequences. Therefore, in each signal processed file, sequences 1 to 5 are noise, 6 to 35 are signal and 36 to 38 are noise. The x-axis is 3.9375 seconds long, the length of the original sequence, and the y-axis is the processed sequence number 1 to 38. Figure 4-1 is representative of most of the 224 Hz signals on 5 May, showing peaks from multiple arrival paths with good SNR.

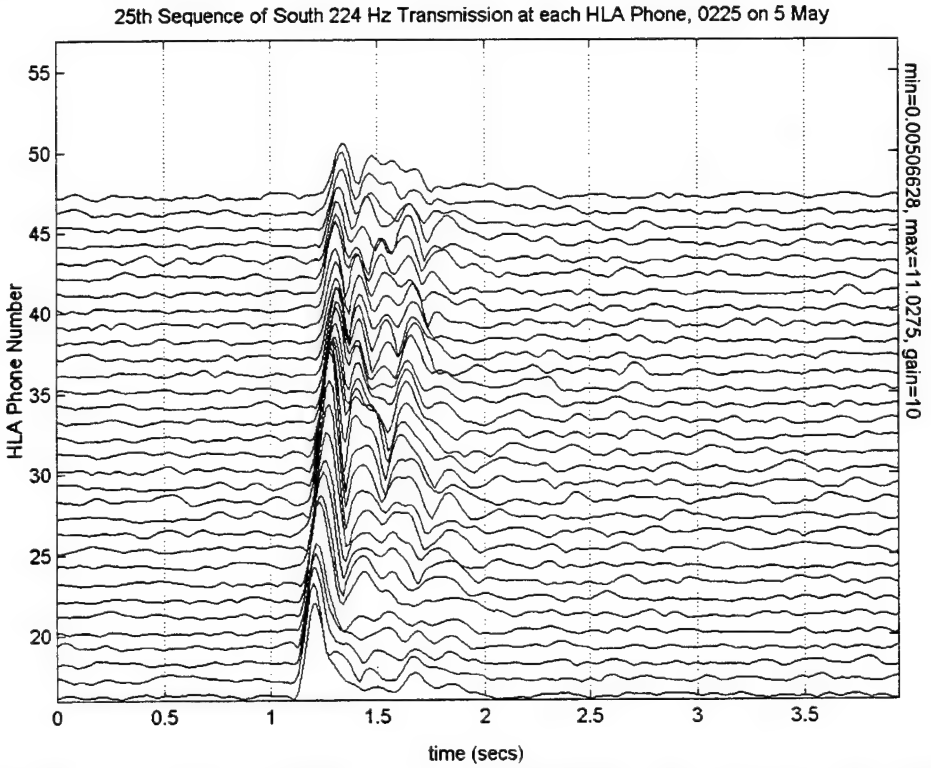

Figure 4-2: The absolute value of the signal processed 25th sequence of the 0225 5 May South 224 Hz transmission as it was received at each one of the HLA hydrophones (hydrophone 16-47 on y-axis). A change in the signal structure is evident.

Figure 4-2 shows the absolute value of the signal processed 25th sequence from the 0225 5 May 224 Hz transmission, as it was received by each of the HLA hydrophones. The y-axis goes from hydrophone number 16 (closest to the tail) to hydrophone number 47 (closest to the sled). At the tail end of the HLA, the signal has most of the energy in the first arrival, while in the middle of the array and closer to the sled the energy is spread into the second and third arrivals.

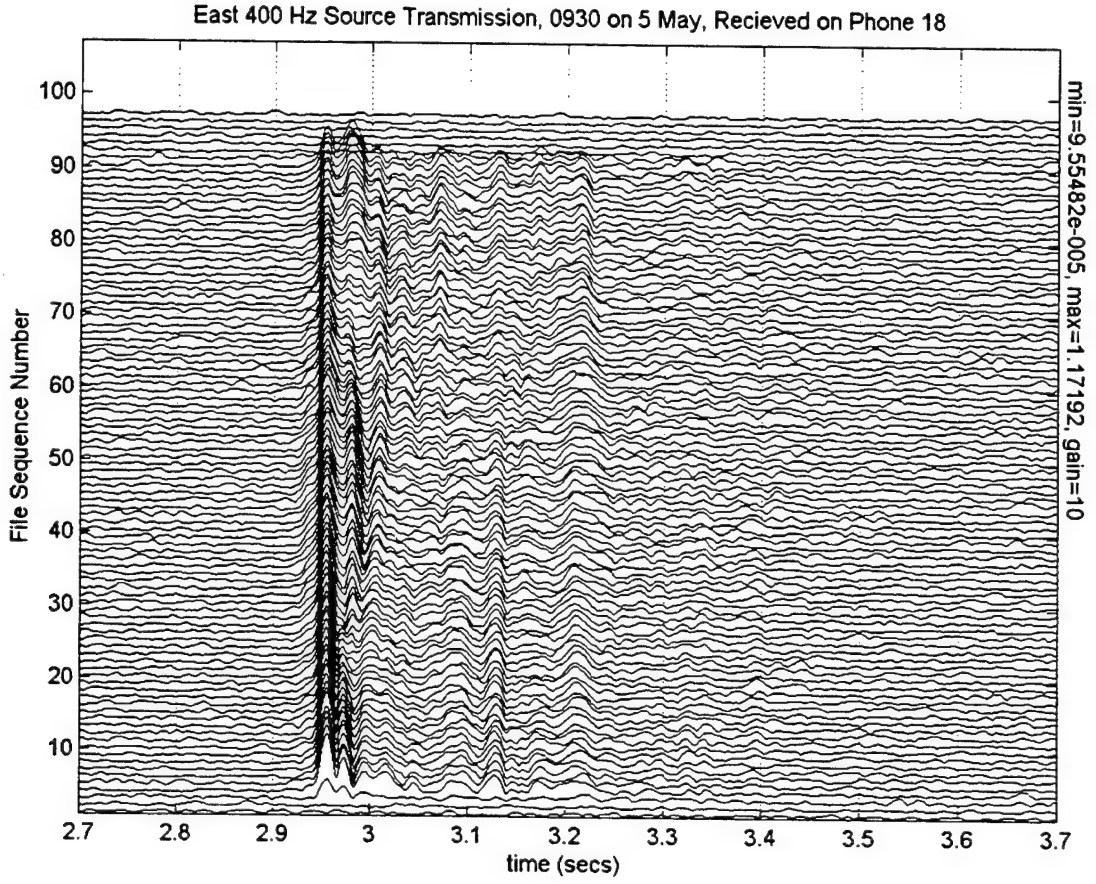

Figure 4-3: East 400 Hz transmission at 0930 on 5 May as it was received by hydrophone 18. The signal processing of the file starts prior to and ends after the reception. Sequences 1 and 2 are processed noise, 3 to 90 are signal and 91 to 97 are again processed noise. The sequences are stacked vertically to allow for comparison.

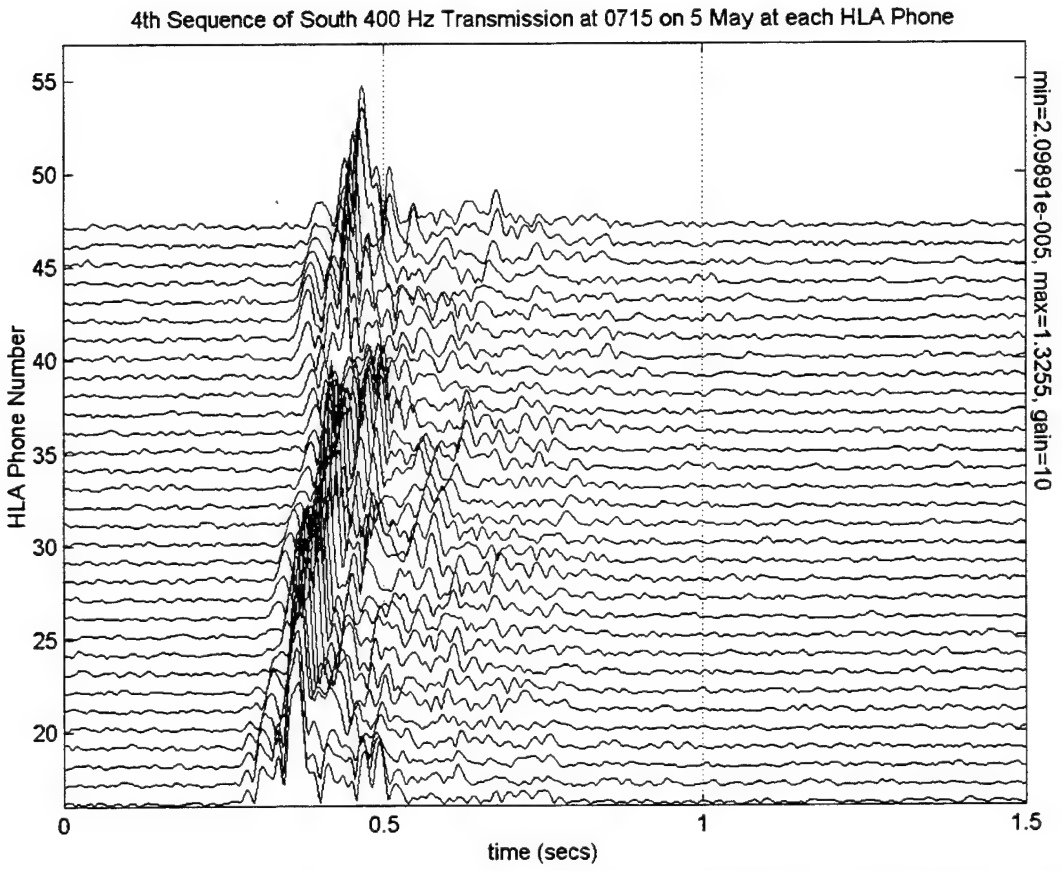

Figure 4-4: Absolute value of the 4th signal sequence from the 0715 5 May transmission of the South 400 Hz source as it was received by each of the HLA hydrophones. The y-axis covers hydrophone 16 (closest to the tail) to hydrophone 47 (closest to the sled).

A processed East 400 Hz source transmission, as received by hydrophone 18, is shown in Figure 4-3. The 400 Hz signals on 5 May, both from the shallow and deep sources, had 88 sequences and were approximately 7.5 minutes long. Like the 224 Hz transmissions, the processed data file started at the time of the transmission and stopped after the end of the reception. This resulted in the 400 Hz data files containing 97 processed sequences. Sequences 1 and 2 were processed noise, 3 to 90 were signal and 91 to 97 were, once again, processed noise.

The absolute value of the fourth signal sequence of the 0715 5 May South 400 Hz transmission, as received at each of the HLA hydrophones, is shown in Figure 4-4. The signals at each hydrophone are stacked for comparison. The y-axis again goes from hydrophone 16 (closest to the tail) to hydrophone 47 (closest to the sled). The 400 Hz

signal has more trapped modes at the receiver (25 versus 14), giving more modal interactions and resulting in more peaks than the 224 Hz signals.

4.3 Coherence and Cross-correlation

4.3.1 Equations

There are many ways to look at spatial coherence. In this thesis, the sensor-to-sensor coherence, or equivalently sensor-to-sensor cross-correlation, is used. Urick [10] defines coherence as the degree of similarity of a waveform of signal and noise between any two elements of the array, and states that coherence is best measured by the cross-correlation coefficient. Defining $v_1(t)$ and $v_2(t)$ as the voltage outputs from two array sensors, the cross correlation function can be written as

$$c_{12} = \frac{\overline{v_1(t)v_2(t)}}{\left[(v_1)^2(v_2)^2\right]^{1/2}} \tag{4.3}$$

where the bars indicate time averages and the denominator normalizes the function[10]. The cross-correlation is also a statistical quantity defined as

$$\rho_{xy}(m) = E\left\{x_n y^*_{n+m}\right\} \tag{4.4}$$

where x_n and y_n are stationary random processes, y^* is the complex conjugate of y, n is defined from $-\infty$ to ∞, and $E\{\ \}$ is the expected value. However, since the signals are finite length discrete-time functions with N samples, the function becomes a deterministic cross-correlation sequence. Defining x_n as the signal processed sequence at one hydrophone and y_n as the signal processed sequence at a different hydrophone, the equation becomes

$$\begin{aligned} \rho_{xy}(m) &= \sum_{n=0}^{N-|m|-1} x_{n+1} y^*_{n+m+1} && m \geq 0 \\ \rho_{xy}(m) &= \rho^*_{yx}(-m) && m < 0 \end{aligned} \tag{4.5}$$

where x_n and y_n are indexed from m equals 0 to N-1 and $\rho_{xy}(m)$ will be indexed from negative (N-1) to (N-1). The cross-correlation function used in the thesis is normalized by the maximum value of x and y to give an auto-correlation value equal to 1 at 0 lag, and ensure the correlation values are less than or equal to 1.

Each sequence within each transmission was cross-correlated separately. The sequence reception at a hydrophone was cross-correlated with the same sequence reception at every other hydrophone on the HLA. This process was repeated for all hydrophones. The cross-correlation values are in terms of lag time between the two signals. For an auto-correlation (the cross-correlation of a signal with itself) the value at 0 lag would be the correlation value. Since the sequences arrived at each hydrophone at different times, the actual correlation of the signal would occur when the two signals line up at the difference between the arrival times or lag time. Therefore, the lag time between the sensors needed to be determined.

4.3.2 Lag Time Determination

The time difference required for the transmission sequence to reach each hydrophone (i.e., lag time) is needed to obtain the correct correlation value. For this first look at coherence, it was decided to determine the lag time from the difference between the actual arrival times of the transmission at each of the hydrophones. This method looks solely at pulse distortion effects across the array, because it processes out phase front irregularities by lining up the initial arrival, i.e. it ignores modal time dispersion. This method should give a good first approximation to coherence without having exact sensor location and propagation characteristics.

To determine the leading edge arrival times, a computer code was used to record the time the magnitude of a transmission sequence exceeded a chosen threshold value at each hydrophone. Since the code would sometimes record spurious times as it triggered on noise peaks, either before or after the actual initial arrival of a sequence, it was decided to discard those sequences with spurious times and simply take the mean of the arrival times of the remaining sequences. This would give one mean arrival time at each

sensor for each full transmission. While this method averages out the variability of the individual sequence arrival times, it was chosen to minimize the effects of code induced spurious times. Figure 4-5 shows the arrival times for the 78 sequences (light lines) used to make the mean arrival times (bold line) for the 1315 5 May transmission of the South 400 Hz source. For this example, the times from 10 of the 88 signal sequences were discarded. Thresholds were chosen that produced good correspondence between 50% or more of the sequences in a transmission.

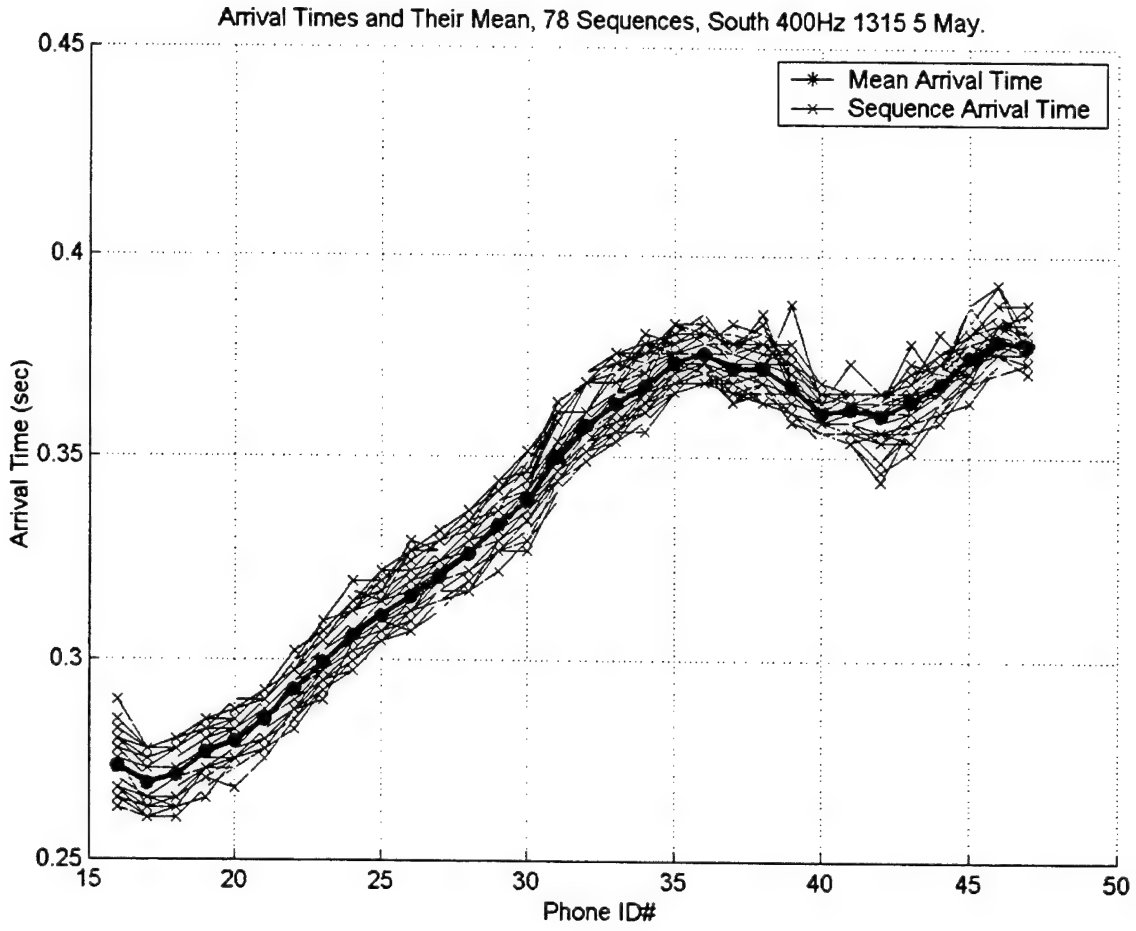

Figure 4-5: Arrival times at each hydrophone for 78 sequences of the South 400 Hz 1315 5 May transmission and their mean. The arrival time curves are representative for most to the 400 Hz transmissions with few spurious results. Ten of the sequence arrival times were discarded due to inaccurate times; the remaining sequences were averaged to obtain the mean arrival time (thick line) for the transmission.

Figure 4-6 shows the arrival times for each of the 21 full transmissions of the South 400 Hz source on 5 May. The curvature of the arrival times corresponds well to the curvature of the array determined in Chapter 3 from the analysis of the light bulb implosions. The variability on the order of 0.04 sec between the transmissions with the slowest and fastest arrival times is due to the change in sound speed throughout the day, i.e. the travel time "wanders."

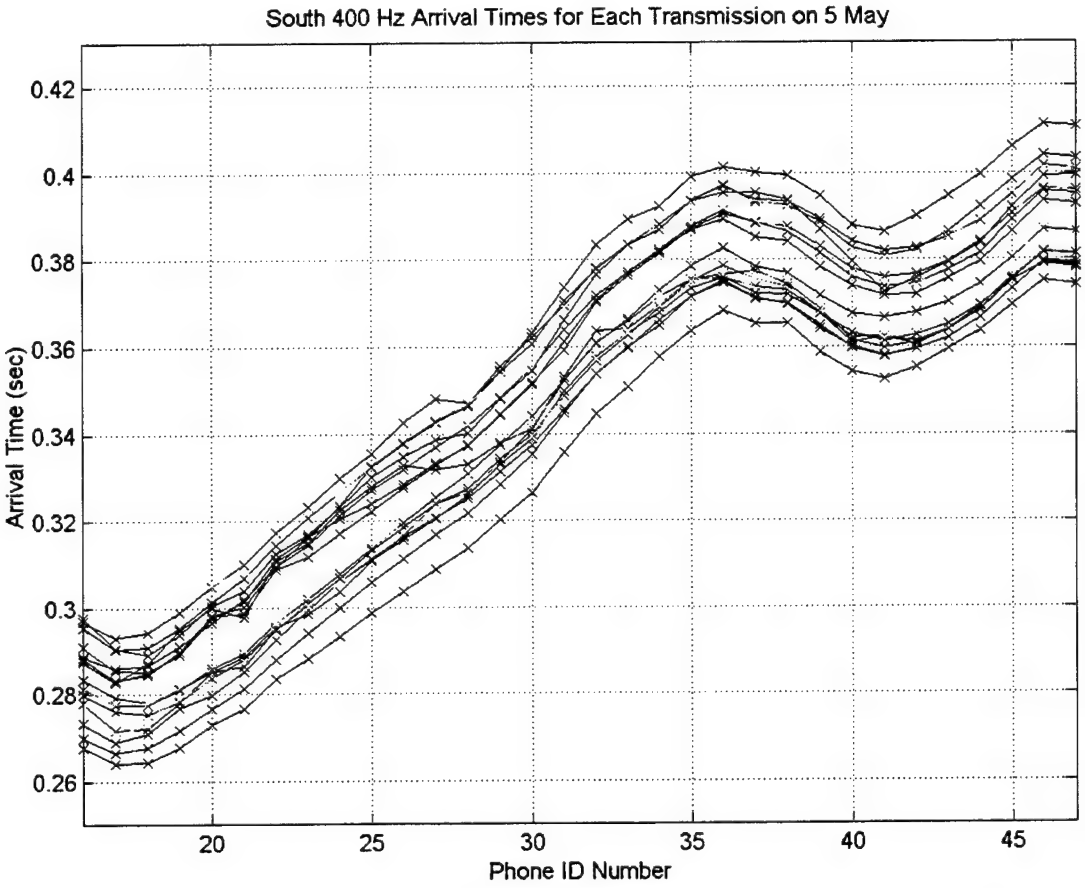

Figure 4-6: Arrival times for the 21 transmissions of the South 400 Hz source used in the correlation calculations. The curvature of the times corresponds well to the array geometry determined from the light bulb implosions covered in Chapter 3.

Arrival times were determined for all of the transmissions of the 224 Hz, and the deep and shallow 400 Hz sources on 5 May, that were contained fully in one data file (full transmission). Once the arrival times were known, the lag times were calculated by

subtracting the arrival time at one hydrophone from the arrival times at all of the other HLA hydrophones.

4.3.3 Correlation Values versus Hydrophone Separation

The goal was to obtain, for each sequence, the correlation value versus sensor separation. This was accomplished by taking a sequence and cross-correlating the reception at CH16 (the HLA sensor closest to the tail) with the reception of that sequence at every other HLA hydrophone. This produced 32 cross-correlations versus lag time. The lag time was then calculated by taking the arrival times for the transmission containing that sequence and subtracting the arrival time at CH16 from the arrival times at each of the other hydrophones. This lag time was used to obtain the correlation value for each hydrophone. Using the locations from the light bulb drop localization, the distance (or hydrophone separation) between CH16 and the other hydrophones was calculated. The correlation values at each hydrophone were then linearly interpolated using the calculated separation to obtain the correlation value versus arbitrary distance. The same process was done for CH17 through CH47, CH18 through CH47 and so on giving 32 correlation versus distance vectors ranging from 0 to 400 m for CH16 to CH47 to the auto-correlation value of CH47. The vectors all used the same range step, so values at the same ranges were then averaged to give one overall vector of correlation value versus separation distance for that sequence. This method gives better accuracy for the shorter distances, as it averages 31 inputs for the first range step and then decreases to one input for the final distance of 400 m.

Figure 4-7 shows the correlation versus hydrophone separation distance for the 30 signal sequences of the South 224 Hz transmission at 1810 on 5 May and eight noise sequences. The noise sequences are the sequences in the data file that were processed at either end of the signal reception. As expected, the correlation of the noise sequences drops off much faster than the signal sequences. The correlations versus distance for the 88 signal sequences from the East 400 Hz transmission at 1730 on 5 May, along with

nine noise sequences, are shown in Figure 4-8. Comparing the two curves, it can be seen the 224 Hz signals stay correlated over a longer distance as they have a longer wavelength than the 400 Hz signals.

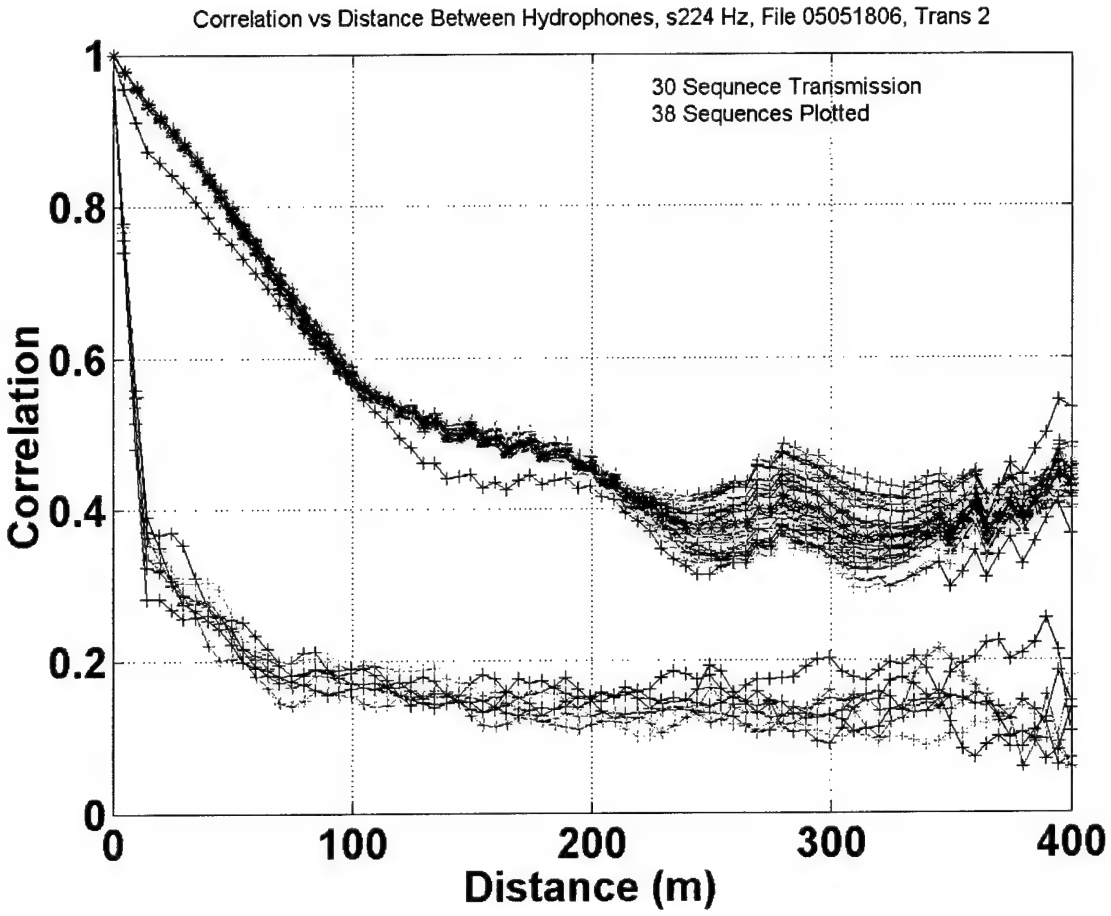

Figure 4-7: Correlation versus distance between hydrophones for the 30 sequences of the South 224 Hz transmission at 1810 on 5 May. Eight noise sequences are also plotted and can be seen dropping off faster than the signal.

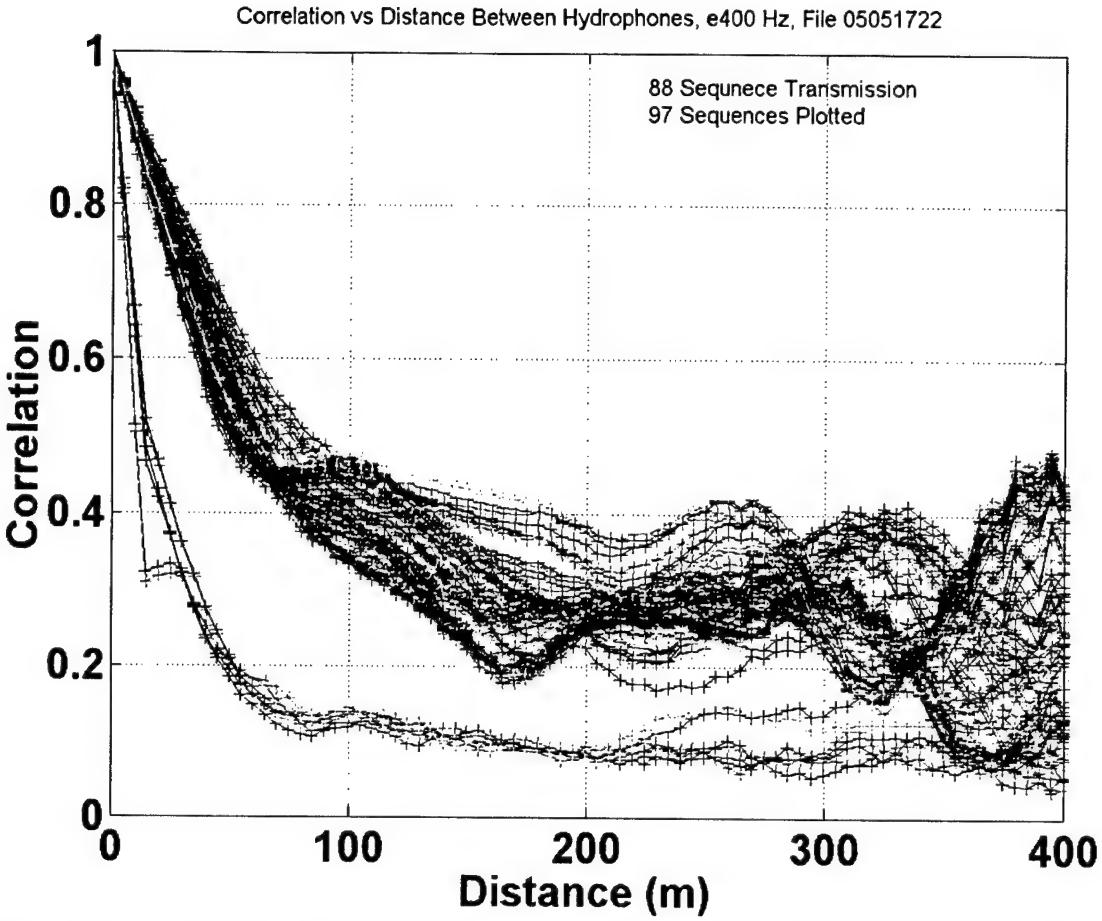

Figure 4-8: Correlation versus distance between hydrophones for the 88 sequences of the East 400 Hz transmission at 1730 on 5 May. Nine noise sequences are also plotted and they drop off faster than the signal sequences.

4.3.4 Correlation Results

For the determination of coherence length, the distance to a correlation value of 0.5 was chosen. Since correlation values for over 5000 sequences from the transmissions on 5 May needed to be dealt with, a readable form for the data was required. A way to do this is by using a histogram representation. Figure 4-9 shows histograms of the hydrophone separation distance resulting in a correlation value of 0.5 for all the analyzed sequences. Each graph shows the analyzed sequences for each of the three sources, with the top two graphs showing the up slope propagation and the lower graph covering the

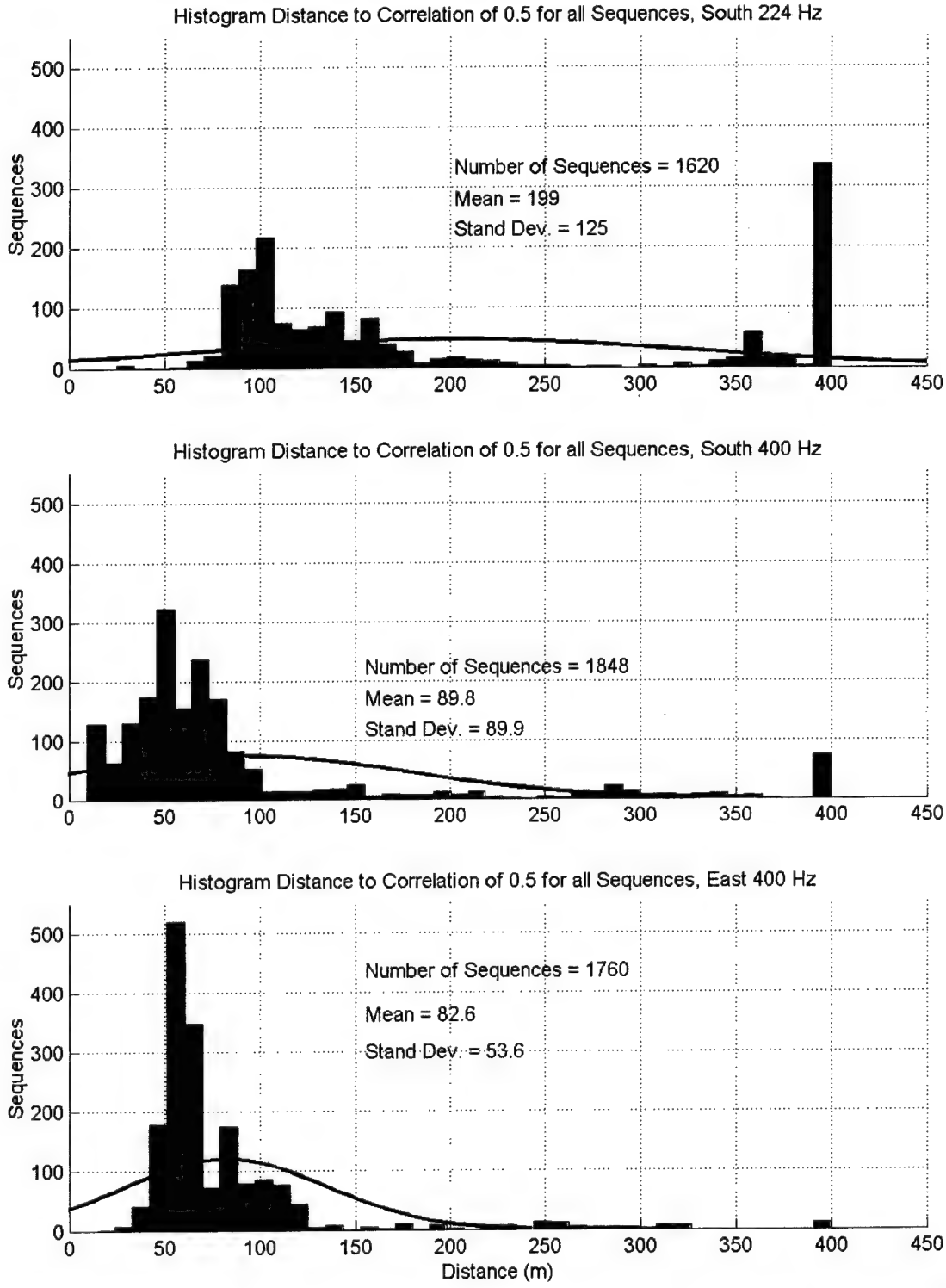

Figure 4-9: Histograms of the distances to a correlation value of 0.5 for the 224 Hz and 400 Hz transmissions on 5 May.

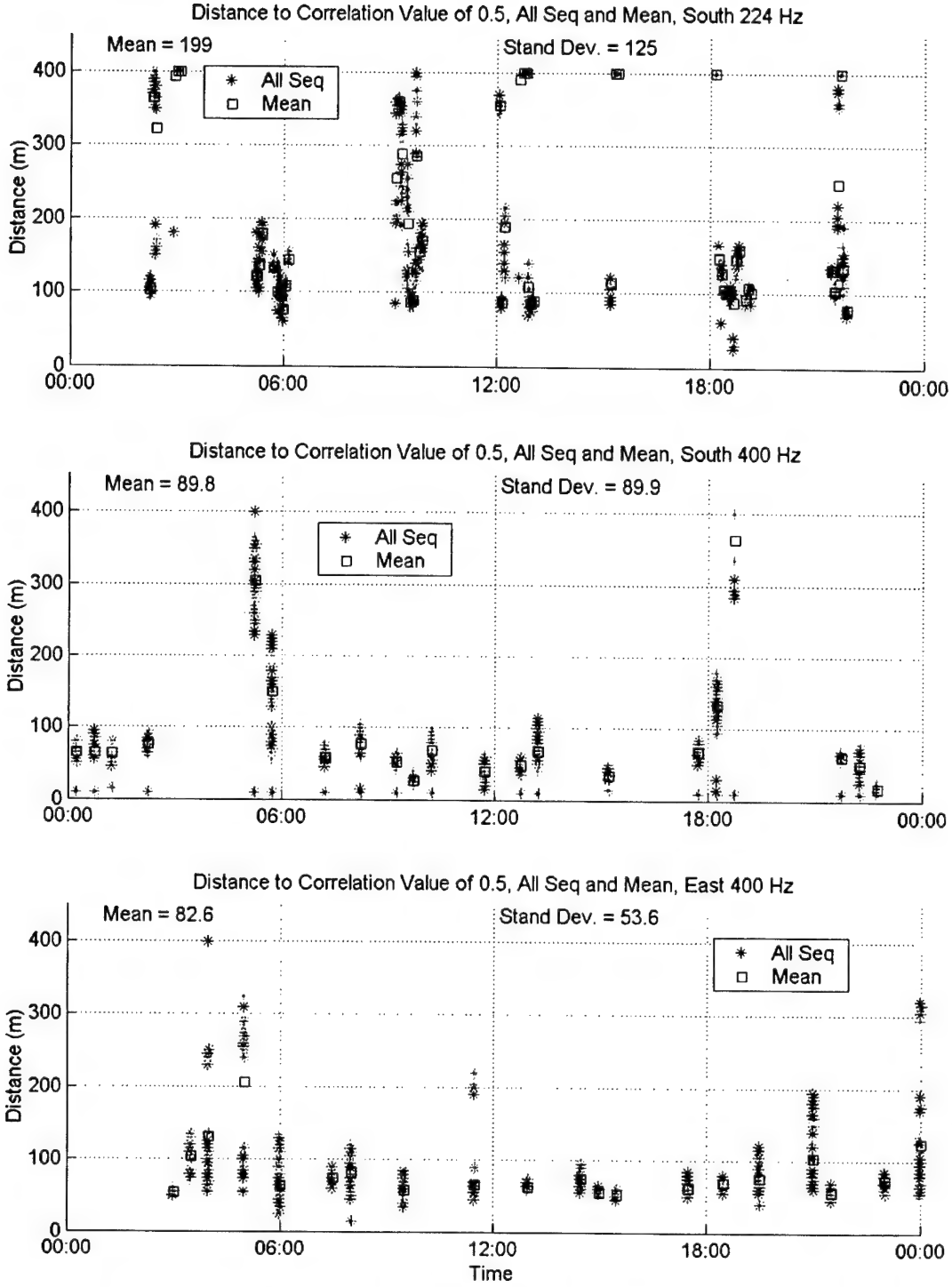

Figure 4-10: Distance to a correlation value versus time for all sequences. The mean for each transmission is also shown.

along shelf propagation. The mean of the values fall within the 15 to 30 λ predicted by Carey [3]. The mean of the sequences are 199 m (~30 λ) for the 224 Hz source, 89.9 m (~23 λ) for the South 400 Hz source and 82.6 m (~22 λ) for the East 400 Hz source transmissions. Another notable trend is that the up slope transmissions from the 224 Hz and 400 Hz sources show somewhat more variability with a larger number of sequences providing longer coherence lengths.

Figure 4-10 shows the distance to a correlation value of 0.5 versus time for all the sequences considered along with the mean value for each transmission. The top two graphs are for the up slope propagation paths of the 224 Hz and 400 Hz sources. The bottom graph shows the along shelf propagation path of the East 400 Hz source. As this data set shows some high frequency "noise," a sliding 4-hour window average was also calculated (Figure 4-11). For this calculation the mean was taken for all the sequences that fell within a 4-hour window as the window was moved at one-hour intervals through the day. With only one day of data, it is difficult to make any substantial conclusions about the origins of the time dependence; however, some substantial variability with time can be seen. Also, again, the up shelf propagation shows some longer correlation distances.

4.4 Discussions and Conclusions

Our first look at sensor-to-sensor correlation and coherence lengths for the ASIAEX SCS experiment HLA gives values that fall within the 15 to 30 λ expected from Carey's work [3]. However, this result considers only part of the "decoherence" causes and has two inherent inaccuracies. First, the method that was used lined up the leading edge of the sequences and therefore it looked only at the signal spreading and distortion across the array. Thus, it ignores (processes out) the phase front irregularities. This approximation will bias the method to produce longer coherence lengths. The second approximation is that the method ignores modal dispersion across the array. This effect will be larger for the East 400 Hz source transmissions, as they are closer to seeing an endfire geometry of the receiving array. Thus, as the modes move down the array at different group speeds,

the phase cancellation between the modes will change. This will cause different interference patterns and nodes along the array. The effect should cause the correlation lengths to be shorter than actual.

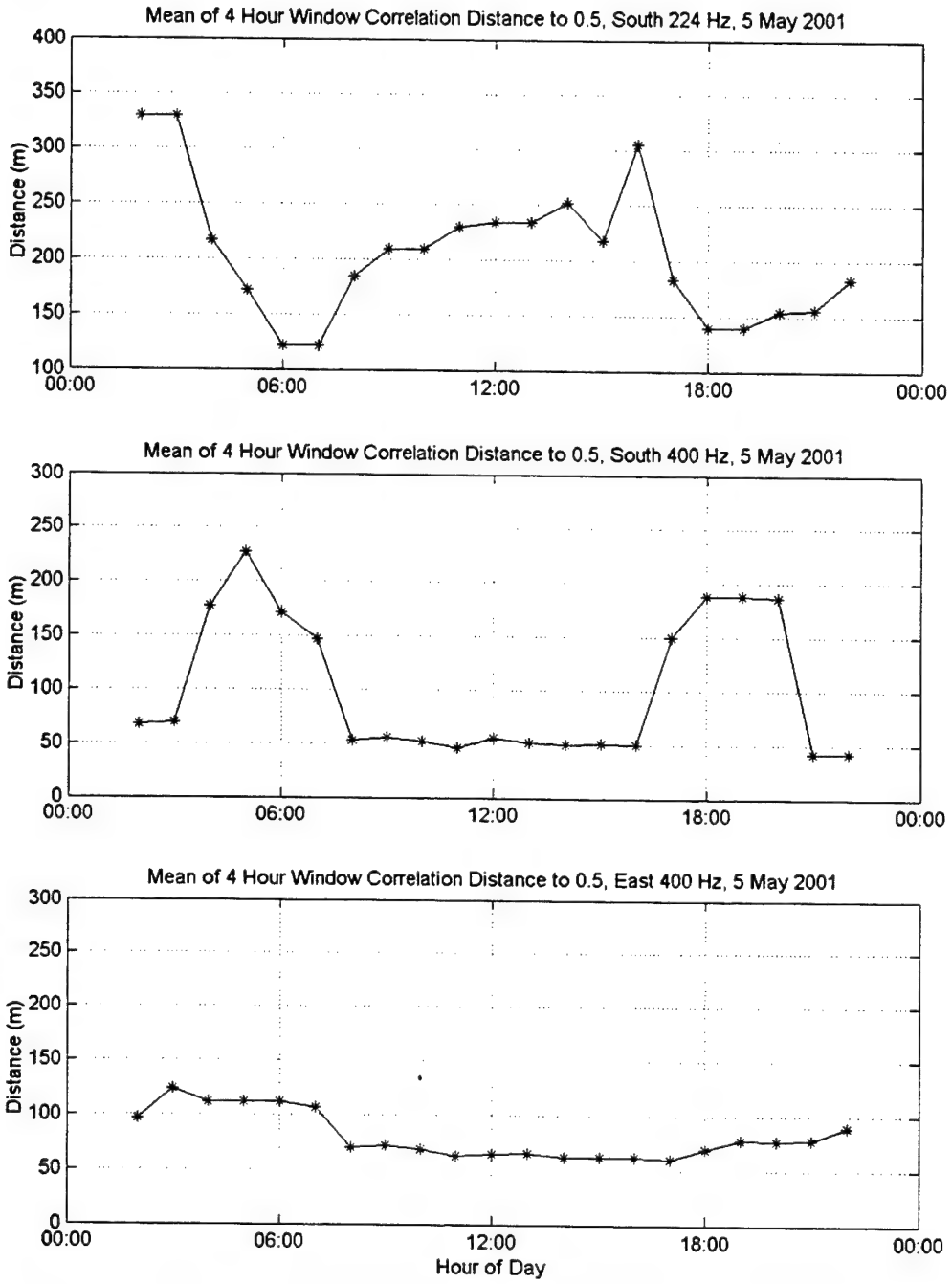

Figure 4-11: 4 Hour sliding window average of the distance to a correlation value of 0.5 of all the sequences.

The up slope propagation paths from the South 400 Hz and 224 Hz sources show more variability in the correlation distances. Specifically, they have more sequences that correlate over longer hydrophone separation distances than the along shelf path. This could be due to two effects. First, because of the geometry of the experiment, the along shelf acoustic path comes in at the endfire aspect of the array, while the up slope path sees closer to a broad-side aspect. This factor would make the along shelf propagation more susceptible to the modal dispersion error. The error should produce shorter correlation lengths in along shelf than up slope propagation. Second, the sound propagating up the shelf from the deep sources stays closer to the bottom and therefore has fewer interactions with scatterers near the surface like internal waves. The combination of the downward refracting sound velocity profile and the deep sources located near the bottom (source depth of 329.5 m for the 400 Hz source and 331.3 m for the 224 Hz source) causes most of the acoustical energy to stay close to the bottom. With fewer interactions with shallow scatterers, the signal will stay coherent over a longer distance.

5 Parallel Work, Conclusions and Future Work

This chapter will discuss some of the parallel work that has been conducted at the Naval Research Laboratory. It will then present the conclusions of the array localization and coherence length calculations. The final section will discuss recommendations for future work.

5.1 Parallel Work

Naval Research Laboratory (NRL) has been working in parallel with us on the ASIAEX SCS experiment HLA element localization and coherence length calculations, emphasizing the 300 Hz and 500 Hz linear frequency modulated (LFM) source transmissions.

5.1.1 Array Element Localization

NRL chose to use the 300 Hz and 500 Hz distant moored sources for the HLA element localization. This avoids the noisiness of the LBL navigation, and the intermittency of the light bulb drops, but comes at the cost of not being able to use the 300 Hz and 500 Hz data for other purposes, e.g. beam forming. In this method, the cross-correlation of the signal reception at subsequent hydrophones was used to determine the hydrophone spacing and the element locations. This analysis has been completed for ~36 hours around 5 May and will be completed for the duration of the experiment in the near future. With reported accuracies of less than 1 m, this method gives much better results then the LBL system. It also will give locations throughout the experiment, unlike the two days of data from the light bulb drops. Figure 5-1 shows the positions of the HLA sensors determined by the moored sources and those determined by the light bulb drops. The two methods correspond well to each other, with differences much less then the 6 m maximum possible error between sensors previously stated in Chapter 3. It appears that

our error bars in Chapter 3 were perhaps too conservative, and that we should be able to perform many phase-sensitive calculations with the positions obtained from the light bulb drops.

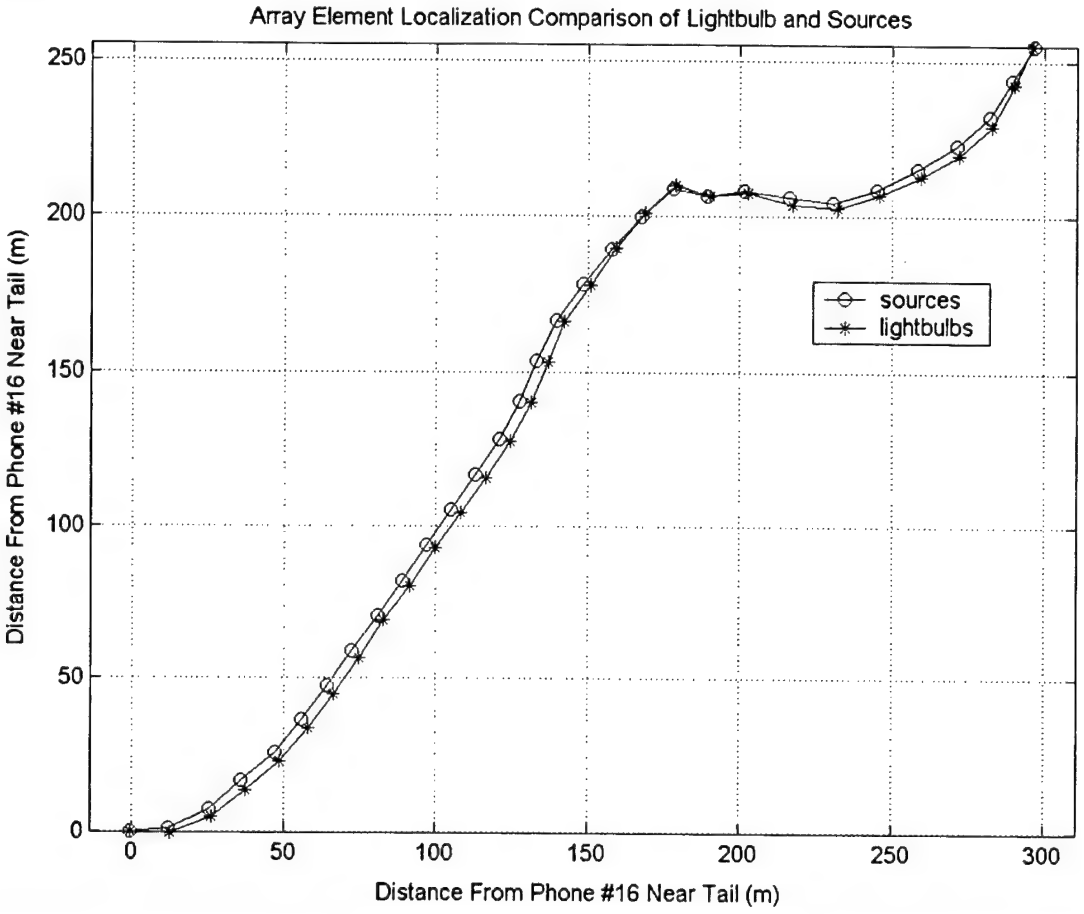

Figure 5-1: Comparison of HLA sensor positions obtained from the distant low frequency moored sources and the light bulb drops. The axes are in meters from the position of hydrophone 16 (closest to the tail).

5.1.2 Coherence Length Calculations

Sensor-to-sensor cross-correlations have been completed by NRL for a few days for the 300 and 500 Hz source transmissions. In their calculations, the peak correlation value was plotted versus hydrophone number. Qualitatively, the results seem similar to those determined for the along shelf 400 Hz source transmissions in this thesis. A larger variability with some longer correlation lengths was seen in the 300 Hz source than in the

400 Hz or the 500 Hz sources. This shows some indications of the frequency dependence of the coherence length.

5.2 Conclusions and Recommendations

The conclusions will be divided into two main parts: sensor localization and coherence lengths. A detailed listing of the conclusions found throughout this thesis is as follows:

5.2.1 Sensor Localization Conclusions and Recommendations

This section is a listing of the conclusions found in Chapter 3 on HLA element localization.

1. A HLA used in an area with high currents, such as the South China Sea, with large internal waves and bottom currents, needs to be more heavily weighted. This will reduce the probability of the array moving during the deployment. However, too much weight sinks the array in the sediment, so some compromise is needed.
2. It is difficult to use a high frequency acoustic long baseline (LBL) array element navigation system for a bottom mounted horizontal array in a complex coastal environment with high bottom currents. Acoustic multipath "hopping" due to internal waves and bottom micro-topography gives frequent jumps in the position estimate. The difficulty lies in trying to determine if the sudden shift in measured acoustic transmission time is due to an acoustic propagation shift or movement of the HLA. Low frequency moored sources positioned at longer ranges should provide better sensor localization than an LBL system. However, this is at the cost of the LF data, as mentioned.
3. While the analysis of the LBL data in this thesis did not fully compensate for all of the propagation shifts it did give indications of the HLA movement and general

geometry. Using the actual physical constraints of the array spacing combined with the LBL locations may provide good enough element locations for beam forming. However, the recommendation is to use the locations determined by the light bulb drops and the low frequency moored sources to provide better results for the beam forming.

4. The absolute position error in the LBL positions is on the order of 100 m unless the propagation path has been well verified, in which case it should be better than 30 m.
5. The implosion of light bulbs provides an excellent broadband pulse, which can be easily used for sensor localization. Using a method such as placing a light bulb on a line with a traveler (messenger) to get more exact implosion position and depth would provide for easier and more accurate calculations.
6. Having a couple of days of light bulb drops would be adequate to localize the sensor positions for an experiment in which the HLA did not move (more heavily weighted array in an area with smaller bottom currents). However, for the ASIAEX SCS experiment the HLA had enough movement that the low frequency moored sources will have to be used to provide locations throughout the experiment. The positions from the light bulb drops will provide a good check for the positions determined from the transmissions of the moored sources. They will also allow the analyses of all the sources for beamforming data on the two days where light bulb positions were available.
7. The sensor locations obtained from the light bulb drops on 5 May, and verified using the LBL positions and the arrival times of the 224 Hz and both 400 Hz sources, seems to be accurate to within 15 m maximum absolute error. The error in the distance between the sensors (relative senor position) is even better, with accuracy within 6 m. These are maximum (conservative) errors and the positions should be adiquate for accurate beam forming.
8. Comparing the sensor positions determined by the light bulb drops to the positions determined from the low frequency moored source transmissions, the

absolute difference is less than 5 m while the difference in hydrophone spacing is less than 2 m.

9. The accuracy of the light bulb drop based locations on 15 May is at least as good as the accuracy for the locations on 5 May. In fact, since the positions on 15 May were determined by 5 drops around the array, instead of just the broadside and endfire drops of 5 May, the accuracy should be better. However, their accuracy still needs to be confirmed by comparing to the positions determined from the LF moored sources.

5.2.2 Sensor to Sensor Correlations and Coherence Lengths

The conclusions for the first look at sensor-to-sensor correlations and horizontal spacial coherence lengths of the ASIAEX SCS HLA for the 5 May 224 Hz and both 400 Hz source transmissions as found in Chapter 4 are listed below.

1. This analysis looked at the pulse spreading across the array and has two inherent errors. First, it factors out the phase front variability by lining up the arrival times. This error would cause the calculated coherence lengths to be an overestimate. Second, modal dispersion was not taken into account, which would be a larger effect for the East 400 Hz transmissions as they come in on the end fire of the array. This error would cause the calculated coherence lengths to be underestimated. However, these errors are believed to be small and should not greatly change the results. The amount of the dispersion effects can be estimated by numerical calculations (Appendix A).
2. Calculating the sensor separation distance to a correlation value of 0.5 for each sequence on 5 May and taking the mean of the values for each source (224 Hz and both 400 Hz) provides values that fall within the 15 to 30 λ predicted by Carey [3]. The mean of the sequences are 199 m (~ 30 λ), 89.9 m (~23 λ) and 82.6 m (~22 λ) for the 224 Hz, South 400 Hz and East 400 Hz sources respectively.

3. While the mean of the transmissions fall within the 15-30 λ, there is a large variability in the correlation distance, with some sequences falling above and below that range. The larger variability seems to occur from the up slope propagation path, with many sequences showing long correlation lengths. In fact, many of the sequences stay correlated over the entire array. This is most likely due to the deep propagation of the up slope path. With a downward refracting sound speed profile, and sources located close to the bottom, much of the acoustic energy stayed below the near surface scatterers. This enabled the signals to stay coherent over longer distances.
4. There seems to be some time dependent variability in the coherence but with only one day of data, it was not yet possible to correlate this with oceanographic forcing.

5.3 Future Work

This thesis presented a first look at the horizontal spatial coherence for the HLA used in the ASIAEX SCS experiment. The following is a list of recommended future work to refine and expand on the results of this thesis.

1. Localize the sensor positions of the HLA for the duration of the experiment using the low frequency moored sources. While this will remove some of the data that can be analyzed, the accurate sensor locations will allow for better analysis on the remaining data. There was plenty of data taken during ASIAEX, so allowing some to be used for localization will not substantially hurt the time series.
2. Use the light bulb drop positions to obtain array coherence, including wave front distortions, for all frequencies (224, 300, 2x400, 500 Hz). The difference between these calculations and the ones performed in this thesis will allow the separation of the pulse distortion/spreading and wave front irregularities.
3. Use computer simulated (e.g. PE) to determine the magnitude of dispersion errors in the calculations.

4. Use Carey's method [3] of determining coherence lengths from the array gain of a beam formed array. This will remove both the modal dispersion and phase front variability errors of this work. The positions determined from the light bulb drops can be used for 5 May and 15 May. The rest of the analysis should wait until the sensor localization is completed.
5. When the data has been analyzed for the duration of the experiment, the time dependent oceanographic effects on the coherence lengths can be determined.

Appendix A

Modal Dispersion Effects on the Array Coherence Estimate

As mentioned, for an off-broadside array such as our ASIAEX SCS HLA, modal dispersion interference effects can produce error in the estimate of the array coherence. The ASIAEX HLA was ~70 degrees off broadside for the along-shelf sources and ~30 degrees off broadside for the cross-shelf source (It was originally planned to have the WHOI/NPS array oriented along shelf and the NRL SGAMS array oriented across-shelf, thus obviating this difficulty. However, the failure of the SGAMS unit, and the deployment of the WHOI/NPS in strong tidal currents forced us into a non-broadside configuration for the HLA.). Though we cannot directly correct our data for dispersion effects, as this would require perfect knowledge of both the acoustic field impinging upon the array and the array geometry, we can at least estimate the magnitude of such effects, in order to put an error bar on our estimates.

We can estimate modal dispersion error due to being at a non-broadside aspect in two ways. The first, and simpler, approach (which we will take here) is to calculate the group velocities of the acoustic normal modes at the receiver location, and then see how the modes get out of phase as they travel along the array. We will consider a purely endfire aspect in doing this calculation, as this is the worst case, and is also trivially extended to any other angle via a trigonometric correction. The second way to perform the error analysis is to directly model the full acoustic field at the receiver, using a full-wave code, such as the RAM parabolic equation code. One can then calculate the coherence directly, as well as use a modal decomposition of the field to see which modes are producing the interference. We will leave this second calculation for a future date.

In calculating how two modes go out of phase as they propagate radially from the source along an endfire horizontal array, we simply use $R = v_n t_n$ for each mode, where R

is the length of the array, v_n is the group velocity of each mode, and t_n is the time it takes the n^{th} mode to transit the array. We then use $\varphi_n = \omega t_n$, where φ_n is the phase, ω is the acoustic pulse center frequency (radians), and t_n is the transit time for each mode, to get what the phase difference is between any two modes after they have transited the array. Using this simple algebra, we can obtain an expression for how far two modes must travel before they are out of phase by π radians, the condition for full destructive interference. (This is a reasonable criterion for interference degradation of the correlation function, though one could certainly use others. A more conservative estimate would be $\pi/4$, which is easily determined by changing the distances by a factor of 1/4).

The expression is:

$$\Delta R = \frac{v_1^2}{\Delta v}\frac{\pi}{\omega} \tag{A-1}$$

where Δv is the difference in group velocity between two modes.

With this expression in hand, we have modeled the distances to the destructive interference point for both the 224 and 400 Hz sources in the ASIAEX SCS experiment. In Figure A-1, we show the radial distance to full interference for nearest neighbor modes for the 224 Hz source. In this figure, the distance to full interference is presented against the "mode pair number," which is just the first number of the mode pair (n, n+1). We do not look at the first three mode pairs (of the thirteen possible), since the distance to full interference for these is much more than a kilometer, and thus far greater than the 400m dimension of the HLA. It is seen from this figure that the nearest neighbor modes do not interfere enough to affect our coherence calculations, as their interference distances are on the order of the array dimension or greater. Also, the additional geometric factor of 1/cos(χ), where χ is the angle off broadside, will further increase the distance to full destructive interference, by a factor of 1.06 for the 70 degree case and by a factor of 2.0 for the 30 degree case (Remember that 90 degrees is endfire.).

However, nearest neighbor modes have the least interference versus range, as their group and phase velocities are close. Thus, we should look at the interferences of distant modes. For this calculation, the interference of the first mode with all other

modes should be a very good indicator of distant mode interference. This calculation is

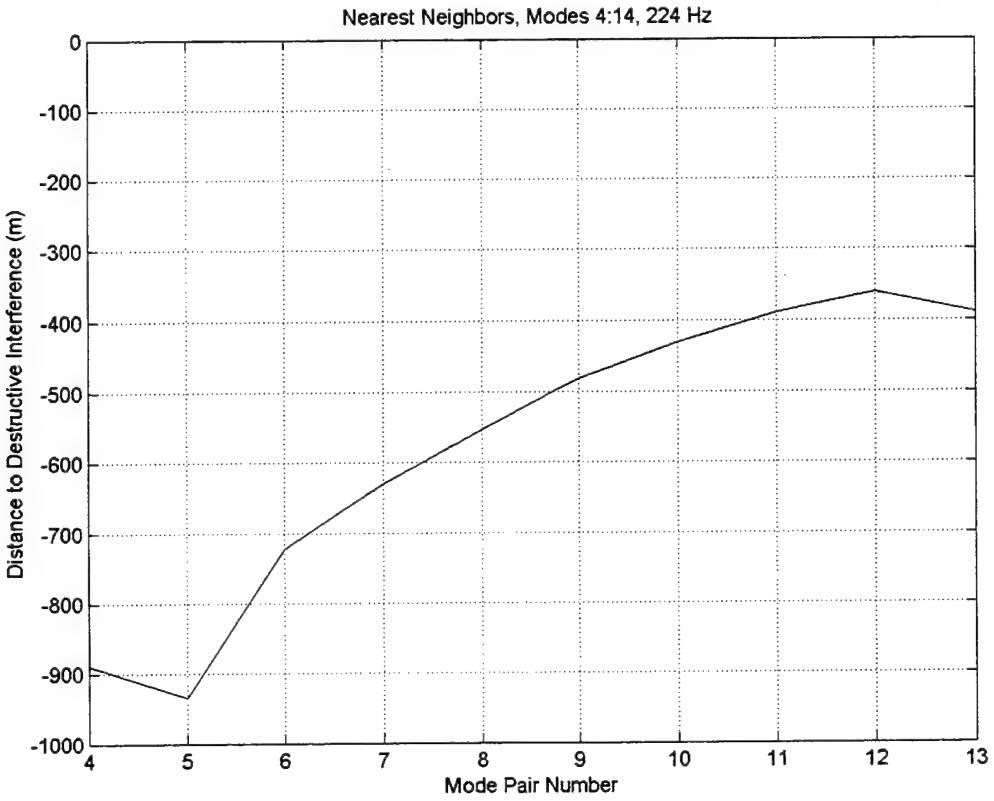

Figure A-1: Distance to destructive interference in meters for the 224 Hz nearest neighbor modes 4 through 14.

shown, again for endfire, in Figure A-2. One immediately sees that for mode pair numbers higher than six (where the mode pair number now means the (1, n) pair), the modes will interfere destructively within the dimensions of the array. However, there is an energetics issue that is not addressed by this figure that may come into play in the real data. Specifically, due to mode excitation, coupling, and attenuation, the higher modes may be largely attenuated at the receiver, making their interference with the stronger, lower modes, somewhat of a moot point. To see how much this effect comes into play, we need to look at the full acoustic field calculation mentioned before. For now, it suffices to say that, based on our calculations, the dispersion effect could introduce some error into our previous calculations.

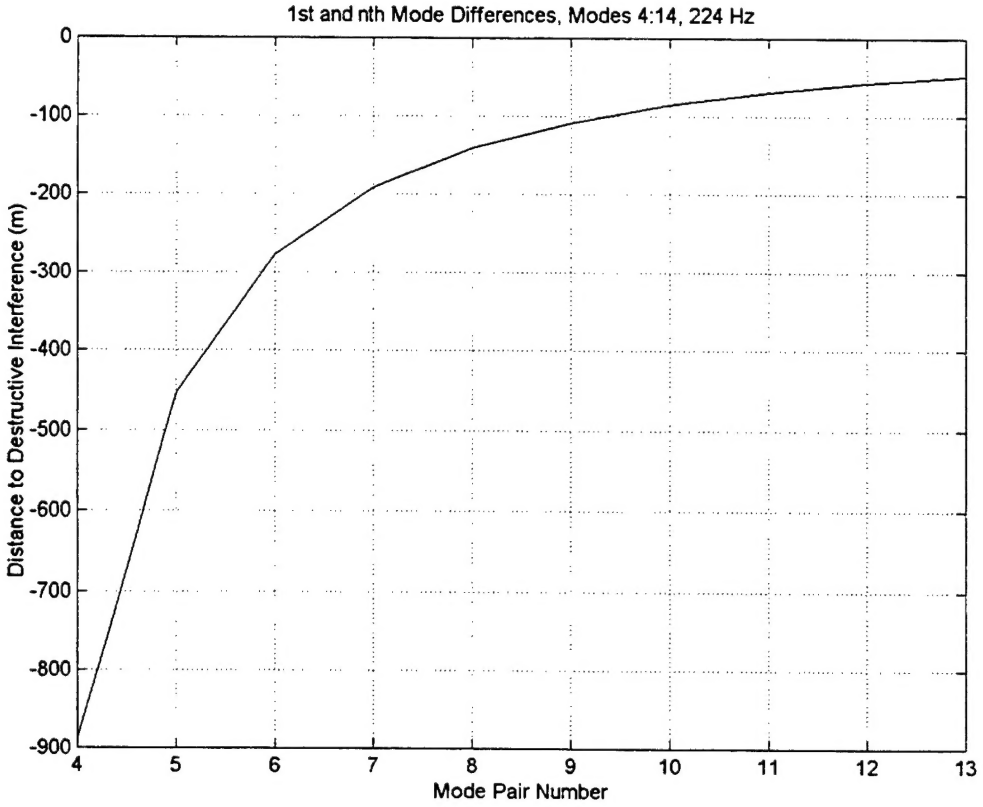

Figure A-2: Distance in meters to the destructive interference for the first and the nth mode of a 224 Hz signal.

We next look at the same type of calculations for the 400 Hz sources. In this case, we have 25 trapped modes, versus the 14 for the 224 Hz. For the nearest neighbors, the result is shown in Figure A-3. As for the 224 Hz case, the nearest neighbor interferences are rather innocuous, and are probably not the cause of significant error. The distant neighbor interferences, as indicated by the (1,n) case, are probably more significant causes of error, as we see in Figure A-4 that the interference distance can be as small as 50m for the (1,25) pair interference. However, there is again the energetics issue to consider, and it is quite likely that many of the higher order modes are energetically insignificant at the receiver location. As before, this issue is best resolved with a full-field computer model.

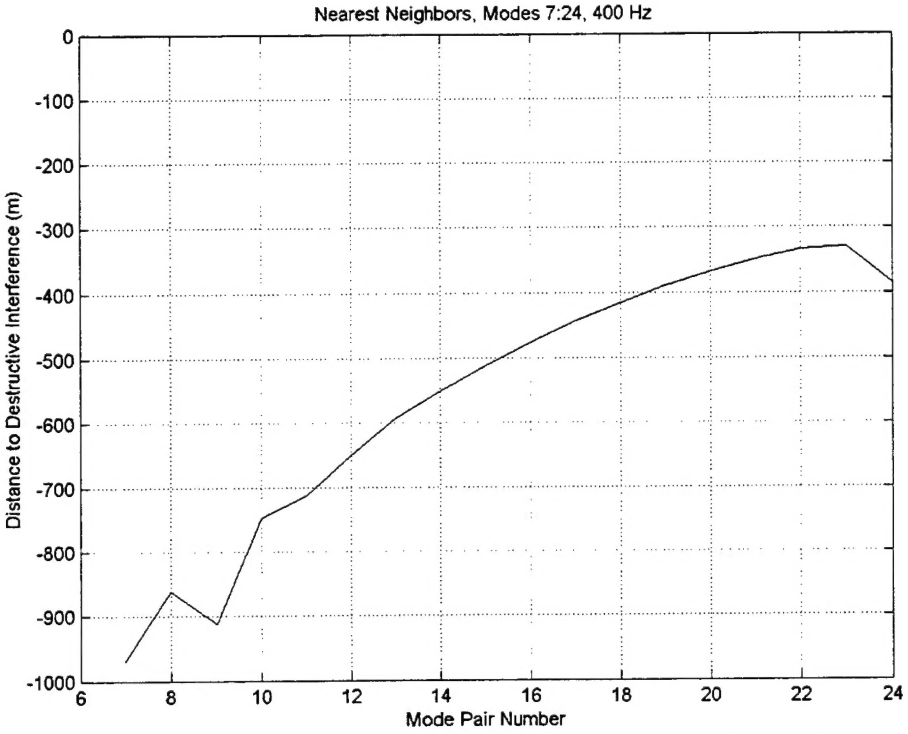

Figure A-3: Distance to destructive interference in meters for the 400 Hz nearest neighbor modes 7 through 24.

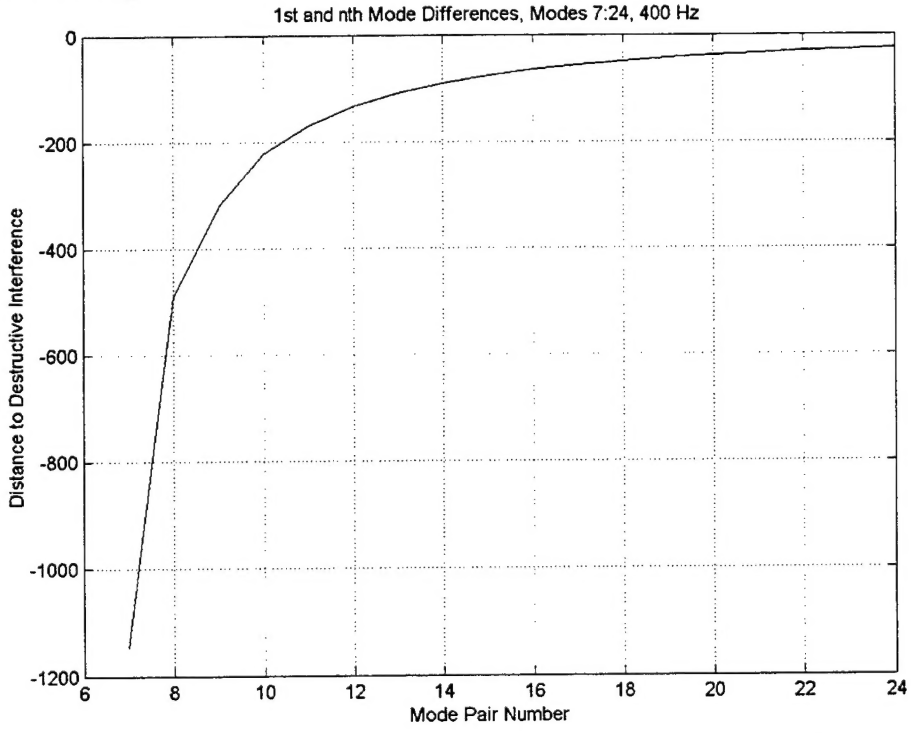

Figure A-4: Distance in meters to the destructive interference for the first and the nth mode of a 400 Hz signal.

Bibliography

1. D. C. Stickler and R. D. Worley and S. S. Jaskot, Bell Telephone Laboratories (unpublished). Summarized by Robertson, G. H., Model for spatial variability effects on single path reception of underwater sound at long ranges. *J. Acoust. Soc. Am.* 69:112-123, 1981

2. W. M. Carey and W. B. Moseley, Space-time processing, environmental-acoustic effects, in *Progress in Underwater Acoustics,* edited by H. M. Merklinger (Plenum, New York, 1987),pp. 743-758, expanded version in IEEE *J Ocean Engineering.* 16, 285-301, 1991

3. W. M. Carey, The determination of signal coherence length based on signal coherence and gain measurements in deep and shallow water. *J. Acoust. Soc. Am.* 104(2):831-837, 1998

4. P. Wille and R. Thiele, Transverse horizontal coherence of explosive signals in shallow water, *J. Acoust. Soc. Am.* 50:348-353, 1971

5. W. M. Carey, Measurement of down-slope sound propagation from a shallow source to a deep ocean receiver, *J. Asoust. Soc. Am.* 79,:49-59, 1986

6. W. M. Carey, I. B. Gereben and B. A. Brunson, Measurement of sound propagation downslope to a bottom-limited sound channel, *J. Acoust. Soc. Am.* 81:244-257, 1987

7. These results are from the ACT series of experiments conducted by W. Carey, P. Cable and J. O'Connor on the Florida Shelf in the Gulf of Mexico, on the Jersey Continental Shelf, and in the Straits of Korea. Explosive sources were developed and deployed by W. Marshall and the analysis was performed by Mike Steele, T. Kooij and J. Angle from BBN Laboratories. In addition, the CW sources were deployed by W. Cary and G. Hunsaker, NRAD. Analysis of the Straits of Korea array data was performed by J. Reese, NRAD.

8. A. Newhall et al., Preliminary acoustic and oceanographic observations from the ASIAEX 2001 South China Sea experiment, Woods Hole Oceanog. Inst. Tech. Rept., WHOI-2001-12.

9. W. Munk, P. Worcester, and C. Wunsch, *Ocean Acoustic Tomography.* Cambridge Monographs on Mechanics. Cambridge University Press, Cambridge. 1995

10. R. Urick. *Principles of Underwater Sound.* McGraw-Hill Inc., New York, 3rd edition. 1983.